

**Experimental and numerical  
investigations on seeding  
options for the multi-beam line  
Free-Electron Laser facility  
FLASH**

**Dissertation**

zur Erlangung des Doktorgrades  
an der Fakultät für Mathematik, Informatik und  
Naturwissenschaften  
Fachbereich Physik  
der Universität Hamburg

vorgelegt von

Diplom-Physiker Sven Ackermann  
aus Hamburg

Hamburg  
2016

**Gutachter der Dissertation** Prof. Dr. Jörg Roßbach  
Dr. Bart Faatz

**Datum der Disputation** Freitag, 02. Dezember 2016

**Mitglieder der Prüfungskommission** Prof. Dr. Ludwig Mathey (Vorsitzender)  
Prof. Dr. Jörg Roßbach (Stellv. Vorsitzender)  
Prof. Dr. Caren Hagner  
Dr. Bart Faatz  
Dr. Juliane Rönsch-Schulenburg

## Abstract

Free-electron laser (FEL) facilities around the world provide scientists from many disciplines with the benefits of the ultra-short, transversely coherent and intense photon pulses with wavelength down to the Ångström regime. Due to the large number of beam time requests facilities start to study options to provide more beam time. One recently extended FEL facilities is FLASH in Hamburg, which was equipped with a second undulator beam line. Since most FELs works as an amplifier for the spontaneous radiation, its stochastic behaviour is imprinted on the photon pulses which means they show poor temporal coherence and large shot-to-shot fluctuations in wavelength, energy, and longitudinal pulse profile.

It has been shown that different seeding schemes can enhance the spectral, temporal and coherence properties of the emitted radiation as well as reducing the fluctuations in arrival time and output energy. One promising approach is direct High-Harmonic Generation (HHG) seeding, where an intense laser pulse with the desired wavelength, overcoming the power of the spontaneous radiation, is overlapped with the electron beam and works as the input signal for the FEL amplifier.

Another approach is High-Gain Harmonic Generation (HGHG) where the electrons get energy modulated by means of an NIR laser and an electromagnetic undulator. Later, this energy modulation is converted into a density modulation which enhances the harmonic content of the electron bunch at the desired wavelength, which is then preferred to be emitted.

In this thesis a summary of the scientific development towards modern FELs as well as their theoretical description is given. The influence of the beam quality on the FEL performance in a directly HHG seeded machine was studied as well as the possibility to use different undulator arrangements for the optimization of longitudinal position of the FEL source point. A method to convert electron beam distribution between different simulation codes is given and used for numerical studies on the initial modulation depth with respect to the seed laser beam quality. The first scientific results of the experimental demonstration of HHG and HGHG seeding at FLASH are presented as well as the results of the commissioning of FLASH2, the worlds first multiplexing FEL facility.

## Zusammenfassung

Freie-Elektronen Laser (FEL) versorgen weltweit Wissenschaftler verschiedenster Fachrichtungen mit den Vorzügen extrem kurzer, transversal kohärenter und intensiver Photonenpulse mit Wellenlängen hinab bis in den Ångström-Bereich. Wegen der hohen Zahl an Strahlzeitanfragen untersuchen einige Forschungszentren Möglichkeiten, mehr Strahlzeit zu generieren. Eine erst kürzlich erweiterte FEL-Anlage ist FLASH in Hamburg, welche mit einer zweiten Undulatorstrahlführung ausgestattet wurde. Da die meisten FELs als Verstärker für die spontane Strahlung arbeiten, ist deren stochastischer Charakter auf die Photonenpulse aufgeprägt; das bedeutet dass diese geringe zeitliche Kohärenz und große Schuss-zu-Schuss Fluktuation in der Wellenlänge, Energie und longitudinalem Pulsprofil aufweisen.

Es wurde gezeigt dass verschiedene Seeding-Schemata sowohl die spektralen, temporalen und Kohärenzeigenschaften der abgestrahlten Strahlung verbessern als auch die Fluktuationen in der Ankunftszeit und Pulsenergie verringern können. Ein vielversprechender Ansatz ist das direkte „HHG“-seeding, bei dem ein intensiver Laserpuls mit der gewünschten Wellenlänge und einer Leistung, die die der spontanen Strahlung übertrifft, mit dem Elektronenstrahl zum Überlapp gebracht wird und als Eingangssignal für den FEL Verstärker dient.

Eine weitere Methode ist „HGHG“, bei dem Elektronen mittels eines NIR-Laserpulses und eines elektromagnetischen Undulators eine Energiemodulation erfahren. Später wird diese Energiemodulation in eine Dichtemodulation konvertiert, welche den Harmonischengehalt auf der ausgewählten Wellenlänge erhöht, welche dann bevorzugt emittiert wird.

In dieser Dissertation wird die wissenschaftliche Entwicklung hin zu modernen FELs und ihre theoretische Beschreibung dargelegt. Der Einfluss der Strahlqualität auf die Leistung eines direkt HHG-geseedeten FELs wurde studiert, zusammen mit der Möglichkeit, unterschiedliche Undulatoranordnungen zu benutzen um die longitudinale Position des FEL Quellpunktes zu optimieren. Eine Methode die Elektronenstrahlverteilung zwischen verschiedenen Simulationscodes zu konvertieren wird gezeigt und genutzt um numerische Studien über den Einfluss der Seedlaser Strahlqualität auf die initiale Modulationsamplitude durchzuführen. Erste wissenschaftliche Ergebnisse aus der experimentellen Demonstration von HHG und HGHG Seeding bei FLASH werden ebenso präsentiert wie die Ergebnisse der Inbetriebnahme von FLASH2, der weltweit ersten FEL-Anlage, die mehrere FELs mit einem Linearbeschleuniger zeitgleich betreiben kann.

# Contents

<b>1</b>	<b>Introduction</b>	<b>12</b>
1.1	Synchrotron radiation . . . . .	12
1.2	Free-Electron Lasers . . . . .	13
1.2.1	The oscillator FEL . . . . .	15
1.2.2	The single-pass FEL . . . . .	16
1.2.3	Properties of SASE radiation . . . . .	16
1.3	Seeded FEL . . . . .	16
1.3.1	Self-seeding . . . . .	17
1.3.2	Direct seeding . . . . .	18
1.3.3	High-Gain Harmonic Generation . . . . .	18
1.3.4	Echo-enabled Harmonic Generation . . . . .	19
1.4	The <b>Free-Electron Laser</b> in <b>Hamburg</b> (FLASH) . . . . .	20
1.5	The extension of the FLASH facility: FLASH2 . . . . .	21
1.6	The sFLASH experiment . . . . .	22
1.7	Organisation of the thesis . . . . .	23
<b>2</b>	<b>Theory</b>	<b>25</b>
2.1	1D FEL Theory . . . . .	26
2.2	Shot noise . . . . .	33
2.3	Transverse and Longitudinal Coherence . . . . .	34
2.4	Production of a seed pulse in a high harmonics-generation target	35
2.5	High-gain harmonic generation . . . . .	38
<b>3</b>	<b>Dependence of HHG seeding on the laser beam quality</b>	<b>45</b>
3.1	Gaussian beams . . . . .	46
3.2	Numerical simulation setup . . . . .	48
3.3	Generation of field distributions with given beam quality factors and waist sizes . . . . .	50
3.4	FEL output power vs. seed pulse beam quality . . . . .	51
3.5	Modal reconstruction of intensity profiles . . . . .	54
3.6	Comparison to experimental results . . . . .	57

## CONTENTS

---

3.7	Conclusion . . . . .	62
<b>4</b>	<b>Optimization of the Source Point of a Direct HHG-seeded FEL</b>	<b>63</b>
4.1	Seeding option at FLASH2 . . . . .	63
4.2	Numerical Simulations . . . . .	64
4.3	Optimization of undulator gaps configuration . . . . .	65
4.4	Summary and outlook . . . . .	70
<b>5</b>	<b>High-gain harmonic generation</b>	<b>73</b>
5.1	Data handling between different simulation codes . . . . .	73
5.1.1	Data exchange from GENESIS1.3 to elegant . . . . .	75
5.1.2	Data exchange from elegant to GENESIS1.3 . . . . .	76
5.1.3	Challenging particle distributions . . . . .	78
5.2	Energy spread measurements . . . . .	78
5.3	Modulation depth vs. seed pulse beam quality . . . . .	80
<b>6</b>	<b>Achievements in seeding at FLASH</b>	<b>82</b>
6.1	High-harmonic generation . . . . .	82
6.2	HGHG . . . . .	87
<b>7</b>	<b>Parallel operation of two FEL beam lines</b>	<b>92</b>
7.1	Introduction . . . . .	92
7.1.1	The timing system . . . . .	93
7.1.2	Intra-bunch train switching . . . . .	95
7.1.3	Dual injector laser setup . . . . .	96
7.1.4	Changes in the RF system . . . . .	97
7.2	FLASH2 hardware commissioning results . . . . .	100
7.3	FLASH2 beam line commissioning . . . . .	108
7.4	Examples for other FEL multiplexing facilities . . . . .	110
<b>8</b>	<b>Summary and Outlook</b>	<b>112</b>
<b>9</b>	<b>Acknowledgements</b>	<b>127</b>

# List of Figures

1.1	Peak brilliance of synchrotron radiation sources. . . . .	14
1.2	Layout of the free-electron laser in Hamburg (FLASH). . . . .	21
1.3	The sFLASH direct XUV seeding experiment. . . . .	23
2.1	Curve showing the power dependence on the longitudinal position. . . . .	31
2.2	Simulation of the FEL output power for different seed pulse powers. The simulation is based on FLASH2 parameters and multi-segmented undulators. . . . .	33
2.3	The semi-classical three step HHG model. . . . .	36
2.4	Design of a QPM target . . . . .	38
2.5	Bunching factors for different seed energies, normalized to the optimum seed energy (maximum in the Bessel function). The different curves show the behaviour for several harmonics $h$ . . . . .	40
2.6	Longitudinal phase space distribution before entering the modulator. . . . .	41
2.7	Longitudinal phase space distribution after energy modulation by the means of a laser in the undulator. . . . .	41
2.8	The charge is still uniformly distributed along the longitudinal bunch coordinate. . . . .	42
2.9	Longitudinal phase space distribution after the dispersive section. The energy modulation was transformed to an electron density modulation. . . . .	42
2.10	The electron density modulation is clearly visible and will radiate on a higher harmonic. . . . .	43
2.11	Dependence of the normalized contrast $(P_S/P_h)/\max(P_S/P_h)$ on the harmonic number $h$ under the absence of energy spread. . . . .	44
3.1	Curvature radius dependence on the longitudinal position. . . . .	47

## LIST OF FIGURES

---

3.2	Gaussian beam propagation. The red solid line is the beam size, the blue dashed line shows the asymptotic behavior. The black line indicates the axis. With the help of the green lines one can see: After traveling a distance of one Rayleigh-Length, the beam radius grows by a factor of $\sqrt{2}$ , thus doubles the beam area. . . . .	47
3.3	Normalized output power of the seeded FEL behind the third undulator vs. the waist size of the seed pulse. . . . .	50
3.4	Seeded FEL power contrast vs. $M^2$ of the seed pulse. The circles show the simulation with the same TEM <sub>00</sub> mode in terms of intensity and size which is embedded in the seed pulse with the given $M^2$ . These pulses have by definition an $M^2$ of 1, however their position on the x-axis refers to the $M^2$ of the seed pulse they are taken from. . . . .	52
3.5	Difference (color coded) of the power gain curves for different $M^2$ in comparison to the $M^2 = 1$ case, normalized to the power after 10 m for each $M^2$ . One can see that for the $M^2 \geq 3$ the gain curve behaviour is the same as for the $M^2 = 1$ case, . . .	53
3.6	Dependence of the $M^2$ of the FEL radiation in saturation on the $M^2$ of the seed pulse at the end of the linear regime. . . .	54
3.7	Longitudinal power distributions for SASE and two different seed pulses of $M^2 = 1$ and $M^2 = 4.8$ . One can see that SASE and $M^2 = 4.8$ have the same double-spike structure while for the fundamental seeded, only one spike is present. . . . .	55
3.8	Spectra for SASE and two different seed pulses of $M^2 = 1$ and $M^2 = 4.8$ . One can see that all three have one dominating spike. For the fundamental seeded FEL, there is only one spike in the spectrum, while for the $M^2 = 4.8$ and SASE case, two spikes are visible. . . . .	55
3.9	Central wavelength in the spectra after three undulators for different $M^2$ (red crosses). The blue line indicates the central wavelength of the SASE case. The clustering at three different wavelength is an artefact of the limited spectral resolution of the used simulation code. . . . .	56
3.10	Transverse intensity distribution of the 38 nm HHG seed beam used at the direct seeding experiment sFLASH. It was measured waist, color coded is the intensity measured by the camera. 58	58

3.11	Power content coefficients $c_{nm}$ of the harmonics beam shown in Fig. 3.10. The TEM <sub>00</sub> mode is with around 90% of the overall intensity the strongest mode. Power content coefficients smaller than $10^{-3}$ are colored white. More than 96% of the pixel value intensity is contained in the 64 reconstructed modes.	59
3.12	Probability distribution of the $M^2$ values determined using Monte Carlo simulation. This only covers uncertainties from the measurement, not bunch-to-bunch fluctuations.	60
3.13	Simulated power contrast along the internal bunch coordinate $s$ . This is one typical result for one electron bunch.	61
4.1	Best undulator gap configuration for a time-dependent simulation of HHG seeding at 38 nm at FLASH 2. Yellow bars mark closed undulators. The green bar is an additional undulator added for the simulation to check whether the FEL is in saturation or not. The blue line is the FEL peak power.	66
4.2	FEL pulse energies and energy contrast. Since the seeded FEL has a shorter saturation length, the energy contrast increases with the active undulator length. At around 30 m, the seeded FEL runs into saturation, while the SASE FEL pulse energy still increases, therefore the contrast decreases.	67
4.3	Longitudinal power distribution (a) and spectra (b) at the position of the highest energy contrast (instead of the end of the last undulator as in Fig. 4.5 and Fig 4.4)) for the optimized temporal offset of 7 fs, optimized in terms of pre-pulse reduction. The head of the pulse is to the right. The radiation pulse yields an energy of 21 $\mu$ J.	68
4.4	Longitudinal power distribution (a) and spectra (b) for a temporal offset of 54 fs, i.e. the electron bunch peak current arrives at the entrance of the first undulator 54 fs earlier than the HHG seed pulse. The head of the pulse is to the right. The radiation pulse yields an energy of 328 $\mu$ J.	69
4.5	Longitudinal power distribution (a) and spectra (b) for a different timing offset. The peak power of the HHG seed radiation pulse arrives 7 fs earlier than the peak current of the electron beam (i.e. the seed pulse has been shifted by +61 fs with respect to Fig. 4.4. The head of the pulse is to the right. The radiation pulse yields an energy of 395 $\mu$ J.	71

## LIST OF FIGURES

---

4.6	Maximum pulse energy contrast in dependence of the HHG seed pulse energy. The simulation assumed the optimum timing offset and undulator configuration and shows values for the position of best contrast along the undulator beam line. . . . .	72
5.1	Usual HGHG simulation using three individual simulations (Modulator, dispersive section, and radiator) . . . . .	74
5.2	Comparison of a GENESIS1.3 and ELEGANT particle distribution. . . . .	77
5.3	Fit of the energy spread against the beam size. The flattening at an additional energy spread of about $5 \cdot 10^{-3}$ is a consequence of the limited energy spread that can be transported without losses. . . . .	79
5.4	Energy modulation at the entrance of the first undulator module for an initial laser seed of 300 MW (blue) and 1 GW (red). . . . .	80
6.1	Result of the seed scan. One can see that for the laser off (blue) cases there is no change of the FEL energy while for the laser on (red) case a significant enhancement of the FEL energy is present within a certain time delay range. The 0 ps is set arbitrarily to the maximum energy contrast. . . . .	84
6.2	Histograms of FEL pulse energies for seeded and unseeded cases. The pulse energy was measured using an multi-channel plate detector. . . . .	85
6.3	Spectrum of the XUV radiation of the sFLASH undulators for SASE at the fundamental undulator wavelength and the HHG seed pulse . . . . .	86
6.4	Individual single-shot spectra of the second harmonic of the FEL radiation for seed laser off (left) and seed laser on (right). One can see that high energy shots on the second harmonic only occur if the seed laser has been switched on. . . . .	86
6.5	Longitudinal phase-space distribution of the electron bunch measured using the transverse deflecting cavity. The energy modulation in the electron bunch induced by the UV seed can be seen as a hole in the curved bunch profile . . . . .	87
6.6	Measured rms width of the electron beam in a given time interval compared to several simulated energy modulation amplitudes. . . . .	88
6.7	FEL pulse energy vs. shot number. The mean FEL energy with the seed laser on is about a factor of 100 higher than for those cases when the laser was switched off. . . . .	89

6.8 Spectra of average HGHG radiation, single-shot HGHG spectra and average SASE radiation. The SASE spectrum has beam multiplied by 1000 in order to enhance visibility, thus having a contrast of about 1000 for the averaged spectra. . . . 90

6.9 Profile of the seeded FEL radiation using a screen. . . . . 91

7.1 Layout of the FLASH facility after the installation of FLASH2. The total length is about 315 m. This sketch is not to scale. . 93

7.2 Timing pattern for FLASH before the extension. The superconducting cavities are filled. Electron bunches are then injected and accelerated during the up to 800  $\mu$ s long flat top, in this example only 500 bunches are present. The remaining flat-top is unused. . . . . 97

7.3 Timing pattern for FLASH after the extension. The superconducting cavities are filled. Electron bunches generated by means of the first injector laser are then injected and accelerated during the first flat top. After the first bunch train ends, the flat top of the RF is changed. At the same time, the kicker voltage is rising to its flat top value. When the RF and the kicker reached the flat top, the second injector laser generates electron bunches which will be kicked to FLASH2. . . . . 98

7.4 Flatness of the long-pulse flat top extraction kicker with (yellow) and without (ocher) casing. One can see that with the casing, the kicker flatness is stable but not constant. . . . . 101

7.5 Envelope of the RF pulse measured at the accelerating module ACC45, gradient (left) and phase (right). There are three flat tops visible where the third flat top is already foreseen for FLASH3. . . . . 102

7.6 Measured photon pulse energy on a Gas Monitor Detector for two bunch trains seperated by 50  $\mu$ s. The first train has 30 pulses while the second one has 20 pulses. The vertical axis shows the photon pulse energy in arbitrary units, the horizontal scale is the time (roughly in microseconds). The yellow line is the maximum value, the green line the exponentially filtered average and blue line the instantaneous value. The gap of about 50  $\mu$ s is foreseen for the kicker to rise and to adjust the RF parameters. For the top figure, the cathode lasers were setup to deliver he same charge, for the bottom figure, for the 2nd pulse train the charge was reduced to half. RF parameters were adjusted to optimize lasing for each bunch train individually. . . . . 104

## LIST OF FIGURES

---

7.7	Charge dependence of the electron bunch length after the optimum compression. Color coded is the bunch number in the train. The black line is the average. . . . .	105
7.8	Energy of the individual bunches. Bunch train 1 consisting of 30 bunches has about 500 MeV total energy, bunch train 2 consisting of 20 bunches about 497 MeV. . . . .	106
7.9	XUV-Spectrometer camera image of the FEL radiation driven by two bunch trains of different energies. Smaller wavelengths are to the left. The yellow box has a width of about 0.1 nm. One can estimate that the two bunch trains are separated by about 3 times the box' width. This would mean a difference of 0.3 nm. This corresponds to an energy deviation of $\frac{\Delta E}{E} = 0.6\%$ which is in a good agreement to the measured energy deviation of $\frac{3\text{MeV}}{500\text{MeV}} = 0.6\%$ . . . . .	107
7.10	Theoretical and achieved wavelength of the FLASH2 undulator system for three different electron beam energies. A filled marker indicates that this wavelength has been demonstrated experimentally. . . . .	108
7.11	Profiles of the FEL radiation on a YAG screen in the photon beam line for different wavelengths between 4 nm and 42 nm. . . . .	109
7.12	Some profiles of the FEL radiation on a YAG screen for a wavelength scan from 13.5 nm to 6 nm that was performed in 0.5 nm steps. FLASH1 was running at 5 nm during the complete scan, which took about 30 min. . . . .	109
7.13	Undulator section of the XFEL. One can see that SASE3 uses the spent beam of SASE1. The grey block between bot undulators is the dipole magnet. . . . .	111
7.14	SACLA Timing pattern . . . . .	111

# List of Tables

2.1	Coherence properties of synchrotrons and Free-Electron Lasers	34
3.1	Simulation parameters and ranges used in the numerical simulation. For the simulated wavelength, only three undulators were considered so that none of the simulated cases reaches saturation. . . . .	49
4.1	Typical FLASH2 parameter set used in the numerical simulations. For seeding only 10 undulators are considered. These parameters are design parameters for the operation of FLASH 2	65
5.1	Coordinate systems and conversion between GENESIS1.3 and elegant . . . . .	76
6.1	Parameters during the first demonstration of HHG seeding at FLASH. . . . .	83
6.2	Parameters during the first demonstration of HGHG seeding at FLASH. . . . .	88
7.1	Expected parameters for FLASH2. . . . .	94
7.2	RF changes within an RF pulse checked for various RF stations. These values were the differences between the first and second flat top for optimum performance of both FEL beam lines individually under SASE conditions. . . . .	103
7.3	This table shows the SASE dependence on the electron bunch charge for two different electron energies. The scans were performed by decreasing the charge, and afterward only touching RF parameters which can be changed within the split RF pulse, and the pointing of the electron beam into the undulator. At the lowest charge, the machine was optimized again for 700 MeV, increasing SASE from 30 to 55 and the scan has been repeated increasing the charge. . . . .	103

# List of symbols

The following table contains the list of symbols used in this thesis. The symbols are in alphanumerical order, while symbols from other alphabets are positioned at the position of their American spelling. One symbol can have different meanings in order to sustain usual conventions in the different field of physics, keeping the notation of cited papers. Each symbol is explained once it occurs or its meaning changes. This thesis uses the MKSA-system.

Symbol	Meaning
$A_b$	Beam crossection
$A_{m,n}$	Complex amplitude coefficient
$\alpha_T$	HHG phase-related coefficient
$B_0$	Peak magnetic field
$B_U$	Peak magnetic field of undulator
$b_n$	Bunching factor on the $n$ -th harmonic
$\beta$	Twiss parameter $\beta$ -function
$\bar{\beta}$	Mean relativistic $\beta$ factor
$BPP$	Beam parameter product
$\mathcal{B}$	Brilliance
$c$	Speed of light in vacuum
$c_{m,n}$	Power content coefficient
$D$	Dispersion
$\delta$	Relative energy deviation
$\Delta\gamma$	Electron beam energy modulation
$\Delta\omega$	FEL spike width
$\Delta\Psi$	Difference in phase advance
$e$	Elementary charge
$E$	Energy of laser field
$E$	Electron beam kinetic energy
$E$	FEL photon pulse energy
$E(r)$	Photon field
$E_0$	Field amplitude

LIST OF SYMBOLS

Symbol	Meaning
$E_c^{\max}$	Maximum kinetic energy of an electron in the nucleus' potential pot
$E_{\text{cutoff}}$	HHG cutoff energy
$E_{\text{HHG}}$	HHG pulse energy
$E_{\text{SASE}}$	FEL pulse energy in SASE operation
$E_x$	Radiation field in $x$ direction
$\epsilon_{n,x}$	Normalized transverse emittance in $x$ -plane
$\eta$	Relative energy deviation
$FWHM$	Full width at half maximum
$G$	Gain function
$G_n$	Hermite-Gaussian generating function of order $n$
$\gamma$	Lorentz-factor
$\gamma_{\text{rel}}$	Lorentz-Factor
$h$	Harmonic number
$H_n$	Hermite polynomial of order $n$
$i$	Imaginary unit
$I$	Current density modulation obtained from charge density modulation
$I(x, y)$	Intensity distribution
$I_A$	Alfven-current
$I_b$	Bunching integral over the first two gain lengths
$I_{\text{ini}}$	Initial laser intensity
$I_{\text{max}}$	Electron beam peak current
$I_{\text{max,slice}}$	Current of the slice with the highest current
$I_P$	Ionizing potential of the atom
$I_{\text{slice}}$	Current of a slice
$j_1$	Current density modulation from charge density modulation
$J_n$	Bessel function $J$
$j_x$	Transverse current in $x$ plane
$K$	Dimensionless undulator parameter
$\hat{K}$	Modified dimensionless undulator parameter
$k_l$	Wave number of emitted radiation
$k_p$	space charge parameter
$k_{s1}$	Wave number of the seed
$k_u$	Wave number of undulator
$k_{w1}$	Wave number of radiator
$L_{\text{Drift}}$	Distance between undulators
$L_{g0}$	Power gain length
$L_n$	Laguerre polynomials of order $n$
$\lambda_{\text{HHG}}$	Wavelength of HHG seed
$\lambda_{\text{rad}}$	Radiated wavelength

LIST OF SYMBOLS

---

Symbol	Meaning
$\lambda_{\text{rad,h}}$	Wavelength of radiated harmonic
$\lambda_U$	Undulator period length
$M$	Longitudinal FEL mode number
$M^2$	Beam quality factor
$M^2_{\text{desired}}$	Optimization target for $M^2$
$m_e$	Electron rest mass
$M_x^2$	$M^2$ for $x$ -plane
$\mu_0$	Magnetic field constant
$n_e$	Number of electrons
$N_\lambda$	Number of electrons per wavelength
$N_{\text{periods}}$	Number of undulator periods
$N_{\text{selected}}$	Number of selected electrons
$N_{\text{slice}}$	Number of particles per simulated slice
$\omega$	Laser field frequency
$\omega_c$	Critical synchrotron frequency
$\mathcal{O}$	Order
$P$	Power
$P_B$	Electron beam power
$P_{\text{beam}}$	Electron beam power
$P_{\text{coh}}$	Power of coherent radiation
$P_h$	Power of seeded harmonic $h$
$P_{\text{max, HHG}}$	HHG peak power
$P_{\text{pk}}$	FEL peak power
$P_S$	Shotnoise power
$P_{\text{SASE}}$	FEL power in SASE operation
$P_{\text{sat}}$	FEL saturation power
$p_x$	Transverse momentum in $x$
$\phi$	Ponderomotive phase
$\mathcal{P}$	Penalty function
$Q_{\text{bunch}}$	Electron bunch charge
$R$	Curvature radius of particle trajectory
$R$	Curvature radius of wavefront
$r$	Radial distance
$\Re$	Real part
$\tilde{\rho}$	Electric charge density
$\rho_0$	Mean charge density inside bunch
$\tilde{\rho}_1$	Amplitude of charge density modulation
$\rho_{\text{FEL}}$	FEL/pierce parameter
$rms$	Root mean square

LIST OF SYMBOLS

Symbol	Meaning
$s$	Longitudinal position inside bunch
$\sigma_E$	Electron beam energy spread
$\sigma_\gamma$	Electron beam energy spread
$\sigma_\omega$	Spectral bandwidth
$\sigma_x$	Transverse electron beam size in $x$
$\sigma_z$	Electron bunch length
$T$	FEL pulse duration
$t$	Time
$T_{\text{bunch}}$	Bunch duration
$\tau_{\text{coh}}$	Coherence time
TEM <sub>mn</sub>	Electromagnetic gaussian mode $n, m$
$\Theta$	Angle between observation and undulator axis
$\Theta$	Far field beam divergence
$\Theta_0$	Far field beam divergence of a multimode beam
$\Theta_{00}$	Far field beam divergence of a gaussian beam
$\Theta_T$	HHG divergence angle
$\theta_{\text{max}}$	Maximum electron deflection angle in undulator
$\theta_{\text{opening}}$	Natural instantaneous opening angle of emitted radiation
$U_P$	Ponderomotive energy
$v_x$	Transverse velocity
$v_z$	Longitudinal velocity
$w$	Photon beam size
$w_0$	Multimode photon beam waist size
$w_{00}$	Gaussian photon beam waist size
$w_{0,\text{desired}}$	Optimization target for photon beam waist
$w_h$	Photon beam size of the $n$ -th harmonic
$w_{\text{ini}}$	Photon beam waist of drive laser
$x$	Transverse deviation in $x$ from local design orbit
$x'$	Angular deviation in $x$ from local design orbit
$z$	Macroscopic longitudinal position, e.g. inside undulator
$Z_0$	Vacuum impedance
$z_R$	Rayleigh-length
$z_{\text{Ray}}$	Rayleigh-length
$z_{\text{w1}}$	Radiation length

# Publications

This thesis is based on the following publications:

## 2016

B. Faatz (1), E. Plönjes (1,15), *S. Ackermann* (1), A. Agababyan (1), V. Asgekar (1,2), V. Ayvazyan (1), S. Baark (1), N. Baboi (1), V. Balandin (1), N. von Bargaen (1), Y. Bican (1), O. Bilani (1), J. Bödewadt (1), M. Böhnert (1), R. Böspflug (1), S. Bonfigt (1), H. Bolz (1), F. Borges (1), O. Borkenhagen (1), M. Brachmanski (1), M. Braune (1), A. Brinkmann (1), O. Brovko (3), T. Bruns (1), P. Castro (1), J. Chen (4), M.K. Czwalinna (1), H. Damker (1), W. Decking (1), M. Degenhardt (1), A. Delfs (1), T. Delfs (1), H. Deng (4), M. Dressel (1), H.-T. Duhme (1), S. Düsterer (1), H. Eckoldt (1), A. Eislage (1), M. Felber (1), J. Feldhaus (1), P. Gessler (5), M. Gibau (1), N. Golubeva (1), T. Golz (1), J. Gonschior (1), A. Grebentsov (3), M. Grecki (1), C. Grün (1), S. Grunewald (1), K. Hacker (6), L. Hänisch (1), A. Hage (1), T. Hans (1), E. Hass (1), A. Hauberg (1), O. Hensler (1), M. Hesse (1), K. Heuck (1), A. Hidvegi (7), M. Holz (1), K. Honkavaara (1), H. Höppner (1,8), A. Ignatenko (1), J. Jäger (1), U. Jastrow (1), R. Kammering (1), S. Karstensen (1), A. Kaukher (5), H. Kay (1), B. Keil (9), K. Klose (1), V. Kocharyan (1), M. Köpke (1), M. Körfer (1), W. Kook (1), B. Krause (1), O. Krebs (1), S. Kreis (1), F. Krivan (1), J. Kuhlmann (1), M. Kuhlmann (1), G. Kube (1), T. Laarmann (1), C. Lechner (1), S. Lederer (1), A. Leuschner (1), D. Liebertz (1), J. Liebing(1), A. Liedtke (1), L. Lilje (1), T. Limberg (1), D. Lipka (1), B. Liu (4), B. Lorbeer (1), K. Ludwig (1), H. Mahn (1), G. Marinkovic (9), C. Martens (1), F. Marutzky (1), M. Maslocv (10), D. Meissner (1), N. Mildner (1), V. Miltchev(11), S. Molnar (1), D. Mross (1), F. Müller (1), R. Neumann (1), P. Neumann (1), D. Nölle (1), F. Obier (1), M. Pelzer (1), H.-B. Peters (1), K. Petersen (1), A. Petrosyan (1), G. Petrosyan (1), L. Petrosyan (1), V. Petrosyan (1), A. Petrov (1), S. Pfeiffer (1), A. Piotrowski (12), Z. Pisarov (1), T. Plath (11), P. Pototzki

(1), M.J. Prandolini (13), J. Prenting (1), G. Priebe (1), B. Racky (1), T. Ramm (1), K. Rehlich (1), R. Riedel (13), M. Roggli (9), M. Röhling (1), J. Rönsch-Schulenburg (1), J. Rossbach (1,11), V. Rybnikov (1), J. Schäfer (1), J. Schaffran (1), H. Schlarb (1), G. Schlesselmann (1), M. Schlösser (1), P. Schmid (1), C. Schmidt (1), F. Schmidt-Föhre (1), M. Schmitz (1), E. Schneidmiller (1), A. Schöps (1), M. Scholz (1), S. Schreiber (1), K. Schütt (1), U. Schütz (1), H. Schulte-Schrepping (1), M. Schulz (1), A. Shabunov (3), P. Smirnov (1), E. Sombrowski (1), A. Sorokin (1), B. Sparr (1), J. Spengler (1), M. Staack (1), M. Stadler (9), C. Stechmann (1), B. Steffen (1), N. Stojanovic (1), V. Sychev (10), E. Syresin (3), T. Tanikawa (1), F. Tavella (14), N. Tesch (1), K. Tiedtke (1), M. Tischer (1), R. Treusch (1), S. Tripathi (1), P. Vagin (1), P. Vetrov (1), S. Vilcins (1), M. Vogt (1), A. de Zubiaurre Wagner (1), T. Wamsat (1), H. Weddig (1), G. Weichert (1,11), H. Weigelt (1), N. Wentowski (1), C. Wiebers (1), T. Wilksen (1), A. Willner (1), K. Wittenburg (1), T. Wohlenberg (1), J. Wortmann (1), W. Wurth (1,11), M. Yurkov (1), I. Zagorodnov (1) and J. Zemella (1)

## PUBLICATIONS

---

- (1) Deutsches Elektronen-Synchrotron (DESY), Notkestrasse 85, D-22607, Hamburg, Germany
- (2) Physics Dept., S P Pune University, Pune 411007, India
- (3) Joint Institute for Nuclear Research (JINR), 141980 Dubna, Russia
- (4) Shanghai Institute of Applied Physics(SINAP), 2019 Jia Luo Road, Jiading District, Shanghai 201800, People's Republic of China
- (5) European XFEL GmbH, Albert-Einstein-Ring 19, D-22761 Hamburg, Germany
- (6) Zentrum für Synchrotronstrahlung (DELTA), Technische Universität Dortmund, Maria-Goeppert-Mayer-Str. 2, 44227 Dortmund, Germany
- (7) Stockholm University Physics Dept., SE 10691, Stockholm, Sweden
- (8) Institut für Physik, Carl von Ossietzky Universität, 26111 Oldenburg, Germany
- (9) Paul Scherrer Institut, CH-5232 Villigen-PSI, Switzerland
- (10) Institute for High Energy Physics(IHEP), Nauki sq. 1, 142 281 Protvino, Russia
- (11) Physics Department and Center for Free-Electron Laser Science, Universität Hamburg, D-22761 Hamburg, Germany
- (12) FastLogic Sp. z o.o., al. T. Kosciuszki 123 office 324 PL-90441 Lodz, Poland
- (13) Helmholtz-Institut Jena, Fröbelstieg 3, D-07743 Jena, Germany
- (14) SLAC National Accelerator Laboratory, 2575 Sand Hill Road, Men

### **Simultaneous operation of two soft x-ray free-electron lasers driven by one linear accelerator**

*New Journal of Physics, 18 062002 (2016)*

**2015**

*S. Ackermann, R. Assmann, J. Boedewadt, N. Ekanayake, B. Faatz, I. Hartl, R. Imanov, T. Laarmann, J. Mueller (DESY, Hamburg, Germany)*

*G.A. Azima, P. Amstutz, M. Drescher, L.L. Lazzarino, C. Lechner, Th. Maltezopoulos, V. Miltchev, T. Plath, J. Rossbach (Universität Hamburg, Hamburg, Germany)*

*K.E. Hacker, S. Khan, R. Molo (DELTA, Dortmund, Germany)*

**Seeding experiment at FLASH**

*PhotonDiag2015, Trieste, Italy*

*V. Ayvazyan, S. Ackermann, J. Branlard, B. Faatz, M. Grecki, O. Hensler, S. Pfeiffer, H. Schlarb, C. Schmidt, M. Scholz, S. Schreiber, A. Piotrowski (DESY, Hamburg, Germany)*

**Low Level RF Control Implementation and Simultaneous Operation of Two FEL Undulator Beamlines at FLASH**

*Low Level RF Workshop 2015, Shanghai, China*

*C. Lechner, A. Azima, M. Drescher, L.L. Lazzarino, Th. Maltezopoulos, V. Miltchev, T. Plath, J. Roensch-Schulenburg, J. Rossbach (Universität Hamburg, Hamburg, Germany)*

*K.E. Hacker, S. Khan, R. Molo (DELTA, Dortmund, Germany)*

*S. Ackermann, J. Boedewadt, G. Brenner, M. Dohlus, N. Ekanayake, T. Golz, T. Laarmann, T. Limberg, E.A. Schneidmiller, N. Stojanovic, M. Yurkov (DESY, Hamburg, Germany)*

**Suppression of FEL Lasing by a Seeded Microbunching Instability**

*Proc. FEL2015, Daejeon, Korea*

*V. Ayvazyan, S. Ackermann, J. Branlard, B. Faatz, M. Grecki, O. Hensler, S. Pfeiffer, H. Schlarb, C. Schmidt, M. Scholz, S. Schreiber, A. Piotrowski (DESY, Hamburg, Germany)*

**Low Level RF Control Implementation and Simultaneous Operation of Two FEL Undulator Beamlines at FLASH**

*Proc. ICALEPS2015, Melbourne, Australia*

*J. Boedewadt, R.W. Assmann, N. Ekanayake, B. Faatz, G. Feng, I. Hartl, R. Ivanov, T. Laarmann, J. Mueller, T. Tanikawa (DESY, Hamburg, Germany)*

*K.E. Hacker, S. Khan, R. Molo (DELTA, Dortmund, Germany)*

*S. Ackermann (DESY, Hamburg, Germany; Universität Hamburg, Hamburg, Germany)*

## PUBLICATIONS

---

Ph. Amstutz, A. Azima, M. Drescher, L.L. Lazzarino, Ch. Lechner, Th. Maltezopoulos, V. Miltchev, T. Plath, J. Rossbach (Universität Hamburg, Hamburg, Germany)

**Recent Results from FEL seeding at FLASH**

*Proc. IPAC2015 (TUBC3), Richmond, USA*

Ph. Amstutz, Ch. Lechner, T. Plath (Universität Hamburg, Hamburg, Germany)

*S. Ackermann, J. Boedewadt, M. Vogt (DESY, Hamburg, Germany)*

**Optics Compensation for Variable-gap Undulator Systems at FLASH**

*Proc. IPAC2015 (TUPWA038), Richmond, USA*

**2014**

C. Lechner, A. Azima, M. Drescher, L.L. Lazzarino, Th. Maltezopoulos, V. Miltchev, T. Plath, J. Rönsch-Schulenburg, J. Roßbach, (Universität Hamburg, Hamburg, Germany)

E.A. Hacker, S. Khan, R. Molo (DELTA, Dortmund, Germany)

*S. Ackermann, J. Bödewadt, G. Brenner, M. Dohlus, N. Ekanayake, T. Gotz, E. Hass, K. Honkavaara, T. Laarmann, T. Limberg, E.A. Schneidmiller, N. Stojanovic, M. Vurkov (DESY, Hamburg, Germany)*

**Demonstration of SASE Suppression Through a Seeded Microbunching Instability** *Proc. FEL2014, Dresden, Germany*

C. Lechner, *S. Ackermann*, A. Azima, J. Boedewadt, G. Brenner, M. Dohlus, M. Drescher, N. Ekanayake, T. Golz, K.E. Hacker, K. Honkavaara, S. Khan, T. Laarmann, L.L. Lazzarino, T. Limberg, Th. Maltezopoulos, V. Miltchev, R. Molo, T. Plath, J. Roensch-Schulenburg, J. Rossbach, E.A. Schneidmiller, N. Tojanovic, M. Yurkov (Universität Hamburg, Hamburg, Germany / DESY Hamburg, Germany / DELTA, Dortmund, Germany)

**Experimental Studies on FEL Gain Controlled by Laser-Induced Longitudinal Space Charge Amplification** *6th Microbunching instability workshop (2014), Trieste, Italy*

*S. Ackermann, V. Ayvazyan, B. Faatz, E. Hass, K. Klose, S. Pfeiffer, M. Scholz, S. Schreiber (DESY, Hamburg, Germany)*

**Simultaneous Operation of Two FEL Undulator Beamlines at FLASH** *Proc. IBIC2014 (MOPF22), Monterey, CA, USA*

*S. Ackermann, B. Faatz (DESY, Hamburg, Germany)*

V. Miltchev (Universität Hamburg, Hamburg, Germany)

**Characterization of the Laser Beam for HHG Seeding**

*Proc. IBIC2014 (TUPF25), Monterey, CA, USA*

G. Feng, *S. Ackermann*, J. Bödewadt, W. Decking, M. Dohlus, Y.A. Kot, T. Limberg, M. Scholz, I. Zagorodnov (DESY, Hamburg, Germany)

K.E. Hacker (DELTA, Dortmund, Germany)

T. Plath (Universität Hamburg, Hamburg, Germany)

**Start-to-End Simulation for FLASH2 HGHG Option**

*Proc. FEL2014 (MOP083), Dresden, Germany*

N. Ekanayake, *S. Ackermann* (DESY, Hamburg, Germany)

*S. Ackermann, C. Lechner, Th. Maltezopoulos, T. Plath (Universität Hamburg, Hamburg, Germany)*

## PUBLICATIONS

---

K.E. Hacker (DELTA, Dortmund, Germany)

**Indirect Measurements of NIR and UV Ultrashort Seed Laser Pulses using a Transverse Deflecting RF-Structure**

*Proc. FEL2014 (MOP094), Dresden, Germany*

C. Lechner, A. Azima, M. Drescher, L.L. Lazzarino, Th. Maltezopoulos, V. Miltchev, T. Plath, J. Rönsch-Schulenburg, J. Roßbach, M. Wieland (Universität Hamburg, Hamburg, Germany)

*S. Ackermann, J. Bödewadt, H. Dachraoui, N. Ekanayake, B. Faatz, M. Felber, K. Honkavaara, T. Laarmann, J.M. Mueller, H. Schlarb, S. Schreiber, S. Schulz (DESY, Hamburg, Germany)*

G. Angelova Hamberg (Uppsala University, Uppsala, Sweden)

K.E. Hacker, S. Khan, R. Molo (DELTA, Dortmund, Germany)

P.M. Salen, P. van der Meulen (FYSIKUM, AlbaNova, Stockholm University, Stockholm, Schweden)

**Measurements of the Timing Stability at the FLASH1 Seeding Experiment**

*Proc. FEL2014 (THP076), Dresden, Germany*

**2013**

*S. Ackermann*, B. Faatz (DESY, Hamburg, Germany)  
V. Miltchev (Universität Hamburg, Hamburg, Germany)

**Modal analysis of a seeded free-electron laser**

*Physical Review Special Topics Accelerators and Beams*. 16, 100702 (2013)

*S. Ackermann* (1,2), A. Azima (1,5,6), S. Bajt (2), J. Bödewadt (1,5), F. Curbis (1), H. Dachraoui (2), H. Delsim-Hashemi (2), M. Drescher (1,5,6), S. Düsterer (2), B. Faatz (2), M. Felber (2), J. Feldhaus (2), E. Hass (1), U. Hipp (1), K. Honkavaara (2), R. Ischebeck (4), S. Khan (3), T. Laarmann (2,6), C. Lechner (1), Th. Maltezopoulos (1,5), V. Miltchev (1), M. Mittenzwey (1), M. Rehders (1,5), J. Rönsch-Schulenburg (1,5), J. Rossbach (1,5), H. Schlarb (2), S. Schreiber (2), L. Schroedter (2), M. Schulz (1,2), S. Schulz (2), R. Tarkeshian (1), M. Tischer (2), V. Wacker (1), and M. Wieland (1,5,6)

(1) Department of Physics, University of Hamburg, 22761 Hamburg, Germany

(2) Deutsches Elektronen-Synchrotron DESY, 22607 Hamburg, Germany

(3) Technische Universität Dortmund, 44227 Dortmund, Germany

(4) Paul Scherrer Institut, 5323 Villigen, Switzerland

(5) Center for Free-Electron Laser Science CFEL, DESY, 22607 Hamburg, Germany

(6) The Hamburg Centre for Ultrafast Imaging CUI, 22761 Hamburg, Germany

**Generation of Coherent 19- and 38-nm Radiation at a Free-Electron Laser Directly Seeded at 38 nm**

*Physical Review Letters* 111, 114801 (2013)

S. Schreiber, *S. Ackermann*, V. Ayvazyan, B. Faatz, K. Klose (DESY, Hamburg, Germany)

**Simultaneous Operation of FLASH1 and FLASH2**

*Proc. FEL2013 (TUPSO70)*, New York, NY, USA

## 2012

C. Lechner, A. Azima, J. Boedewadt, M. Drescher, E. Hass, U. Hipp, T. Maltezopoulos, V. Miltchev, M. Rehders, J. Roensch, J. Rossbach, R. Tarkeshian, M. Wieland (Universität Hamburg, Hamburg, Germany)  
S. Khan (DELTA, Dortmund, Germany)

*S. Ackermann, S. Bajt, H. Dachraoui, H. Delsim-Hashemi, S. Düsterer, B. Faatz, K. Honkavaara, T. Laarmann, M. Mittenzwey, H. Schlarb, S. Schreiber, L. Schroedter, M. Tischer (DESY, Hamburg, Germany)  
F. Curbis (MAX-lab, Lund, Sweden)  
R. Ischebeck (PSI, Villigen, Switzerland)  
V. Wacker (University of Hamburg, Hamburg, Germany)*

### **First Direct Seeding at 38nm**

*Proc. FEL2012 (TUOAI01), Nara, Japan*

*S. Ackermann, B. Faatz (DESY, Hamburg, Germany)  
V. Miltchev, J. Rossbach (Universität Hamburg, Hamburg, Germany)*

### **Optimization of HHG Seeding at Flash II**

*Proc. FEL2012 (TUPD11), Nara, Japan*

B. Faatz, *S. Ackermann*, V. Ayvazyan, W. Decking, C. Gruen, K. Klose, F. Obier, S. Pfeiffer, M. Scholz, J. Wortmann (DESY, Hamburg, Germany), E. Hass (Universität Hamburg, Hamburg, Germany)

### **Simultaneous Operation of a Multi Beamline FEL Facility**

*Proc. FEL2012 (TUPD32), Nara, Japan*

K. Honkavaara, *S. Ackermann*, V. Ayvazyan, N. Baboi, V. Balandin, W. Decking, S. Düsterer, H.-J. Eckoldt, B. Faatz, M. Felber, J. Feldhaus, N. Golubeva, M. Koerfer, M. Kuhlmann, T. Laarmann, A. Leuschner, L. Lilje, T. Limberg, N. Mildner, D. Noelle, F. Obier, A. Petrov, E. Plönjes, K. Rehlich, H. Remde, H. Schlarb, B. Schmidt, M. Schmitz, M. Scholz, S. Schreiber, H. Schulte-Schrepping, J. Spengler, M. Staack, N. Stojanovic, K.I. Tiedtke, M. Tischer, R. Treusch, M. Vogt, H.C. Weddig, T. Wohlenberg (DESY, Hamburg, Germany)

F. Tavella (HIJ, Jena, Germany)

M. Drescher, A. Hage, V. Miltchev, R. Riedel, J. Roensch-Schulenburg, J. Rossbach, M. Schulz, A. Willner (Universität Hamburg, Hamburg, Germany)

### **Status of the FLASH II Project**

*Proc. FEL2012 (WEPD07), Nara, Japan*

**2011**

*S. Ackermann, V. Miltchev, J. Rossbach (Universität Hamburg, Hamburg, Germany)*

**Transverse Phase-space Studies for the Electron Optics at the Direct XUV-seeding Experiment at FLASH (DESY)**

*Proc. FEL2011 (TUPA31), Shanghai, China*

*E. Hass, S. Ackermann, J. Boedewadt, J. Rossbach (Universität Hamburg, Hamburg, Germany)*

**Transverse Overlap Diagnostics with Wire Scanners in the XUV-seeding Experiment at FLASH**

*Proc. FEL2011 (TUPB01), Shanghai, China*

*V. Miltchev, S. Ackermann, A. Azima, J. Boedewadt, F. Curbis, M. Drescher, E. Hass, T. Maltezopoulos, M. Mittenzwey, J. Roensch-Schulenburg, J. Rossbach, R. Tarkeshian (Universität Hamburg, Hamburg, Germany)*

*H. Delsim-Hashemi, K. Honkavaara, T. Laarmann, H. Schlarb, S. Schreiber, M. Tischer (DESY, Hamburg, Germany)*

*R. Ischebeck (Paul Scherrer Institut, Villigen, Switzerland)*

**sFLASH - Present Status and Commissioning Results**

*Proc. FEL2011 (TUPA04), Shanghai, China*

*V. Miltchev, S. Ackermann, A. Azima, J. Bödewadt, F. Curbis, M. Drescher, E. Hass, Th. Maltezopoulos, M. Mittenzwey, J. Rönsch-Schulenburg, J. Roßbach, R. Tarkeshian (Universität Hamburg, Hamburg, Germany)*

*H. Delsim-Hashemi, K. Honkavaara, T. Laarmann, H. Schlarb, S. Schreiber, M. Tischer (DESY, Hamburg, Germany)*

*R. Ischebeck (PSI, Villigen, Switzerland), S. Khan (DELTA, Dortmund, Germany)*

**sFLASH - Present Status and Commissioning Results**

*Proc. IPAC11 (TUZA02), San Sebastian, Spain*

# Chapter 1

## Introduction

### 1.1 Synchrotron radiation

In 1947 Frank Elder, Anatole Gurewitsch, Robert Langmuir, and Herb Pollock published a paper describing their observation of radiation in the visual wavelength regime emitting from the General Electric synchrotron, hence the name “synchrotron radiation” [1]. Synchrotron radiation is produced when relativistic charged particles are forced to have bent trajectories by magnetic fields. This radiation is emitted tangentially to the curvature of the particles’ trajectory. With particle physics demanding higher electron beam energies and stored beam currents, the development of accelerators led to the invention of storage rings, which are the technological basis for all circular light sources today. For a given particle energy, synchrotron radiation power is inversely proportional to the forth power of particle mass, therefore in all light sources electrons or positrons are used rather than protons.

Synchrotron radiation has become a very powerful diagnostics tool for many scientific disciplines like physics, biology, chemistry and medicine. The history of synchrotron radiation sources can be subdivided into four so-called generations [2].

The 1<sup>st</sup> generation light sources used synchrotron radiation emitted in bending magnets of storage rings operated for particle physics. The radiation could be extracted and used parasitically. Two examples for this kind of synchrotron radiation sources were the DORIS (Double Orbit Ring System) at DESY and CESR (Cornell Electron-positron Storage Ring) at Cornell, which were later upgraded to 2<sup>nd</sup> generation light sources [3].

The 2<sup>nd</sup> generation light sources were necessary due to the changed demands of high-energy physics experiments: Searching the  $J/\Psi$  particle demanded lower beam currents to have smaller background noise. This limited

the synchrotron radiation output in a severe way. Therefore the synchrotron radiation was produced in machines solely built and operated for the purpose of producing synchrotron radiation using the technology known from the 1<sup>st</sup> generation light sources. However the geometry of the machines was changed in a way that longer arcs were installed to be able to deliver more synchrotron radiation. This had been done at the DORIS storage ring, which was then renamed DORIS-II. Even whole new research complexes, not only the accelerator but also photon experimental facilities were built for synchrotron radiation studies. One such example was BESSY, now part of HZB (Helmholtz Zentrum Berlin). Some of these machines already featured undulators.

The 3<sup>rd</sup> generation synchrotron light sources are similar to 2<sup>nd</sup> generation sources, however they were optimized for smaller emittances and used many undulator straight sections. Synchrotron radiation emitted from bending magnets has a broad spectral range and therefore the brilliance is only in the order of  $\mathcal{B} = 10^{12} \text{ mm}^{-2} \cdot \text{mrad}^{-2} \cdot \text{s}^{-1} \cdot (0.1 \% \text{ bandwidth})^{-1}$  [4], see Fig. 1.1. This is of course not sufficient for investigation of atomic structures. In 1947 Vitaly Ginzburg proposed the concept of the undulator for the first time [5]. The first undulator built and tested was constructed by Motz et al. [6]. An undulator is an array of alternating magnets whose field forces the electrons to move on sinusoidal trajectories as they pass through. It decreases the radiated bandwidth and the opening angle, which increases the brilliance, which is also referred to as brightness in the USA. The undulator radiation has a narrower spectral range than the synchrotron radiation and typically achieves peak brilliance in the order of  $\mathcal{B} = 10^{21} \text{ mm}^{-2} \cdot \text{mrad}^{-2} \cdot \text{s}^{-1} \cdot (0.1 \% \text{ bandwidth})^{-1}$ . One example is the PETRA III synchrotron light source at DESY which also is one of the most brilliant 3<sup>rd</sup> generation synchrotron light sources [4]. The 4<sup>th</sup> generation light sources are the free-electron lasers, which are the main topic of this thesis and discussed in the next section.

## 1.2 Free-Electron Lasers

In 1971 John Madey came up with the revolutionary idea of the free-electron lasers (FEL) [7], which can be classified as the 4<sup>th</sup> generation of light sources, which was a leap in peak brilliance by many orders of magnitude. One way to make this possible is building the undulator within an suited optical cavity allowing the radiation power to build up during the passes of several electron bunches, which results in fully temporal coherent pulses. Another way is sending electron bunches with increased peak currents in a single pass through an undulator with increased length, having a similar effect, but with

## 1.2. FREE-ELECTRON LASERS

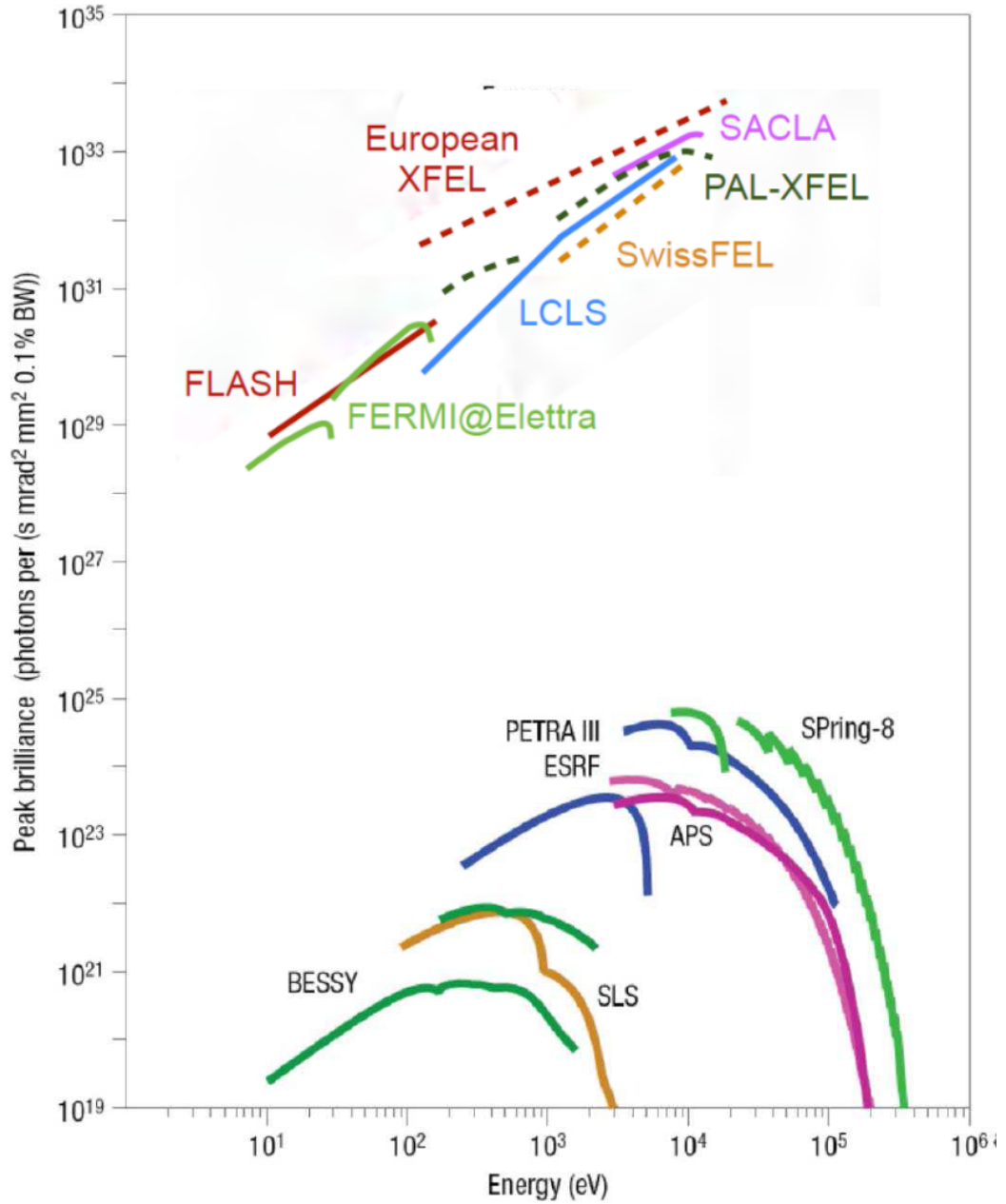


Figure 1.1: Peak brilliance of synchrotron radiation sources as a function of photon energy.

only limited longitudinal coherence. (See Section 2.3).

The first option was almost exclusively used during the first two decades of the operation of free-electron lasers, which were operated in a wavelength range from THz down to the UV, either in linear accelerators (LINACs) [8–11] or at storage rings [12–16].

Single pass FELs, based on groundbreaking theoretical work in the 1980s [17,18] and technological development, especially on the electron guns which was needed to improve the quality of the electron beam [19,20] have been used since the 1990s for wavelength regimes from the UV to the X-rays [21–30]. Others are under construction or have been proposed [31–33]. A summary of existing and proposed FEL facilities can be found in Ref. [34].

Because the degree of coherence is limited for FELs without an optical cavity where electron only pass the undulator once, so-called seeding schemes have been proposed, built and studied to increase the coherence. These sources are often referred to as 5<sup>th</sup> generation light sources.

In the section 1.3, the advantages and disadvantages for different FEL schemes are discussed.

### 1.2.1 The oscillator FEL

In an oscillator FEL the light emitted from the electron bunch inside the undulator is captured in an optical cavity where it gets amplified during multiple passage of fresh electron bunches. Oscillator FELs are used if the electron beam peak current is low, thus many passes through the undulator are needed to reach saturation and if broad band extraction mirrors are available and therefore the oscillator has no draw back and is more cost-efficient in addition to deliver superior radiation properties. Example for FELs implemented in storage rings are VEPP-3 [12], SuperACO [13], Duke [14], DELTA [15], and Elettra [16]. Also in most FELs in the infrared regime (IR-FELs) oscillators are used, for example in FELIX [9], CLIO [10], the Darmstadt FEL [11], and ELBE [35]. Even though mirrors can be highly reflective in many wavelength ranges, a controlled, broadband transmission is hard to achieve. In order to couple out radiation from the optical cavity an old extraction mechanism, as used in the early days of conventional lasers, the so-called hole coupling [36], is used. An aperture in the center of one of the two cavity-building mirrors is used as a broad-band extraction mechanism for a part of the radiation [9].

#### 1.2.2 The single-pass FEL

For wavelength in the deep ultra-violet (DUV) and beyond no broadband, high-reflectivity mirrors for normal incidence are available. Therefore one either has to limit a machine to one fixed wavelength and use multi-layer mirrors, or one needs to achieve saturation within one single pass of the undulator. This requires electron bunches with high peak currents of high beam quality and at the same time a very long undulator. One advantage of such FEL over a conventional laser is that the electron bunch itself is the lasing medium, offering continuously tunable radiation wavelength. A conventional laser is always using an active material with the correct energy bands to reach a certain wavelength, which for some wavelengths might not even be available. Optical Parametric Chirped Pulse Amplifier offer large tune-ability in wavelengths in the ultra-violet [37], but the soft- and hard X-ray regime is out of reach, laser diodes only offer wavelength down to 346 nm [38], and fluorine excimer laser down to 157 nm [39].

#### 1.2.3 Properties of SASE radiation

The electron bunch used in an FEL consists of stochastically distributed electrons. The generated radiation shares this behavior. The radiation pulse of a SASE FEL features several radiation spikes, where the duration of one spike is about the coherence time as it will be discussed in section 2.3. The spectrum also shows a structure consisting of spikes. The width of a spike is about  $1/T$  with  $T$  being the pulse duration. The complete spectral width is in terms about  $1/\tau_{\text{coh}}$  with  $\tau_{\text{coh}}$  being the coherence time.

### 1.3 Seeded FEL

In order to improve the properties of the radiation emitted from an FEL several techniques were developed and/or applied in the experimental research. One way to improve the longitudinal coherence of a SASE FEL is to create electron bunches short enough to confine all electrons that contribute to lasing within one cooperation length. This will lead to one singular longitudinal mode in the temporal distribution of the FEL radiation. However, since there are practical limits for the charge density of the electron bunches, the radiation power, thus pulse energy, is limited. This method does only offer longitudinal coherence. It does not benefit from the advantages that are introduced when using seeding techniques described below. Disadvantages of single-spike operation are the 100% shot-to-shot fluctuation of the photon pulse energy due to the stochastic behavior of the SASE radiation and the

spectral fluctuations. When a high-gain FEL [40] operates in the SASE mode the lasing starts from noise and therefore the radiation consists of a number of uncorrelated modes which might lead to a poor longitudinal coherence. In addition the FEL output energy is fluctuating with an rms value in the order of about 20 % [41] while the synchronization between the FEL pulse arrival time and an external laser without special synchronization techniques is typically in the order of about 100 fs rms [42], while 100 fs FWHM at FLASH are world record, which defines a lower limit to the temporal resolution of pump-probe experiments for standard operation in FLASH. However using more advanced techniques, the synchronization can be done much better [43]. Furthermore for reaching the saturation at a SASE FEL one typically needs an undulator section of at least about 20 power gain lengths [18, 40].

### 1.3.1 Self-seeding

For self-seeding the undulator is divided into two sections. The first section produces radiation due to the SASE process. The undulator is short enough to prevent saturation from being reached. The generated radiation pulse is then sent through a monochromator which transmits only a narrow frequency band, confining the radiation in a small spectral bandwidth. At the same time, the electron beam is sent through a chicane serving two purposes: First, to destroy the density modulation accumulated so far by the FEL and second, to synchronize the electron bunch with the monochromatized photon pulse.

In the second undulator the photon beam is overlapped with the electrons and amplified by FEL gain. This scheme was originally proposed for the soft X-Ray range by Feldhaus et al. [44] and a technical design report on the possible implementation a FLASH was finished in 2003 [45]. Further studies performed can be found in [46]. For the hard X-ray regime, a concept was proposed by Saldin et al. [47] and has been implemented at the LCLS at SLAC [48]. Although the self-seeding process is internally synchronized, it is not stabilized to an external device, such as a pump-probe laser for example. In addition the intensity fluctuations of the FEL radiation increase as consequence of the fact that by selecting a single spike - or even less - of the SASE spectrum the amplification process in the second undulator starts with a huge power fluctuation of the initial radiation. The advantage of this technique is that it produces a single-mode FEL radiation pulse and therefore an significantly increased peak brilliance.

#### 1.3.2 Direct seeding

While the seed for self-seeding is produced by the same electron bunch as the one that is to be seeded, direct seeding uses an externally generated photon pulse which is then to be overlapped six-dimensionally with the electron bunch. Because the radiation process starts from the seed instead of from noise, this leads directly to some improvements: The spectrum is stabilized at the seeding wavelength, the longitudinal coherence is improved, and due to the intrinsic temporal correlation between the arrival of FEL photons and the HHG drive laser, this technique offers the possibility to drive pump-probe experiments with femtosecond synchronization. In addition, the achieved saturation length can be reduced significantly.

At DELTA at the TU Dortmund, the harmonics of an 800 nm Ti:Sa laser generated in nonlinear crystals (second harmonic generation "SHG" and third harmonic generation "THG") are used to seed a low current electron beam. This brings the radiation wavelength down to the UV (266 nm). In order to reach shorter wavelength one needs a different radiation source.

Depending on the source of the external seed there is a variety of names from hyponyms to direct seeding. One of them, the high-harmonic generation (HHG) uses a gas target to generate and provide the external seed. This is one of the seeding methods discussed in this thesis. The HHG process is briefly discussed in Section 2.4. Sources of radiation exploiting the HHG principle are available down to the nanometer range [49, 50]. However, with decreasing wavelength the HHG radiation pulse intensity goes down. A so-called quasi phase matching (QPM) source has been developed. [51–53] which increases the HHG pulse energy at short wavelengths by more than an order of magnitude. It has been shown that seeds produced in HHG sources can be amplified. The SCSS demonstrated the usage of HHG seeds in the UV [54], while the SPARC has shown similar results at longer wavelengths. FLASH at DESY was the first facility to demonstrate HHG seeding at a wavelength below 40 nm [55]. However seed pulses with sufficient power are only available at low repetition rates, mainly due to the unavailability of suited laser systems in terms of power output and possibility to be synchronized to external sources. Therefore further development on sources and laser systems is needed to make practical use for an FEL using superconducting technology like FLASH exploiting long bunch trains.

#### 1.3.3 High-Gain Harmonic Generation

Instead of directly amplifying an external seed in an FEL as described in the previous section one can also induce microbunching to the electron beam

at a longer wavelength which will then radiate also at higher harmonics of the bunching period according to its harmonic content. The microbunching is initiated by a laser that is overlapped with the electron beam inside a short undulator, the so called modulator. The laser field imprints an energy modulation on the electron bunch which is then converted to an electron density modulation by the means of a dispersive section. The generated harmonic content will then radiate. The first theoretical work on this field was done by Li-Hua Yu et al. [56,57], a demonstration in the UV was shown by the same group at Brookhaven National Lab (BNL) in [58].

Facilities operating this principle are FERMI at Elettra and the SDUV at SINAP. Because HGHG is very sensitive to energy spread of the electron beam, the harmonic that can actually be reached using this method is limited to below the 15<sup>th</sup> harmonic in practice. In order to circumvent this limitation a cascaded scheme has been proposed, in which only a small longitudinal fraction of the electron bunch is modulated by the seed laser. Then, in the following undulator, the introduced bunching will radiate at some high harmonics. By the means of a chicane, the electrons are retarded in time with respect to the photons so that the photons will be overlapped with an unmodulated part of the electron bunch. In the next undulator, this part gets modulated on a harmonic of the wavelength of the previous radiation stage.

This has also been demonstrated experimentally at FERMI [59].

### 1.3.4 Echo-enabled Harmonic Generation

The idea of the echo-enabled harmonic generation was first proposed by G. Stupakov and D. Xiang in 2009 [60]. It uses a double modulator setup, each modulator followed by a dispersive section, and a radiator. In the first modulator an energy modulation is introduced by a laser, which is later converted to an electron density modulation. In contrast to HGHG the chicane is set to over-compress the bunch, not to optimize its harmonic content. This bunch is then sent through another modulator where a certain correlation is imprinted on the electron beam. In the second dispersive section this correlation is used to create an electron density modulation which contains very high harmonic content that will lase in the radiator. The concept of EEHG promises to be able to reach very high harmonics, in the order of 100.

## 1.4 The Free-Electron Laser in Hamburg (FLASH)

The Free-electron LASer in Hamburg (FLASH) is a high-gain, single pass FEL that operates in the SASE mode and generates coherent XUV photon pulses down to fundamental wavelengths of 4.12 nm [25]. All the work presented in this thesis has been done for and measured at this facility. The electron bunches are generated using a normal conducting 1.3 GHz RF gun with a Cesium Telluride ( $\text{Cs}_2\text{Te}$ ) photo cathode [61] and accelerated by seven superconducting, 1.3 GHz TESLA type accelerating modules [62, 63]. The electrons leaving the cathode have a kinetic energy of about 5 MeV and are then accelerated to about 164 MeV using the first superconducting module. The following module operates at the third harmonic (3.9GHz) of the standard accelerator frequency [64]. This third harmonic module allows to linearize the electrons' phase-space distribution which leads to a more linear bunch compression in the two magnetic chicanes and thus higher peak currents (in the kA range). After the first bunch compressor the electrons are accelerated in two more modules up to 450 MeV, compressed the second time, and finally accelerated by the remaining four modules up to 1.25 GeV. In order to separate the electrons from dark current and beam halo, the electrons need to pass through transverse and energy collimation. Downstream the energy collimator, the sFLASH direct HHG seeding experiment has been installed. A detailed description of the sFLASH experiment will be given in section 1.6 and in Ref. [55]. Further downstream the FLASH main undulators are installed. At FLASH six fixed gap planar hybrid undulators are installed. Each undulator has a length of 4.5 m, a period length of  $\lambda_u = 27.3$  mm and a peak magnetic field  $B_0 = 0.46$  T corresponding to a K-value of 1.23 [23, 65] as defined by

$$K = \frac{eB_u\lambda_u}{2\pi m_e c} \quad (1.1)$$

An additional undulator offers the possibility to produce radiation in the Terahertz-regime. As it is driven by the spent beam of the main FLASH undulators, it is intrinsically synchronized to the XUV photon pulse and thus perfectly useable for pump-probe experiments. The FEL radiation is then separated from the electron beam and characterized. Position, angle and energy of each individual photon pulse can be measured by means of the ionization of gas [66–68]. After characterization the photons are transported and, if needed, attenuated by a gas absorber before they are distributed to one of the five experimental stations in the experimental hall. In the hall, further diagnostics are available as well as filters for further attenuation and, depending on the beam line, several high-resolution spectrometers [69–71]. For pump-probe experiments, a laser synchronized to the FEL can be used.

## 1.5. THE EXTENSION OF THE FLASH FACILITY: FLASH2

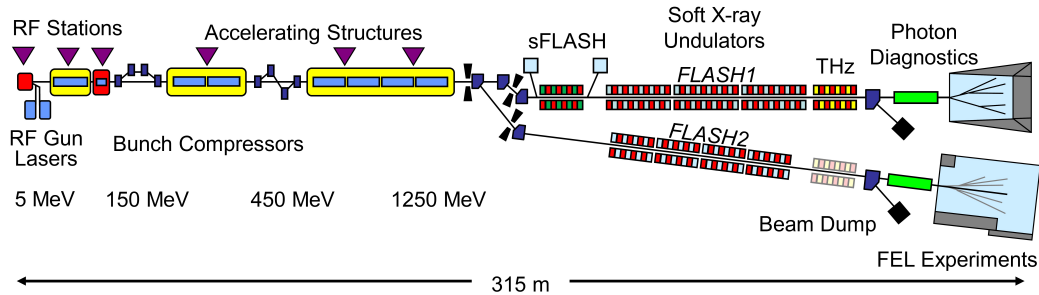


Figure 1.2: Layout of the free-electron laser in Hamburg (FLASH).

## 1.5 The extension of the FLASH facility: FLASH2

Over the past decade the FLASH facility has been steadily improved and extended its wavelength range. The number of requests for user time has also been growing in time. The usage of fast-switching XUV mirrors and stacking experiments behind each other have been exploited or are foreseen for coming user runs. However, this is insufficient. The extension of beam time by a second undulator beam line is - besides the option to realize a seeding scheme at that beam line - an important argument for enlarging the facility. FLASH2 uses a significant fraction of already existing infrastructure and facilities, see Fig. 1.2. A detailed description can be found in [26]. Behind the last accelerating module the electron beam can be switched between the fixed-gap undulator beam line of FLASH (now referred to as FLASH1) and the new variable gap undulators of FLASH2 within one FLASH linac bunch train. The modification of the existing facility is minor. The FLASH2 undulators are housed in a separate tunnel for several reasons: First, the tunnel of FLASH1 is too small to allow the placement of a second undulator beam line as well as there is only little more space in the experimental hall of FLASH1. Second, the construction of a new tunnel offers the possibility to ensure enough space for future upgrades and extensions. Third, if the electron beam line is installed in a separate tunnel it does only minimally interfere with the FLASH1 user operation as it is possible to run FLASH1 without making the FLASH2 tunnel a prohibited area in terms of radiation safety. The only shutdowns needed is when the tunnels and beam lines are getting connected. The FLASH2 tunnel comprises a matching beam line, an electron beam diagnostics section, a section reserved for the subsequent installation of a seeding scheme, and a long undulator section, sufficient to reach saturation in SASE mode. Further downstream, space is foreseen for an afterburner and more diagnostics. Around 20 m of space are assigned to of photon diagnostics similar to what has been used at FLASH [68] and

an additional on-line spectrometer [72]. In the experimental hall, space is foreseen for at least five experimental stations, not including the possibility of experiments in a row, or experiments at larger angles for longer wavelengths.

## 1.6 The sFLASH experiment

The seeding experiment at FLASH was built to study possible seeding schemes

The setup installed during a shutdown in 2009 offers the unique possibility to study a variety of seeding schemes, although the initial focus was laid on direct seeding using an HHG seed source.

The section begins with the final dipole magnet of the energy collimator of FLASH1, see Fig. 1.2. At this position, the electron beam pipe merges with the photon beam pipe used for the injection of the seed pulse. Two different injection beam lines exist: One to transport XUV radiation of 38 nm, the 21<sup>st</sup> harmonic of an 800 nm Ti:Sa laser system, in vacuum, and a second beam line transporting 800 nm directly to the tunnel where nonlinear crystals are used to convert the radiation to the second and third harmonic (400 nm and 267 nm, respectively). Downstream, two short electromagnetic undulators, each followed by a chicane, and with deflection planes orientated perpendicular to each other are installed [73, 74]. The following sFLASH undulator system consists of three two-meter long U32-type [75] undulators and one four-meter long U33-type, refurbished PETRA-II, undulator separated by electron beam diagnostic sections. After the undulators an electromagnetic chicane is situated used to separate the electrons from the photon beam. The photon beam can be sent to a high resolution spectrometer for the wavelength range around 38 nm or to a laboratory outside the tunnel to use the undulator radiation. The electrons are further transported downstream where a transverse deflecting structure (TDS) [76] is installed. It is an important piece of diagnostics for the seeding experiments as it provides information about the longitudinal phase-space distribution of electrons. For long seed pulses and low peak current electron bunches the effect of energy modulation imprinted on the bunch can be directly observed.

The sFLASH experiment was the first experiment to demonstrate HHG seeding on wavelength below 40 nm [77], where the sFLASH main undulators were used as an amplifier.

In order to study HHG, one of the electromagnetic undulators can be used as a modulator, while the main undulator serves as the radiator. Even EEHG studies can be performed.

All seeding schemes can be operated in parallel to FLASH1. The laser system used for seeding is operated at 10 Hz, which means that out of the

up to 800 bunches of a bunch train of FLASH1 (or 750 bunches in the sum of FLASH1 and FLASH2), only one bunch can be seeded. A kicker magnet, originally installed to kick one bunch out of the bunch train to measure its length is used to prevent the seeded bunch to reach the main undulator. All other bunches pass the sFLASH setup unaffected by the laser and should only experience minor modulations, as the length of the sFLASH undulators is chosen to be shorter than the SASE saturation length. The seeding experiment has been successfully operated in parallel to in-house research beam times several times.

The experimental setup can be seen in Fig. 1.3

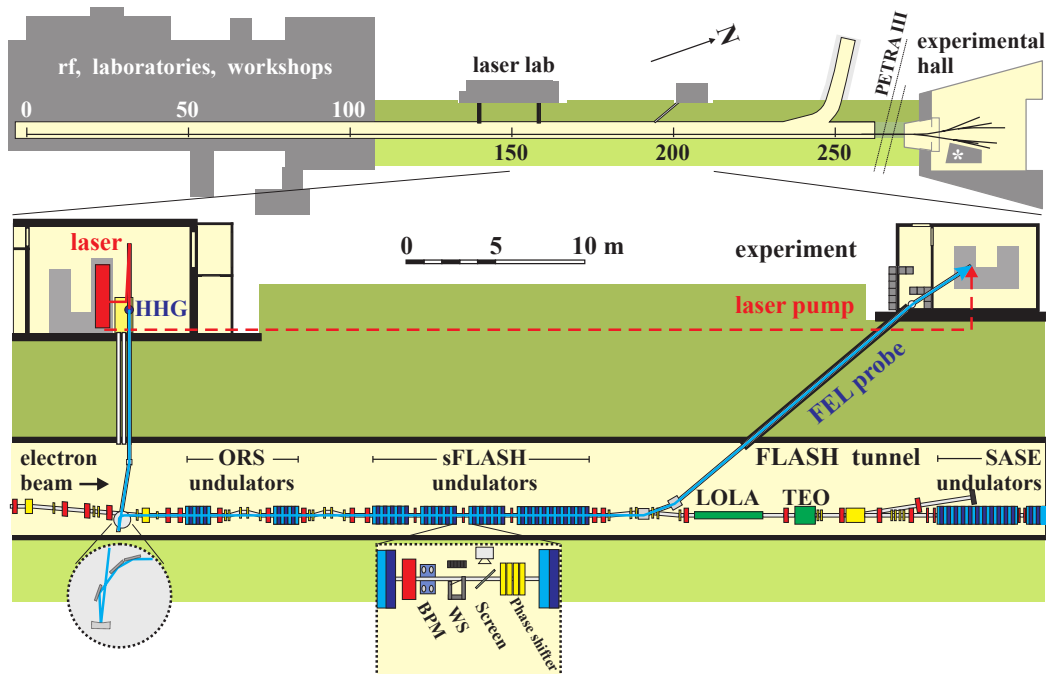


Figure 1.3: The sFLASH direct XUV seeding experiment. (Taken from [55].)

## 1.7 Organisation of the thesis

After the present introduction, a short resume on the FEL theory and the theory of the seeding schemes discussed in this thesis is given. The following chapters deals with the effects of seed radiation beam quality on the performance of HHG seeding. Also, a study on the operation of the FLASH2 moveable gap undulators for the optimization of HHG seeding is performed. A similar study on the performance of HGHG with different beam quality

## 1.7. ORGANISATION OF THE THESIS

---

factors is done. Later, the experience and performance of the FLASH facility, operating two FEL beam lines, is explained and discussed. Finally, a review of the achieved results of seeding experiment at FLASH is given, and an outlook on future seeding plans is given.

# Chapter 2

## Theory

In this chapter we will describe the basic mechanisms for the production of light from relativistic electron beams from bending magnets to Free-Electron Lasers (FELs). In addition methods to improve the properties of the radiation emitted from such FEL are discussed. The complete deduction of the formulae presented in this chapter can not be covered by this thesis, but important steps as well as references to literature will be presented. This chapter will roughly follow the notation and reasoning used by Schmüser et al. [40].

If charged particles are deflected by a bending magnet they emit radiation according to Maxwell's equation. The spectrum of this radiation is wide and continuous. The spectrum can be divided at a certain frequency such that the integrated power content of frequencies below and above that so-called "critical frequency" are equal.

$$\omega_c = \frac{3c}{2R}\gamma^3 \quad (2.1)$$

where  $\gamma = E/(m_e c^2)$  is the Lorentz factor and  $R$  the radius of curvature of the particle trajectory. The major part of the power is radiated into the tangential forward direction of the particle with an opening angle of  $\gamma^{-1}$ . In order to increase the total energy extracted from the electron beam into photons, one can use shorter and alternatingly orientated dipole magnets. These so-called "insertion devices" (IDs) allow for a higher photon pulse energy. IDs are characterized by the undulator parameter

$$K = \frac{eB_u \lambda_u}{2\pi m_e c} \quad (2.2)$$

where  $e$  is the elementary charge,  $m_e$  the electron rest mass,  $c$  the speed of light in vacuum,  $\lambda_u$  the period length of the alternating dipole magnets,

## 2.1. 1D FEL THEORY

---

and  $B_u$  the peak magnetic field. One can show that for  $K \leq 1$  the deflection angle of the electrons in the insertion device is smaller than the opening angle of the emitted radiation cone. In this case, the ID is also called "undulator". For  $K > 1$  the ID is called "wiggler". An insertion device forces the particles to sinusoidal trajectories, where the maximum deflection angle is

$$\theta_{\max} = \frac{K}{\gamma} \quad (2.3)$$

The natural instantaneous opening angle of the emitted radiation is

$$\theta_{\text{opening}} = \frac{1}{\gamma} \quad (2.4)$$

Thus for an undulator ( $K \leq 1$ ) the radiation cones of the electron at different longitudinal positions inside of the undulator overlap each other. The radiated wavelength for such undulator setup is then given by

$$\lambda_{\text{rad}} = \frac{\lambda_u}{2\gamma^2} \left( 1 + \frac{K^2}{2} + (\Theta\gamma)^2 \right) \quad (2.5)$$

with  $\Theta$  being the observation angle with respect to the undulator axis.

## 2.1 1D FEL Theory

In the 1D theory any dependency of bunch- or radiation parameters on the lateral coordinates is neglected. We assume the case of a planar undulator with linear polarization as it is used in both FLASH beam lines [78, 79]. Assuming the electron bunch has a small periodical density modulation, the electrical charge density  $\tilde{\rho}$  can be expressed as  $\tilde{\rho}(\psi, z) = \rho_0 + \tilde{\rho}_1(z) \exp(i\psi)$  where the tilde indicates complex variables,  $\psi$  the so called ponderomotive phase,  $z$  the longitudinal position along the macroscopic undulator beam line.  $\rho_0$  is the mean charge density inside the bunch while  $\tilde{\rho}_1$  is the amplitude of the charge density modulation. Inside the undulator the electrons travel on a sinusoidal trajectory which leads to an oscillatory part in the longitudinal velocity. One can then consider the time-dependence of the longitudinal position inside the undulator as

$$z(t) = \bar{\beta}ct = \left( 1 - \frac{1 + \frac{K^2}{2}}{2\gamma^2} \right) ct \quad (2.6)$$

In order to obtain the radiation Field  $E_x(z)$  one needs to solve the wave equation

$$\left[ \frac{\partial^2}{\partial z^2} - \frac{1}{c^2} \frac{\partial}{\partial t^2} \right] E_x(z, t) = \mu_0 \frac{\partial j_x}{\partial t} \quad (2.7)$$

as we neglect any dependencies on transverse positions. We now need to find a solution for the complex field amplitude

$$E_x(z, t) = \tilde{E}_x(z) \exp(ik_1(z - ct)) \quad (2.8)$$

with  $\tilde{E}_x(0) = E_0$  and  $k_1$  the wave number of the initial radiation. As the change of the amplitude should be small over the distance of one light wavelength, one can use the slow varying amplitude ansatz, which is justified by FLASH for a not prebunched beam: At 4.12 nm all six undulators with a length of 4.5 nm, so 27 m are sufficient to bring the FEL into saturation. As we will see later, this is equivalent to about 20 power gain lengths. After each gain length, the radiated power is e-fold-amplified which gives 1.35 m as an estimate for the gain length. The period length of FLASH is 27.1 mm, so one gain length is approximately 50 period lengths. This means that on one undulator period the radiated power changes by only 2 %. Assuming slow-varying means that changes per undulator period in the amplitude are small compared to the momentous value

$$|\tilde{E}'_x(z)| \lambda_{\text{rad}} \ll |\tilde{E}_x(z)| \quad (2.9)$$

where the prime indicates the derivative with respect to  $z$ . This is equivalent to exchanging light wavelength and wave number

$$|\tilde{E}'_x(z)| \ll |\tilde{E}_x(z)| k_l \quad (2.10)$$

Since the first derivative of the field amplitude is assumed small for any given  $z$ , one can safely say that the second derivative is even smaller and thus negligible. The differential equation of the slowly varying amplitude is then

$$\tilde{E}'_x(z) = -i \frac{\mu_0}{2k_1} \frac{\partial j_x}{\partial t} \exp(-ik_1(z - ct)) \quad (2.11)$$

The transverse current  $j_x$  needs to be found.

$$j_x = j_z \frac{v_x}{v_z} \approx j_z \frac{K}{\gamma} \cos(k_u z) \quad (2.12)$$

which can be inserted into the formula of the electric field amplitude 2.11 yielding

## 2.1. 1D FEL THEORY

---

$$\tilde{E}'_x = -\frac{\mu_0 c K}{2\gamma} \tilde{j}_1 \exp(i(k_1 z - \omega_1 t) + i k_u z) \exp(-i(k_1 z - \omega_1 t)) \cos(k_u z) \quad (2.13)$$

with  $j_1$  being the current density modulation which can be obtained from the charge density modulation. The derivative of the electric field amplitude can then be expressed as

$$= -\frac{\mu_0 c K}{4\gamma} \tilde{j}_1 (1 + \exp(2i k_u z)) \approx -\frac{\mu_0 c K}{4\gamma} \tilde{j}_1 \quad (2.14)$$

in order to cover the longitudinal oscillations of the electron beam during their path through the undulators magnetic field one needs to use the modified undulator parameter  $\hat{K}$ .

$$\hat{K} = K \cdot \left( J_0 \left( \frac{K^2}{4 + 2K^2} \right) - J_1 \left( \frac{K^2}{4 + 2K^2} \right) \right) \quad (2.15)$$

For the high-gain FEL the field amplitude depends on  $z$ . This means also the relative energy deviation  $\eta = \gamma/\gamma_r - 1$  has a  $z$ -dependence.

$$\eta'|_t = -\frac{e\hat{K}}{2m_e c^2 \gamma_r^2} \Re \left( \tilde{E}_x \exp(i\Psi) \right) \quad (2.16)$$

Combining Energy and Space charge term we can state

$$\tilde{E}_z(z) = i \frac{4\gamma c}{\omega_l K} \frac{d\tilde{E}_x}{dz} \quad (2.17)$$

Finally, one can end up with a set of  $2N + 2$  coupled differential equations for a bunch consisting of  $N$  particles where  $n$  indicates the  $n$ th particle.

$$\Psi'_n = 2k_u \eta_n \quad (2.18)$$

$$\eta'_n = -\frac{e}{m_e c^2 \gamma_r} \Re \left( \left( \frac{\hat{K} \tilde{E}_z}{2\gamma_r} - i \frac{\mu_0 c^2}{\omega_l} \tilde{j}_1 \right) \exp(i\Psi_n) \right) \quad (2.19)$$

$$\tilde{j}_1 = j_0 \frac{2}{N} \sum_{n=1}^N (\exp(-i\Psi_n)) \quad (2.20)$$

$$\tilde{E}'_x = -\frac{\mu_0 c \hat{K}}{4\gamma_r} \tilde{j}_1 \quad (2.21)$$

Speaking of an electron bunch with common bunch charges of 100 pC, about  $10^9$  particles need to be considered which renders this a true many-body problem with the consequence that it cannot be solved analytically. However, one can benefit from these equations by using them to numerically investigate the FEL amplifier.

For small density modulations that are periodic one can formulate a normalized particle distribution function:

$$F(\psi, \eta, z) = \Re\left(\tilde{F}(\psi, \eta, z)\right) = F_0(\eta) + \Re\left(\tilde{F}_1(\eta, z) \cdot \exp(i\psi)\right) \quad (2.22)$$

This can be used in a generalized continuity equation, the so-called Vlasov-equation:

$$\frac{dF}{dz} = \frac{\partial F}{\partial z} + \frac{\partial F}{\partial \psi} \frac{\partial \psi}{\partial z} + \frac{\partial F}{\partial \eta} \frac{\partial \eta}{\partial z} = 0 \quad (2.23)$$

A third-order differential equation can be found describing the exponential growth of the radiation power along the undulator which is analytically solvable.

$$\frac{1}{\Gamma^3} \tilde{E}_x''' + 2i \frac{\eta}{\rho_{\text{FEL}}} \frac{1}{\Gamma^2} \tilde{E}_x'' + \left( \frac{k_p^2}{\Gamma^2} - \left( \frac{\eta}{\rho_{\text{FEL}}} \right)^2 \right) \frac{1}{\Gamma} \tilde{E}_x' - i \tilde{E}_x = 0 \quad (2.24)$$

where  $\Gamma$  is the gain parameter defined as

$$\Gamma = \sqrt[3]{\frac{\mu_0 \hat{K}^2 e^2 k_u n_e}{4 \gamma_r^3 m_e}} \quad (2.25)$$

and  $k_p$  the space charge parameter

$$k_p = \sqrt{\frac{2k_x u}{\mu_0} e^2 c n_e \gamma_r m_e \omega_1} \quad (2.26)$$

$$\rho_{\text{FEL}} = \frac{\Gamma}{2k_u} = \frac{1}{4\pi\sqrt{3}} \frac{\lambda_u}{L_{g0}} \quad (2.27)$$

where  $L_{g0}$  is the power gain length, the length after that the FEL output power is amplified by a factor of  $e$ . A solution of the third order differential equation can be found for  $\eta = k_p = 0$ , where all electrons are perfectly in resonance and space charge is negligible. These assumptions are valid for high electron beam energies and low electron beam densities. From the Ansatz  $\alpha^3 = i\Gamma^3$ . This leads to solutions

## 2.1. 1D FEL THEORY

---

$$\alpha_1 = \frac{1}{2} (i + \sqrt{3}) \Gamma \quad (2.28)$$

$$\alpha_2 = \frac{1}{2} (i - \sqrt{3}) \Gamma \quad (2.29)$$

$$\alpha_3 = -i\Gamma \quad (2.30)$$

The solution for the third order differential equation is then a linear combination of the three solutions:

$$\tilde{E}_z(x) = \sum_{j=1}^3 c_j \exp(\alpha_j z) \quad (2.31)$$

One now needs to find the correct coefficients  $c_j$ . They are determined by the initial condition, for example  $\tilde{E}_z(0) = E_{\text{ini}}$ ,  $E'_z(0) = E''_z(0) = 0$ . For these conditions to be fulfilled all  $c_j$  need to be the same  $c_j = \frac{1}{3} E_{\text{ini}} \forall j$  if  $\eta$  and  $k_p$  vanish which means the  $\alpha_n$  are the eigenvalues of the equation.

$$\tilde{E}_x(z) = \frac{E_{\text{ini}}}{3} \left( \underbrace{\exp\left(\frac{1}{2}(i + \sqrt{3})\Gamma z\right)}_{\text{exponentially growing term}} + \underbrace{\exp\left(\frac{1}{2}(i - \sqrt{3})\Gamma z\right)}_{\text{exponentially damped term}} + \underbrace{\exp(-i\Gamma z)}_{\text{oscillatory term}} \right) \quad (2.32)$$

The first term is exponentially growing, which dominates the electric field after some distance. The exponentially damped term will eventually vanish, while the oscillatory term is small compared to the exponentially growing term after some gain lengths.

In the so called "lethargy regime", about 2 gain lengths after the beginning of the undulator, the FEL power only rises slightly due to the presence of the two non-exponential terms. Making a Taylor expansion up to the second real term, one gets

$$\tilde{E}_x(z) \Big|_{z=0} = E_{\text{ini}} \left( 1 + \frac{1}{6} i \Gamma^3 z^3 - \frac{1}{720} \Gamma^6 z^6 \right) + \mathcal{O}(7) \quad (2.33)$$

After those 2 gain lengths the growth rate for large  $z$  is mainly dominated by the real and positive part of the  $\alpha_1$  solution, which leads to an exponential growth of the field:

$$P(z) \propto \frac{1}{9} P_{\text{ini}} \exp(2 \cdot \Re(\alpha_1)) = \frac{1}{9} P_{\text{ini}} \exp(\sqrt{3}\Gamma z) = \frac{1}{9} P_{\text{ini}} \exp\left(\frac{z}{L_G}\right) \quad (2.34)$$

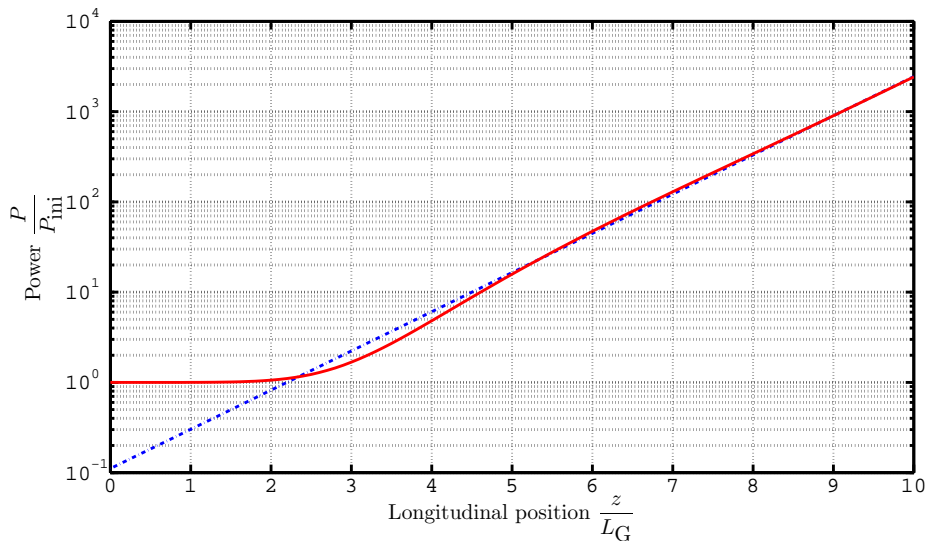


Figure 2.1: Curve showing the power dependence on the longitudinal position.

$$L_G = \frac{\lambda_u}{4\pi\rho_{\text{FEL}}\sqrt{3}} \propto \gamma \sqrt[3]{\frac{\sigma_r^2}{I_0}} \quad (2.35)$$

where  $\rho_{\text{FEL}}$  is the so called Pierce- or FEL-parameter [80] defined as

$$\rho_{\text{FEL}} = \sqrt[3]{\frac{I}{I_A} \frac{\gamma \lambda_{\text{rad}}^2}{16\pi^2 \sigma_x^2} \frac{K^2}{\left(1 + \frac{K^2}{2}\right)^2} \hat{K}^2} \quad (2.36)$$

with the Alfvén current  $I_A = (4\pi m_e c)/(\mu_0 e) = 17$  kA, and  $\sigma_x$  the transverse rms beam size. The FEL parameter is approximately the fraction of beam power converted into photons at saturation.

$$P_{\text{sat}} \approx \rho_{\text{FEL}} P_{\text{beam}} \quad (2.37)$$

The numerical value is typically in the order of  $10^{-3}$ . The gain function of the FEL as an amplifier depends on the position inside the FEL and the relative energy deviation  $\eta$ .

$$G(\eta, z) = \left| \frac{\tilde{E}_x(\eta, z)}{E_{\text{ini}}} \right|^2 - 1 \quad (2.38)$$

The bandwidth, i.e. the width of the gain curve, gets narrower with the length of the undulator. It is about  $2\rho_{\text{FEL}}$  at a longitudinal position of 4 gain lengths and at about  $\rho_{\text{FEL}}$  after 16 gain lengths.

## 2.1. 1D FEL THEORY

---

Up to now, only the FEL amplification using electron bunches on the resonant energy of the undulator were covered. But the electron energy might not comply with the resonance energy. More important, in case of spontaneous start-up or a frequency spectrum in the initial radiation field, several frequencies are present. In that case one has to formulate the general form of solutions

$$\tilde{E}_x(z, \eta) = \sum_{j=1}^3 [c_j(\eta) \exp(\alpha_j(\eta) z)] \quad (2.39)$$

which depends on  $\eta$  since the eigenvalues are functions of it  $\alpha(\eta)$ . The coefficients  $c_j$  are again defined by the initial conditions. Once all coefficients for the individual frequency coefficients are calculated one can find the resulting field as a superposition of the individual detuned cases:

$$E_x(z, t) = \Re \left( \sum_{\nu} \left( \tilde{E}_x^{\nu}(z) \exp(i\omega_{\nu}(z/c - t)) \right) \right) \quad (2.40)$$

Apart from amplifying an input seed, the FEL can also start from a periodically modulated electron distribution. Assuming the beam current is periodically modulated in its ponderomotive phase leads to

$$j_z = j_0 + \tilde{j}(z) \exp(i\Psi) \quad (2.41)$$

Here,  $j$  denotes the current density in analogy to the charge density  $\rho$ . Previously it was shown that under this assumption the first and second derivative of the electric field do not vanish. At the begin of the FEL,  $z = 0$ , the derivatives are

$$E_0' = -\frac{\mu_0 c \hat{K}}{4\gamma_r} \cdot \tilde{j}_1(0) \quad (2.42)$$

$$E_0'' = -\frac{\mu_0 c \hat{K}}{4\gamma_r} \cdot \tilde{j}_1'(0) \quad (2.43)$$

Following Ref. [40], one can find a bunching-equivalent input field to be

$$E_{\text{equiv}} = \frac{\mu_0 c \hat{K}}{4\gamma_r} \frac{\sqrt{cI_0 \Delta\omega}}{\sqrt{\pi} A_b} \quad (2.44)$$

with  $A_b$  the cross-section of both, electron beam and photon pulse. The third possibility to start the FEL process is an energy-modulated electron beam.

Since during the amplification process energy is taken from the electron beam and transferred to the photon field the electrons can move to areas in the phase space where photons get absorbed by the electrons. One important result of the 1D-Theory is that the saturation power does not depend on the initial seed power, see Fig. 2.2.

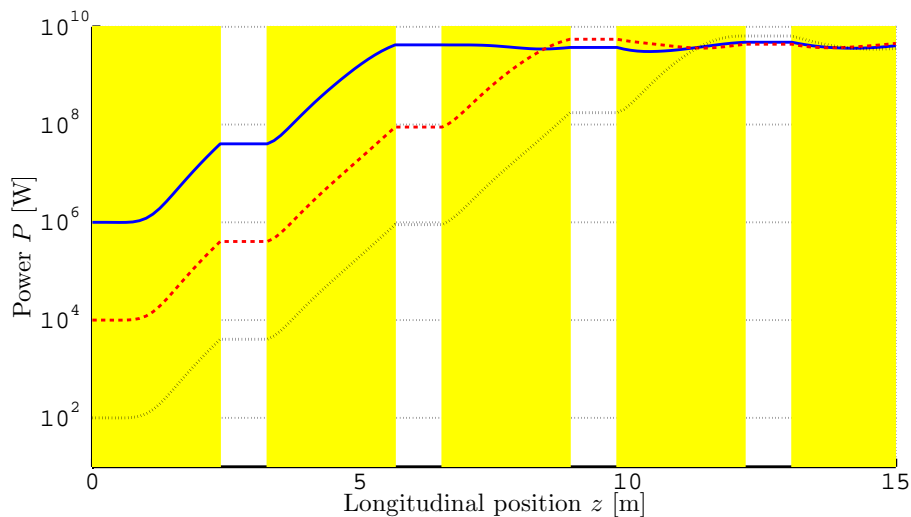


Figure 2.2: Simulation of the FEL output power for different seed pulse powers. The simulation is based on FLASH2 parameters and multi-segmented undulators.

## 2.2 Shot noise

So far the FEL was treated as an amplifier only. However, many FELs built are not genuinely designed to be seeded. They start up from the internal and stochastic electron density distribution inside the bunch, the so-called "shotnoise" which is approximated by

$$P_0 = \frac{3\sqrt{4\pi}\rho_{\text{FEL}}^2}{N_\lambda\sqrt{\ln\left(\frac{N_\lambda}{\rho_{\text{FEL}}}\right)}} P_b \quad (2.45)$$

with the number of electrons per wavelength

$$N_\lambda = \frac{I\lambda_{\text{rad}}}{ec} \quad (2.46)$$

### 2.3. TRANSVERSE AND LONGITUDINAL COHERENCE

---

Due to the stochastic behavior of the electrons inside the bunch, the dominant wavelength and intensity of the shotnoise varies from shot to shot.

## 2.3 Transverse and Longitudinal Coherence

One of the biggest advantages of Free-Electron Lasers compared to Synchrotron-based light sources is the degree of temporal coherence. See Table 2.1

*Table 2.1: Coherence properties of synchrotrons and Free-Electron Lasers. Data taken from [81–84].*

Property	PETRA III	FLASH
	Horizontal / Vertical	Horizontal / Vertical
Coh. length at source	0.9 $\mu\text{m}$ / 7.7 $\mu\text{m}$	$6.2 \pm 0.2 \mu\text{m}$ / $8.7 \pm 1.0 \mu\text{m}$
Coh. length at observation position	58 $\mu\text{m}$ / 390 $\mu\text{m}$	$300 \pm 15 \mu\text{m}$ / $250 \pm 13 \mu\text{m}$
Degree of coherence	0.01 / 0.52	$0.74 \pm 0.08$ / $0.59 \pm 0.10$

The spectral bandwidth in the FEL is a function of the longitudinal position inside the undulator

$$\sigma_\omega = 3\sqrt{2}\rho_{\text{FEL}}\omega_1\sqrt{\frac{L_{\text{g0}}}{z}} \quad (2.47)$$

and therefore also the coherence time which is given by

$$\tau_{\text{coh}} = \int \left( \exp\left(-\frac{\sigma_\omega(z)^2 t^2}{2}\right) \right)^2 dt \approx \frac{\sqrt{\pi}}{\sigma_\omega(z)} \quad (2.48)$$

For a bunch with a flat-top energy distribution duration that is shorter than the coherence time only a single spike in the wavelength spectrum is generated. For longer bunches the average number of spikes in the spectrum (sometimes called "longitudinal modes") is

$$M = \frac{T_{\text{bunch}}}{\tau_{\text{coh}}} \quad (2.49)$$

The number of spikes in the spectrum  $M$  is not to be confused with beam quality factor  $M^2$  of the following chapters. The width of such a spike is equal to the Fourier transform limit of the bunch duration

$$\Delta\omega_{\text{spike}} = \frac{2\sqrt{2\ln(2)}}{T_{\text{bunch}}} \quad (2.50)$$

## 2.4. PRODUCTION OF A SEED PULSE IN A HIGH HARMONICS-GENERATION TARGET

---

In addition to the temporal coherence, FELs offer radiation with a high degree of transverse coherence which has been shown in double-slit experiments. One can show that on the undulator-electron beam axis the fundamental  $\text{TEM}_{00}$  content has the highest intensity, while higher order  $\text{TEM}_{mn}$  modes have larger radial extents and thus reduced power densities, and some even vanish on the undulator-electron beam axis (those where at least one of  $m$  or  $n$  is an odd integer). Once saturation is reached the  $\text{TEM}_{00}$  will dominate the FEL modal composition, however some higher order modes are still present (see chapter 3) resulting in an  $M^2$  bigger than one [85].

### 2.4 Production of a seed pulse in a high harmonics-generation target

In order to produce higher harmonics, one has to overlap an intense laser pulse with a noble gas target. In experiments [50, 86], a number of high harmonics is generated, and the spectrum of the harmonics shows a plateau of several harmonics having the same energy. This could not be explained until in 1993, when Corkum et al. came up with a semi-classical description of the HHG process [87, 88]. This so-called three-step model works as follows: First, the strong laser field bends the atomic potential (Fig. 2.3(a)) of the noble gas atoms, which also means that the laser field intensity needs to be in the order of the coulomb potential of the noble gas. The electron has now a higher probability to tunnel through the Coulomb barrier (Fig. 2.3(b)). After leaving the central potential pot, the electron is accelerated in the electric field of the laser.

The second step takes place one half-cycle of the laser field later. The noble gas atom's potential is bent now in a way that the electron has gained energy and is accelerated towards the atom (Fig. 2.3(c)).

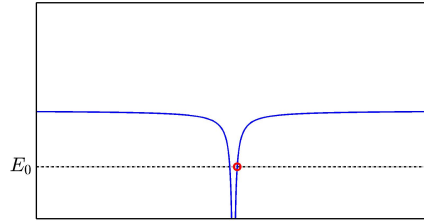
In the third step, the electron recombines with the atom and emits a high-energy photon, whose energy is defined by the kinetic energy of the electrons. (Fig. 2.3(d)) The maximum energy one can achieve with the electrons defines the cut-off of the energy spectrum with  $E_{\text{cutoff}} = I_p + E_c^{\text{max}}$ , and  $E_c^{\text{max}} \approx 3.17U_p$ , where  $U_p$  is the ponderomotive energy

$$U_p = \frac{e^2 E^2}{4m_e \omega^2} \quad (2.51)$$

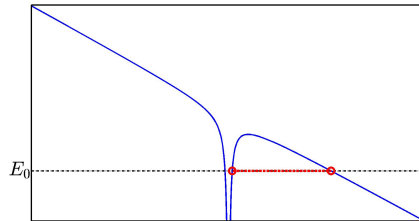
with electron rest mass  $m_e$ , elementary charge  $e$  and the frequency  $\omega$  and energy  $E$  of the electric field of the laser. Depending on the time of the ionization of the atom, two different electron trajectories can lead to the same photon energy. Those trajectories differ in path lengths (and recombination

## 2.4. PRODUCTION OF A SEED PULSE IN A HIGH HARMONICS-GENERATION TARGET

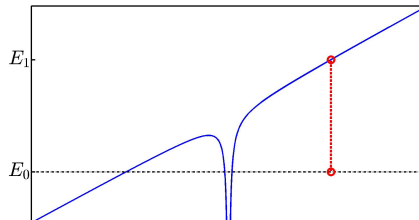
---



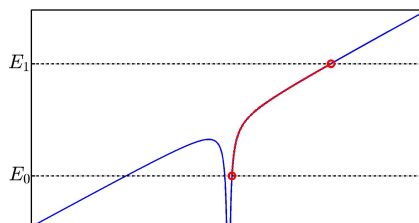
(a) Electron inside the nucleus' coulomb potential.



(b) The coulomb potential is bent under the influence of an external laser field. Electrons can now tunnel through the potential barrier.



(c) One half-period later the laser has bent the coulomb potential to the other direction, giving higher energy to the electrons.



(d) The electron accelerates by the means of the coulomb potential towards its ground state, doing photo emission, and finally recombination.

*Figure 2.3: The semi-classical three step HHG model.*

## 2.4. PRODUCTION OF A SEED PULSE IN A HIGH HARMONICS-GENERATION TARGET

---

times) and are therefore called "long" and "short" trajectory. In order to calculate the HHG radiation properties correctly one needs to follow a complete quantum mechanical approach. This allows to predict phase information of the harmonic radiation for both trajectories which depends on the drive laser phase and the phase of the recombining electron.

In order to understand the plateau one needs to understand the macroscopic emission process. In order to emit the  $h$ -th harmonic, constructive interference between the drive laser field and the radiation emitted in the single atom HHG process needs to take place. The phase difference is defined by the dispersion of the medium and the electrons, the focusing geometry and the single-atom phases. The laser intensity and divergence and waist size of the laser as well as the geometry of the gas target together with the pressures and the gas type can be exploited to control the phase matching. For direct seeding, one would optimize an HHG source in terms of the highest possible photon number on the desired harmonic and a bandwidth as small as possible because many users request small-bandwidth, Fourier-limited photon pulses. In addition, the divergence has to be kept small enough to overlap the harmonic radiation with the FEL electrons in the undulator for a sufficiently long distance.

The divergence of the emitted radiation is given by

$$\theta_T = \frac{\lambda_{\text{rad},h}}{\pi w_h} \sqrt{1 + \left( \alpha_T^2 I_{\text{ini}}^2 \left( \frac{w_h}{w_{\text{ini}}} \right)^2 \right)^2} \quad (2.52)$$

with the wavelength  $\lambda_{\text{rad},h}$ , beam waist size  $w_h$  of the  $h$ -th harmonic, the intensity  $I_{\text{ini}}$ , and waist size  $w_{\text{ini}}$  of the drive laser.  $\alpha_T$  is the phase-related coefficient of the corresponding trajectory. From the beam divergence one can estimate the beam quality factor  $M^2$  :

$$M^2 = w_h \frac{\theta_T}{\lambda_{\text{rad},h}} \quad (2.53)$$

For the direct seeding of an FEL, an HHG source with a high photon flux and optimal spatial and temporal coherence is needed. In contrast to other nonlinear processes like second harmonic generation (SHG) or third harmonic generation (THG), the phase information of the drive laser is not simply imprinted onto the harmonics produced. To ensure fully coherent beams, one needs to control the contributions of the short and long trajectories. A possible concept is to segregate the harmonic production process and the phase matching process. This is realized by alternatingly adding passive areas and harmonic generation areas driven by one single laser. The length of the zones is typically one coherence length, which is one HHG half period.

## 2.5. HIGH-GAIN HARMONIC GENERATION

---

Since under phase-matching conditions the intensity of the coherent radiation increases quadratically as with the number of harmonic generation zones, the pulse energy is increased. A design for such so-called quasi-phase matched target is shown in Fig. 2.4.

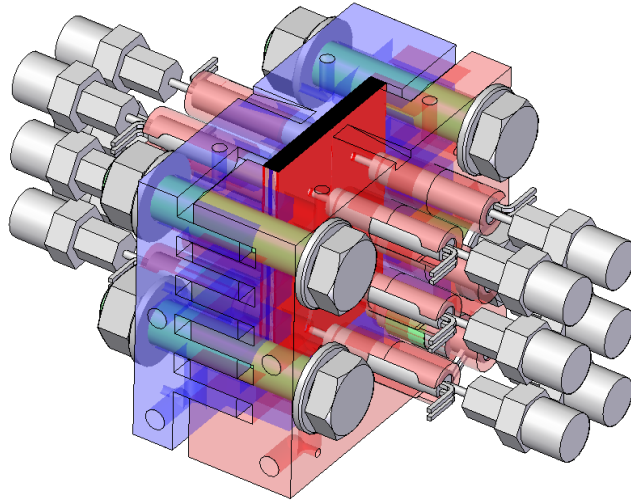


*Figure 2.4: Design of a Quasi-Phase Matching HHG source, as described in [53]. The target consists of several thin foils, kept tight together by the big screws. Each foil has a channel that allows gas to flow into the target area and is connected to a valve that can control the pressure of the gas.*

## 2.5 High-gain harmonic generation

While direct seeding amplifies the provided photon pulse, high-gain harmonic generation (HG) [56,57,89] uses the laser to produce initial bunching. The HG process consists of four parts:

### Energy modulation

The modulator, a short undulator, is usually shorter than two gain lengths so that the spontaneous radiation will not be amplified exponentially. Within this undulator the electron bunch (Fig. 2.6) are overlapped with a laser field which introduces an energy modulation of

$$\Delta\gamma = k_{s1} K_{s1} \hat{K}_{w1} K_{w1} z_{w1} \frac{1}{\gamma} \quad (2.54)$$

with  $k_{s1}$  being the wave number of the seed,  $K_{s1} = eA_{s1}/mc$  the dimensionless rms vector potential of the seed,  $K_{w1}$  the K-parameter of the modulator,  $z_{w1}$  the length of the modulator,  $\hat{K}_{w1}$  as defined in Eq. 2.15 and  $\gamma$  the electron beam energy [57] (Fig. 2.7). The current is not yet modulated (Fig. 2.8). This formula approximates the photon field to be constant along the undulator.

## Dispersion

The introduced energy modulation is then converted to microbunching (sheared in phase-space, see Fig. 2.9) by means of betatron phase advance due to dispersion. The current density has been modulated (See Fig. 2.10). In the radiator, the phase advance due to the maximum energy modulation is

$$\Delta\Psi = \frac{\partial\Psi}{\partial\gamma} \Delta\gamma \quad (2.55)$$

where  $\frac{\partial\Psi}{\partial\gamma}$  is the dispersion strength. Three terms are contributing:

$$\frac{\partial\Psi}{\partial\gamma} = \underbrace{h \frac{k_{w1}}{\gamma} z_{w1}}_{\text{Modulator}} + \underbrace{\left( \frac{\partial\Psi}{\partial\gamma} \right)_{\text{dispersion}}}_{\text{Dispersive section}} + \underbrace{2 \frac{k_{w2}}{\gamma} z_{w2}}_{\text{Radiator}} \quad (2.56)$$

The first term, the dispersion of the modulator, and the third term, the dispersion of the radiator differ by a factor of  $n/2$ . The factor of  $n$  is due to the fact that the phase in the modulator is the  $n$ -fold of the phase in the radiator. The factor  $1/2$  comes from the energy modulation that increases linearly with the modulator length. Integrating over  $z_{w1}$  contributes a factor of  $1/2$ . such that

## Microbunching

After passing the modulator, dispersive section, and radiator, the energy modulation is transformed to an electron density modulation, i.e. bunching factor  $b_n$ :

$$b_n = \exp\left(-\frac{1}{2} \left(\frac{\partial\Psi}{\partial\gamma} \sigma_\gamma\right)^2\right) J_n\left(\frac{\partial\Psi}{\partial\gamma} \Delta\gamma\right) \quad (2.57)$$

## 2.5. HIGH-GAIN HARMONIC GENERATION

A bunching-equivalent field can be calculated (Eq. 2.44), thus the bunching factor has to be optimized. In Eq. 2.57 one can see two terms: One exponential term that is at its maximum for an energy spread of 0, and a Bessel function-term. The Bessel function term depends on energy modulation  $\Delta\gamma$  and the total dispersion. The product of modulation depth and total dispersion is usually chosen such that the first maximum (which is also the global maximum) of the Bessel function is achieved. In Fig. 2.5, one can see the bunching factor as a function of the energy of the seed pulse in units of the optimum seed energy.

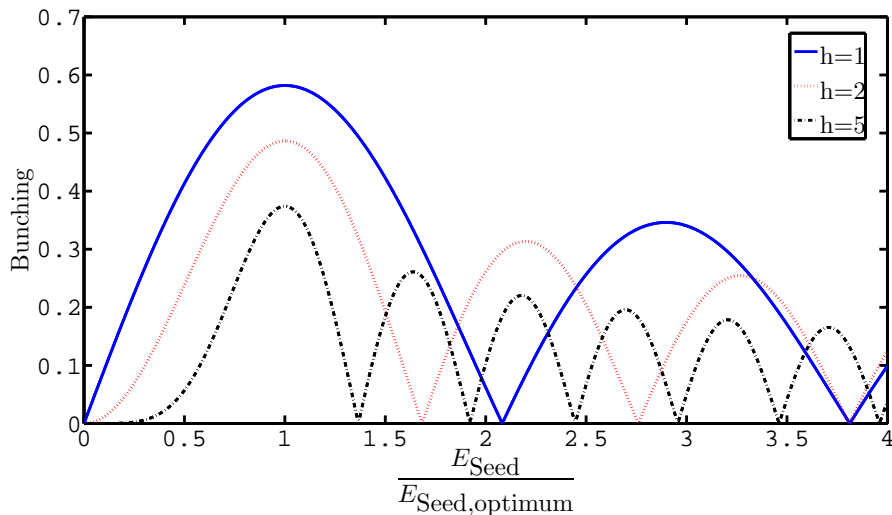


Figure 2.5: Bunching factors for different seed energies, normalized to the optimum seed energy (maximum in the Bessel function). The different curves show the behaviour for several harmonics  $h$ .

Following L.H. Yu and J. Wu [57] one can calculate the power of the coherent radiation in the first two gain lengths:

$$P_{\text{coh}} = \frac{(I_0)^2 Z_0}{8} \left( \frac{K \hat{K}_{B2}}{\gamma} \right)^2 \frac{1}{4\pi\sigma_x^2} |I_b|^2 \quad (2.58)$$

with electron beam current  $I_0$ , vacuum impedance  $Z_0 = 377 \Omega$ , undulator parameter  $K = \sqrt{2}K_{w2}$ , Bessel factor  $\hat{K}_{B2}$  as defined in Eq. 2.15,  $\sigma_x$  the electron beam size and  $I_b = \int_0^{2L_G} b_n(z, r) dt$  the bunching integral over the first two gain lengths.

As one can see in the term for the bunching, it decreases exponentially with the energy spread  $\sigma_\gamma$ . The coherent radiated power will decrease with

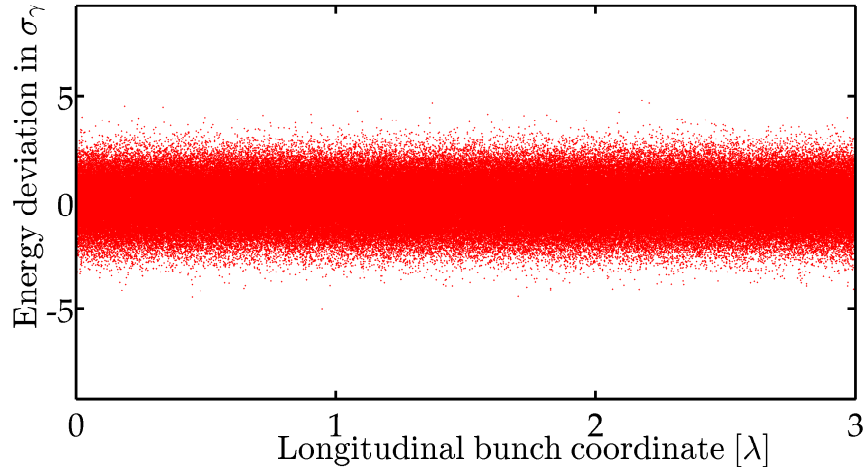


Figure 2.6: Longitudinal phase space distribution before entering the modulator.

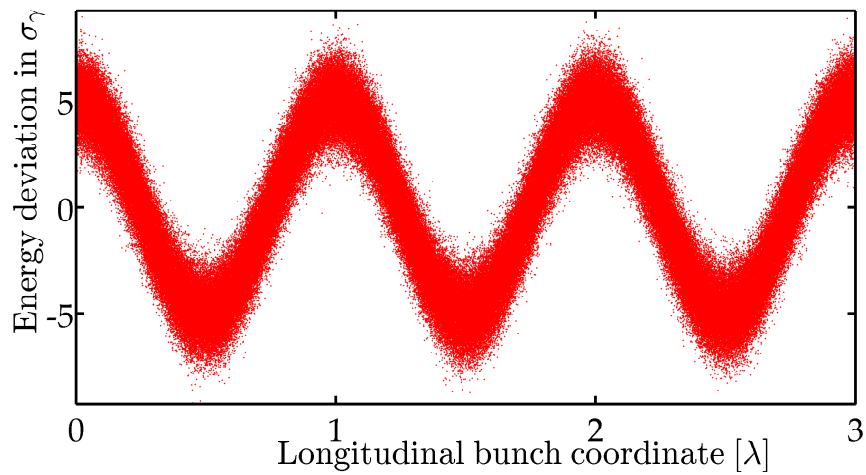


Figure 2.7: Longitudinal phase space distribution after energy modulation by the means of a laser in the undulator.

## 2.5. HIGH-GAIN HARMONIC GENERATION

---

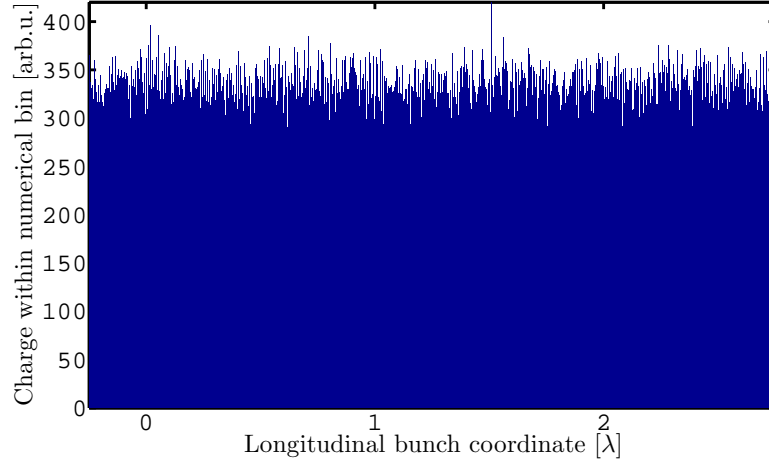


Figure 2.8: The charge is still uniformly distributed along the longitudinal bunch coordinate.

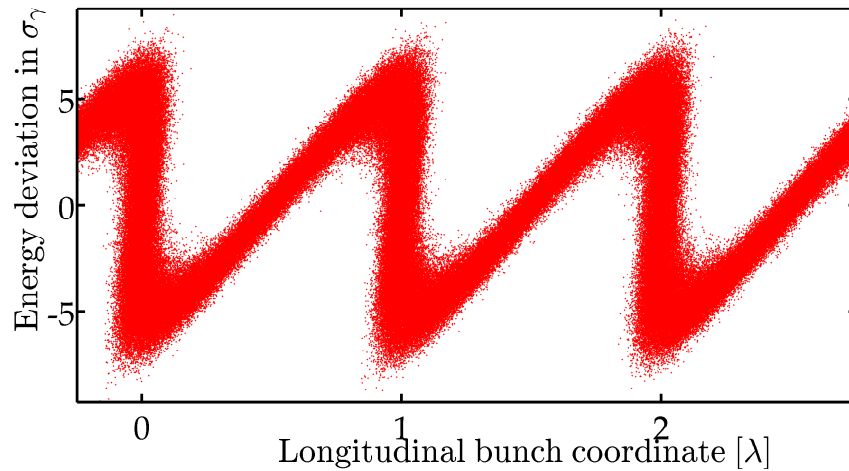


Figure 2.9: Longitudinal phase space distribution after the dispersive section. The energy modulation was transformed to an electron density modulation.

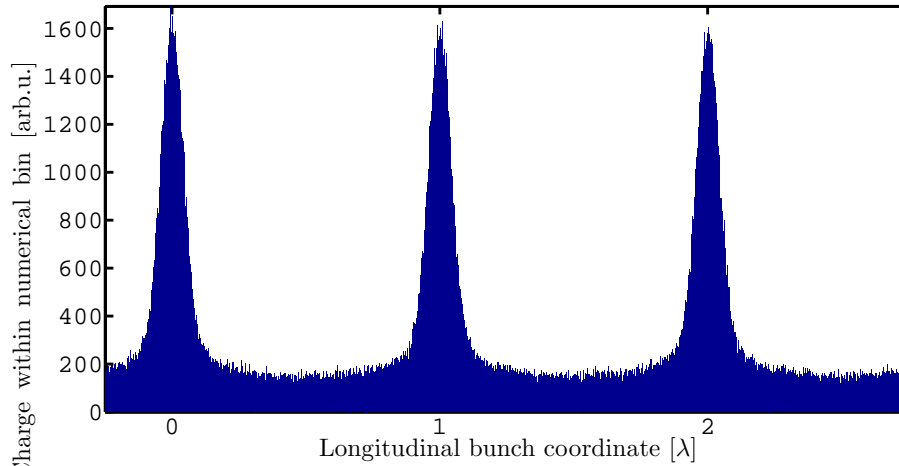


Figure 2.10: The electron density modulation is clearly visible and will radiate on a higher harmonic.

the second power of the bunching factor.

The signal-to-noise ratio of the HGHG process is given in [90] to be

$$\left(\frac{P_S}{P_h}\right)_{\text{out}} = \frac{1}{h^2} \left(\frac{P_S}{P_h}\right)_{\text{in}} \quad (2.59)$$

with  $P_S$  the power of the FEL amplifier from shot noise,  $P_h$  the power of the FEL amplifier starting from seeding. The contrast is inversely proportional to the harmonic  $h$  of the fundamental laser wavelength, while the maximum bunching factor is proportional to the global maximum of  $J_h(x)$ , when no energy spread is present. Using the analytical approximation for  $h > 4$  :  $\max(J_h(x)) \approx 0.67/\sqrt[3]{h}$  from Stupakov et al. [60], the achievable contrast scales like

$$\left(\frac{P_S}{P_h}\right)_{\text{out}} \propto \frac{0.67}{\sqrt[3]{h^8}} \quad (2.60)$$

In Fig. 2.11 the first maxima have been calculated numerically.

## 2.5. HIGH-GAIN HARMONIC GENERATION

---

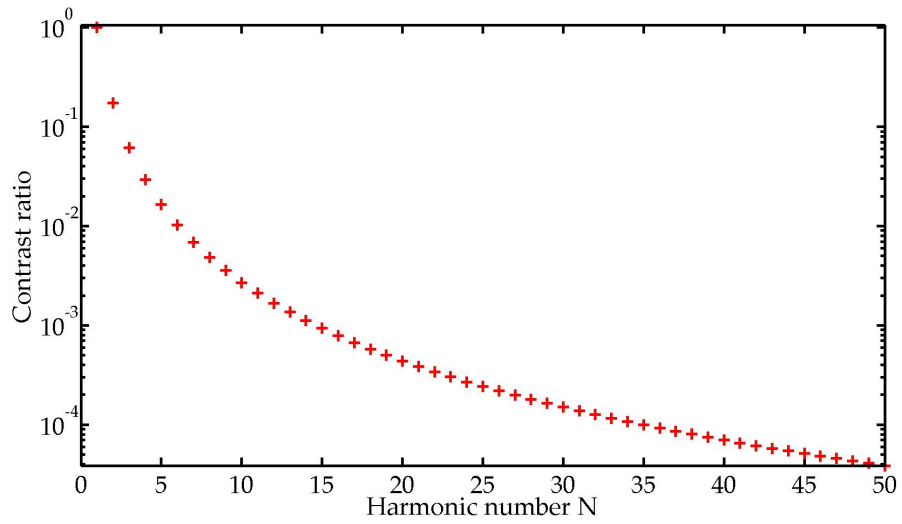


*Figure 2.11: Dependence of the normalized contrast  $(P_S/P_h)/\max(P_S/P_h)$  on the harmonic number  $h$  under the absence of energy spread.*

## Chapter 3

# Dependence of HHG seeding on the laser beam quality

A disadvantage of SASE FELs is that the FEL pulses show large intensity fluctuations and shot-to-shot variation in spectral content. This can be avoided by seeding the FEL with an external laser. It is clear that in the direct seeding process the quality of the external photon pulse ("Seed") plays an important role since the coupling and energy transfer between the electromagnetic field of the seed pulse and the electrons depend on the wavefront of the photon pulse [91]. The wavefront itself can in principle be measured, e.g. using a Shack-Hartmann wavefront sensor [92]. In practice, in an FEL a direct measurement of the wavefront at the beginning of the undulator is very difficult due to space limitations e.g. at sFLASH [75]. Therefore another figure of merit which describes the quality of the seed beam, the  $M^2$ -value [93], can be used. In this chapter the impact of  $M^2$  on the performance of an FEL, directly seeded using higher harmonics generated in gas, is presented. The simulation results are compared with experimental data from the seeding experiment sFLASH [77]. The  $M^2$  of the sFLASH seed [94] has been estimated using a technique based on the modal decomposition proposed in [95]. A study on the quality of the photon pulse generated by a SASE FEL using modal decomposition can be found in [96]. There are several other methods to measure the  $M^2$ -value, e.g. the focus scan technique [97] or modal decomposition using computer generated holograms [98]. In contrast to these, the  $M^2$  measurement technique used here [96] needs a single transverse intensity profile, e.g. a CCD-camera image. Thus, this technique becomes a viable alternative in the cases when due to space limitations other methods cannot be used and knowledge on the modal content of the laser radiation is required.

### 3.1 Gaussian beams

Gaussian beams are photon beams with an axially symmetric field distribution following the formula:

$$E(r) = E_0 \exp\left(-\frac{r^2}{w_{00}^2}\right) \quad (3.1)$$

where  $r$  is the radial coordinate and  $w_{00}$  that radial distance from the center where the intensity drops down to  $e^{-2}$  of the central intensity, usually called "Gaussian radius". Here,  $w_{00}$  denotes the radius of a pure TEM<sub>00</sub> beam, while  $w_0$  is the radius of a multimode beam, which is discussed later. At a distance of  $2w_0$ , the intensity is only about  $(\exp(-(2w_0)^2/w_{00}^2))^2 = 3 \cdot 10^{-4}$  of the central field amplitude, and thus almost always negligible. Since the Fourier-transform of a Gaussian distribution is still a Gaussian distribution no integration is needed to propagate a Gaussian beam.

The beam radius of a Gaussian beam with its waist at  $z = 0$  is given by

$$w^2(z) = w_{00}^2 \left(1 + \left(\frac{\lambda z}{\pi w_{00}^2}\right)^2\right) = w_{00}^2 \left(1 + \left(\frac{z}{z_R}\right)^2\right) \quad (3.2)$$

and the radius of curvature of the wave front.

$$R(z) = z \left(1 + \left(\frac{\pi w_{00}^2}{\lambda z}\right)^2\right) = z \left(1 + \left(\frac{z_R}{z}\right)^2\right) \quad (3.3)$$

, see Fig. 3.1

One can show that the minimum curvature radius as a function of  $z$  is achieved for  $z_R = \pi w_{00}^2/\lambda$ , which is called the "Rayleigh-length".

For distances much longer than the Rayleigh-length  $z \gg z_R$  the beam size increases almost linearly with  $z$  and the beam evolution no longer appears as hour-glass shaped, but cone-like, see Fig. 3.2. From this one can estimate the far field beam divergence as

$$\theta \approx \frac{\lambda}{\pi w_{00}} \quad (3.4)$$

During propagation, a longitudinal phase delay occurs, also called "Gouy-phase" which is given by

$$\zeta(z) = \arctan\left(\frac{z}{z_R}\right) \quad (3.5)$$

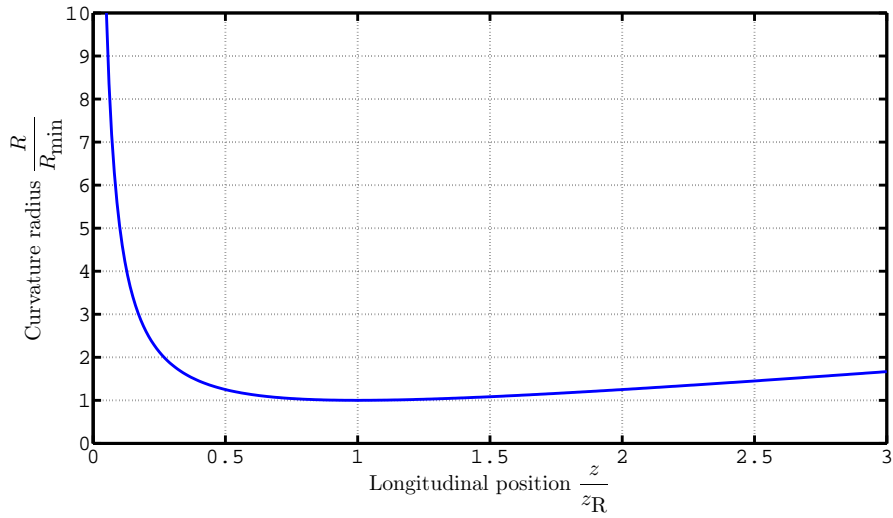


Figure 3.1: Curvature radius dependence on the longitudinal position.

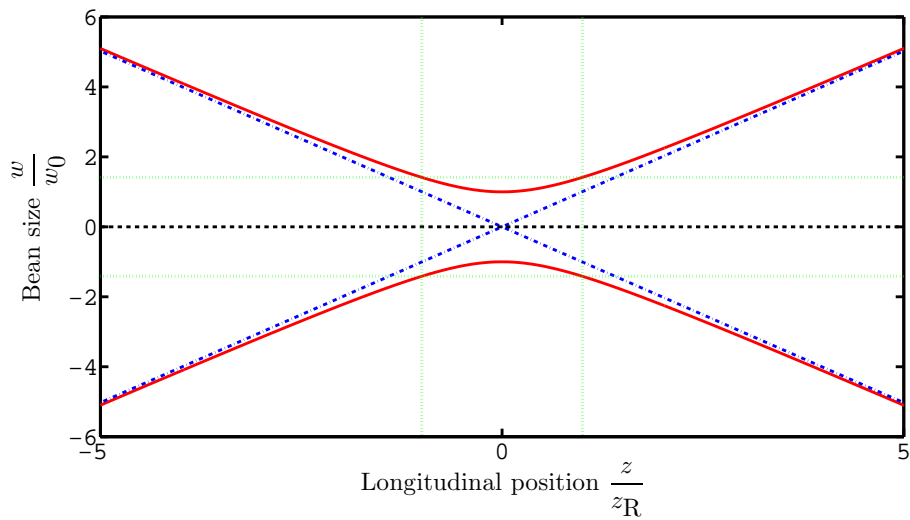


Figure 3.2: Gaussian beam propagation. The red solid line is the beam size, the blue dashed line shows the asymptotic behavior. The black line indicates the axis. With the help of the green lines one can see: After traveling a distance of one Rayleigh-Length, the beam radius grows by a factor of  $\sqrt{2}$ , thus doubles the beam area.

## 3.2. NUMERICAL SIMULATION SETUP

---

One number to quantify how Gaussian a beam is, is called  $M^2$ . It describes the ratio of the beam parameter product of a real beam and a Gaussian beam. The beam parameter product is the product of the rms beam divergence and minimum rms beam size:

$$M^2 = \frac{BPP_{\text{real}}}{BPP_{\text{gauss}}} = \frac{\theta_0 w_0}{\theta_{00} w_{00}} = \frac{\theta_0 w_0 \pi}{\lambda} \quad (3.6)$$

The  $M^2$  changes Eq. 3.4 to

$$\theta_0 = M^2 \frac{\lambda}{\pi w_0} \quad (3.7)$$

and

$$w^2(z) = w_0^2 + \left( \frac{M^2 \lambda z}{\pi w_0} \right)^2 \quad (3.8)$$

## 3.2 Numerical simulation setup

The studies presented in this chapter have been done using the time-dependent 3D FEL code "GENESIS 1.3, v2" [99]. This means that an appropriate model for the FEL start-up from shot noise has been used. The electron beam line considered in the simulations is similar to the FLASH2 beam line of the FEL facility FLASH at DESY, Hamburg, Germany [24, 26]. All the relevant beam line parameters for the simulation are listed in Table 3.1.

The goal of the simulations is to study the FEL output power and contrast at the end of the beam line as a function of the  $M^2$ -value of the seed pulse. It has been assumed that the seed waist is located at the entrance of the first undulator module. In all cases the waist size  $w_0$  is kept constant and equal to  $55 \mu\text{m}$ . As shown in Figure 3.3 this value corresponds to the optimum beam size for a seed pulse consisting of the fundamental  $\text{TEM}_{00}$  mode only. The seeds with different  $M^2$ -values have been prepared as field distribution files for GENESIS all with the same total seed power of 2.5 kW and the same longitudinal power profile. The 2.5 kW for the given temporal profile lead to a pulse energy of 70 pJ, which is estimated to be the laser power that has coupled in successful HHG experiments. This means that the fraction of the power in the fundamental mode is decreasing as  $M^2$  increases. These field distributions have been generated by superposition of different Hermite-Gaussian modes. The amplitude and phase of each individual mode has been adjusted using a direct-search numerical algorithm [100] so that the following boundary conditions have been fulfilled:

## 3.2. NUMERICAL SIMULATION SETUP

---

*Table 3.1: Simulation parameters and ranges used in the numerical simulation. For the simulated wavelength, only three undulators were considered so that none of the simulated cases reaches saturation.*

<b>Undulators</b>		
Lattice		FODO
Number of undulators		3
Undulator period	$\lambda_u$	31.4 mm
Periods per undulator	$N_{\text{periods}}$	76
Undulator intersection	$L_{\text{drift}}$	91.36 cm
Max. K parameter (rms)	$K_{\text{rms}}$	2.0
<b>HHG pulse</b>		
Temporal shape		Gaussian
Wavelength	$\lambda_{\text{HHG}}$	37.6 nm
Pulse energy	$E_{\text{HHG}}$	70 pJ
Peak power	$P_{\text{max,HHG}}$	2.5 kW
Waist size	$w_0$	55 $\mu\text{m}$
Duration (rms)	$\tau_{\text{HHG}}$	12 fs
<b>Electron beam</b>		
Peak current	$I_{\text{max}}$	2.5 kA
Beam size	$\sigma_x$	49 $\mu\text{m}$
	$\sigma_y$	100 $\mu\text{m}$
Bunch Length (rms)	$\sigma_z$	30 $\mu\text{m}$
Energy	$E$	700 MeV
Slice energy spread	$\sigma_E$	500 keV
Normalized emittance	$\epsilon_{x,n}$	1.4 mm · mrad
	$\epsilon_{y,n}$	1.4 mm · mrad

### 3.3. GENERATION OF FIELD DISTRIBUTIONS WITH GIVEN BEAM QUALITY FACTORS AND WAIST SIZES

---

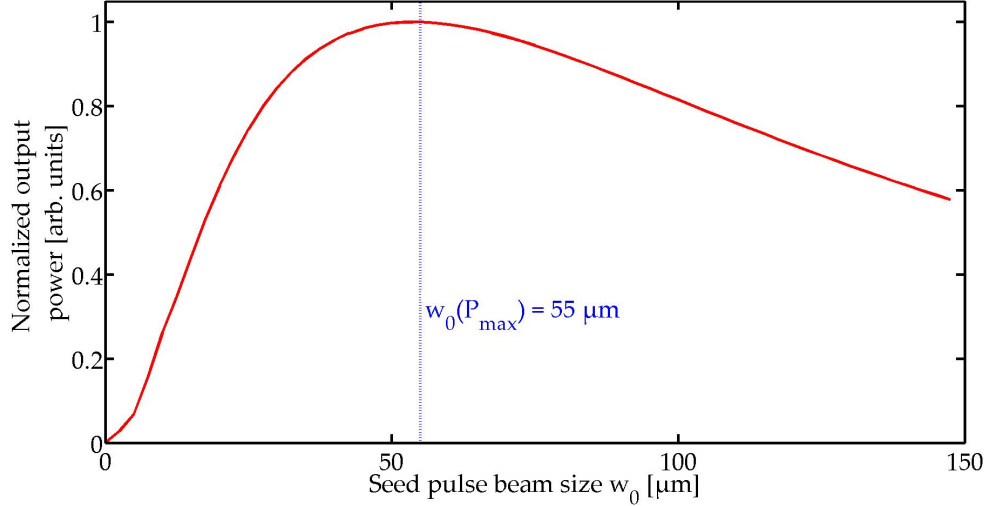


Figure 3.3: Normalized output power of the seeded FEL behind the third undulator vs. the waist size of the seed pulse.

- The waist size has to be  $55 \mu\text{m}$ , as discussed above.
- $M^2$  is equal to the desired  $M^2$  -value for both planes.
- In order to keep the axial symmetry of the multimode seed field, only TEM<sub>mn</sub> modes with even  $n, m$  are taken into account.

Obviously, there are many sets of Hermite-Gaussian modes that fulfill the aforementioned boundary conditions. Out of them, the one consisting of the smallest possible number of higher order modes was picked. Technically, this is implemented in the numerical algorithm, which starts with the fundamental mode and higher order modes are being added in steps of one to the field only if a solution with the desired  $M^2$  could not be found.

### 3.3 Generation of field distributions with given beam quality factors and waist sizes

In order to generate seed pulse files  $E(x)$  containing field distributions used in seeding simulations a generation routine has been developed. A seed pulse field consists of a superposition of Hermite-Gaussian generating functions

$$G_n(x) = \left(\frac{2}{\pi}\right)^{\frac{1}{4}} \frac{1}{\sqrt{2^n n! w(z)}} H_n\left(\frac{\sqrt{2}x}{w(z)}\right) \exp\left(-\frac{x^2}{w^2(z)}\right) \quad (3.9)$$

---

### 3.4. FEL OUTPUT POWER VS. SEED PULSE BEAM QUALITY

with the Hermite polynomials

$$H_n(x) = (-1)^n \exp(x^2) \frac{d^n}{dx^n} \exp(-x^2) \dots \quad (3.10)$$

$$E(x) = \sum_j (c_j G_j(x)) \quad (3.11)$$

with  $c_j$  being complex amplitudes describing the phase and amplitude of the Gaussian mode. Of course, a given  $M^2$  value can be achieved by an infinite number of modal compositions. For real  $c_j$  one can state that [96]

$$M_x^2 = \frac{\sum_{n=0}^{\infty} ((2n+1) c_n)}{\sum_{n=0}^{\infty} c_n} \quad (3.12)$$

In order to maintain the axial symmetry of the field one needs to exclude all odd  $n$ . Produced seed pulses should maintain as few modes as possible, thus the algorithm starts with the TEM<sub>00</sub> only. Of course the only possible parameter that can be optimized here is the radius of the fundamental mode as its phase is defined as 0 (all other phases refer to the TEM<sub>00</sub> phase) and its amplitude  $c_0$  is defined as 1. The radius of the fundamental mode is also a fit parameter.

If the number of modes is not sufficient to model the desired  $M^2$ , the next higher order modes are considered. The best setting is used as an optimization starting point. In order to maintain symmetry for the two-dimensional case  $c_{nm} = c_{mn}$  can be chosen. The optimization is performed until another local minimum on the penalty function (Eq. 3.13) is reached.

$$\mathcal{P} = \left( |w_0 - w_{0,\text{desired}}| \cdot \frac{10^5}{\text{m}} + |M_0^2 - M_{\text{desired}}^2| \cdot 10^1 \right) \cdot 10^3 \quad (3.13)$$

The factor of  $10^3$  is needed to provide a sufficiently large penalty function, making the used computer program more stable. If the value of the penalty function is still too high ( $\mathcal{P} > 50$ ) after the maximum number of optimization steps is reached, higher order modes are added as described in this paragraph.

## 3.4 FEL output power vs. seed pulse beam quality

The simulation results have been summarized in Figure 3.4 with the power contrast  $\frac{P_{\text{pk}} - \langle P_{\text{SASE}} \rangle}{\langle P_{\text{SASE}} \rangle}$  as the figure of merit.  $P_{\text{pk}}$  stands for the peak output

### 3.4. FEL OUTPUT POWER VS. SEED PULSE BEAM QUALITY

power for the seeded FEL,  $\langle P_{\text{SASE}} \rangle$  for the SASE power time averaged over the FEL photon pulse. Apparently the contrast has a maximum at  $M^2$

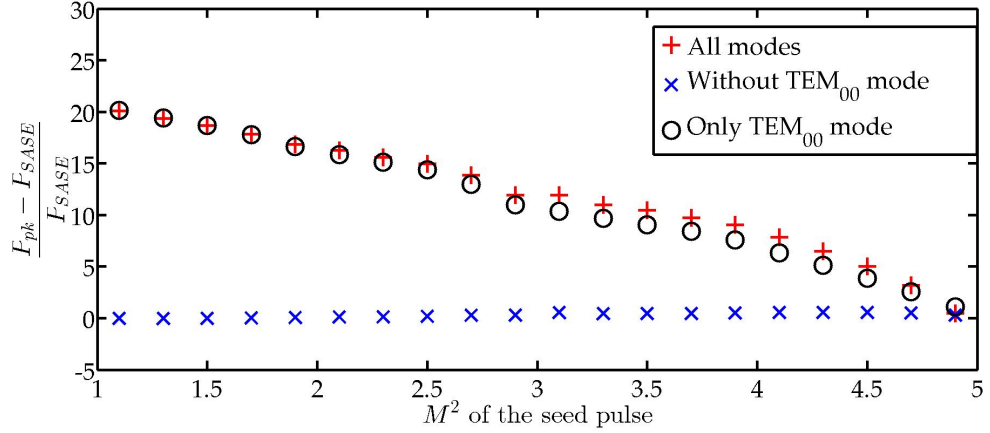


Figure 3.4: Seeded FEL power contrast vs.  $M^2$  of the seed pulse. The circles show the simulation with the same  $TEM_{00}$  mode in terms of intensity and size which is embedded in the seed pulse with the given  $M^2$ . These pulses have by definition an  $M^2$  of 1, however their position on the x-axis refers to the  $M^2$  of the seed pulse they are taken from.

$=1$  and drops rapidly to 0 at an  $M^2$  of about 5, where the power of the fundamental mode is almost zero. In order to give a proper interpretation of these results, all the higher order modes in the seed field distributions have been taken out except for the fundamental  $TEM_{00}$  mode. This seed pulse has by definition an  $M^2$  of 1. It is the embedded  $TEM_{00}$  mode out of the seed file in terms of size and intensity. Then the simulations have been repeated and the results are shown in Figure 3.4 as circles. The comparison between the seeding with the full modal content and the  $TEM_{00}$  only shows that mainly the fundamental mode is amplified in the FEL process. One can see that the power contrast comes almost completely from the embedded fundamental mode, while higher order modes do not contribute to the power contrast. But their presence shows no evidence of destructing the gain of the fundamental mode. This conclusion is supported by the simulation results using the same seed field distribution but without the fundamental mode. The results, also shown in Figure 3.4 as crosses show that the FEL seeded with such fields have almost zero output contrast. Furthermore the drop in the FEL power contrast can be understood in a way that with increasing  $M^2$ , given the waist size is fixed, the  $TEM_{00}$  mode transverse size is decreasing. This means that the fundamental mode does not couple effectively to the electron beam

### 3.4. FEL OUTPUT POWER VS. SEED PULSE BEAM QUALITY

which explains the decreasing contrast. In addition, for larger  $M^2$  the seed pulse energy is distributed among more higher order modes, which means less power in the fundamental mode. This effect further contributes to the decrease of the power contrast. Since in the exponential growth regime the FEL works as a linear amplifier, the plot above should be independent on position along the undulator as long as the FEL is not saturated. This can be seen in Fig. 3.5.

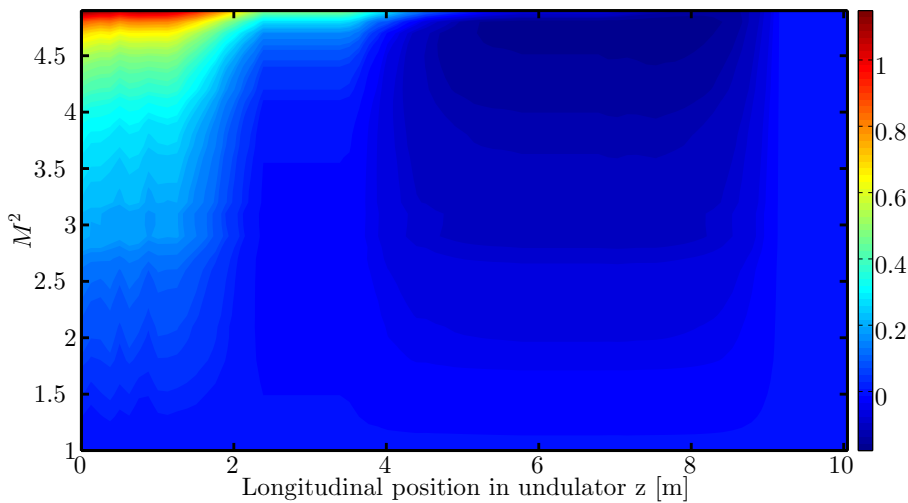


Figure 3.5: Difference (color coded) of the power gain curves for different  $M^2$  in comparison to the  $M^2 = 1$  case, normalized to the power after 10 m for each  $M^2$ . One can see that for the  $M^2 \leq 3$  the gain curve behaviour is the same as for the  $M^2 = 1$  case,

One has to note that power contrast is considered, while in practice one usually measures energy contrast. Therefore in the exponential growth regime the expected energy contrast can be estimated from Figure 3.4 by scaling the power contrast with the ratio between the seed pulse length and the SASE photon pulse length. In addition, the influence of the  $M^2$  of the seed on the  $M^2$  of the FEL has been studied, leading to the following result: For our simulation setup and for any simulated  $M^2$  of the seed pulse the resulting  $M^2$  at the end of the FEL is 1.38, independent from the initial  $M^2$  as shown in Fig. 3.6. This is also the case when the FEL starts from noise, e.g. in SASE mode. This is in agreement with the theoretical description in [85].

As one can see in Fig. 3.8 for the case of  $M^2 = 5$ , that seeding with higher order modes leads to spectra that still show that the FEL did not start from

### 3.5. MODAL RECONSTRUCTION OF INTENSITY PROFILES

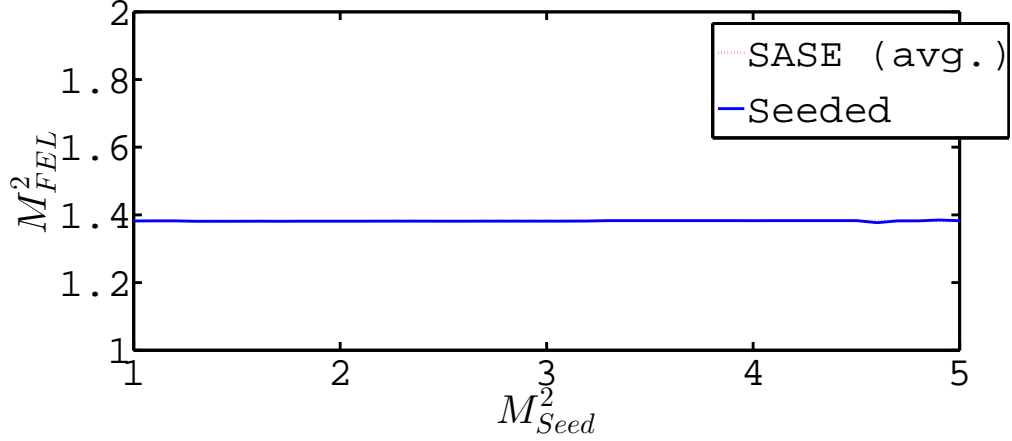


Figure 3.6: Dependence of the  $M^2$  of the FEL radiation in saturation on the  $M^2$  of the seed pulse at the end of the linear regime.

noise, as a second spike at around 37.9 nm is clearly suppressed. However they have the same features as the pure SASE reference spectra. In comparison, the spectra of the fundamental Gaussian mode (Fig. 3.8) show clearly all the advantages that were discussed for HHG seeding. The wavelength of the seeded FEL differs from the SASE case slightly. The central wavelength is shorter for the seeded case, but also dependent on the  $M^2$  of the seed laser, which is visible in Fig. 3.9

## 3.5 Modal reconstruction of intensity profiles

As already mentioned, due to limited space in the electron beam line it is challenging to install a wave front sensor in the vicinity of the undulator. For that reason the  $M^2$  -value is often the only measure for the quality of the seed pulse.  $M^2$  is usually measured using the focus scan technique [97]. An alternative method is to use a mode decomposition of the transverse seed pulse intensity profile as proposed in [95]. The advantage of this technique is that one can measure  $M^2$  from a single intensity profile, provided that the observation screen is at the waist of the seed beam. In the single plane case, the field amplitude can be considered as superposition of Hermite-Gaussian functions [95] as in Eq. 3.9. This approach can be extended into two dimensions as it has been derived in [96]. The two-dimensional time-

### 3.5. MODAL RECONSTRUCTION OF INTENSITY PROFILES

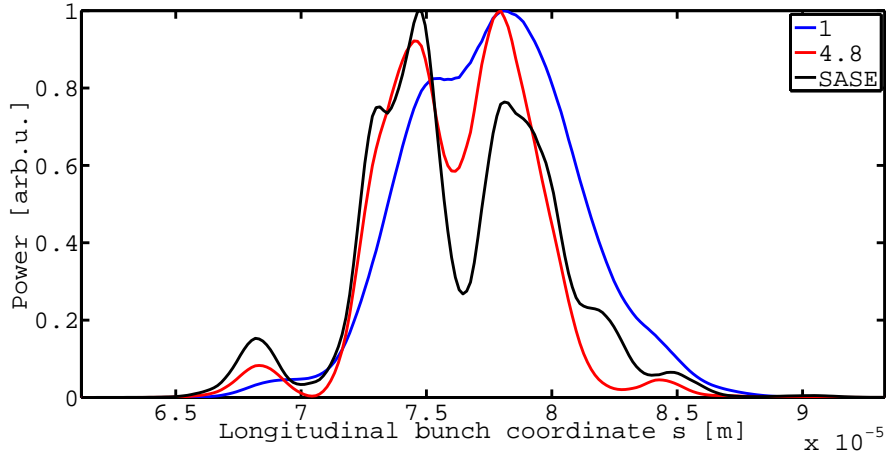


Figure 3.7: Longitudinal power distributions for SASE and two different seed pulses of  $M^2 = 1$  and  $M^2 = 4.8$ . One can see that SASE and  $M^2 = 4.8$  have the same double-spike structure while for the fundamental seeded, only one spike is present.

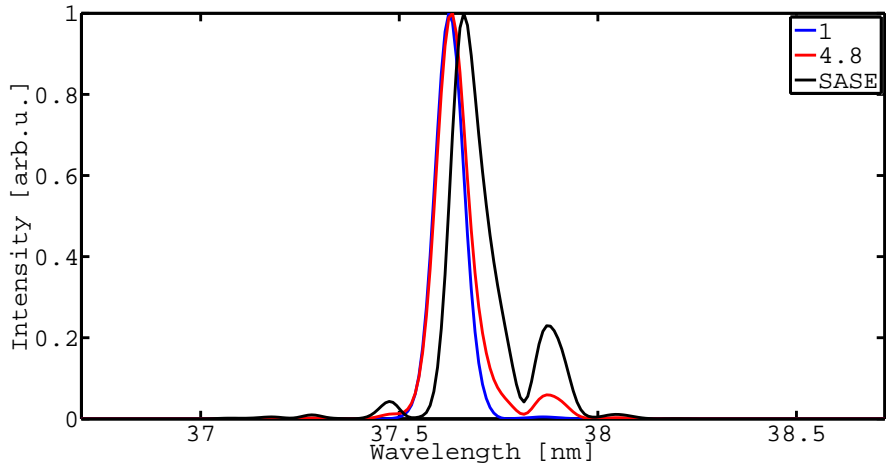


Figure 3.8: Spectra for SASE and two different seed pulses of  $M^2 = 1$  and  $M^2 = 4.8$ . One can see that all three have one dominating spike. For the fundamental seeded FEL, there is only one spike in the spectrum, while for the  $M^2 = 4.8$  and SASE case, two spikes are visible.

### 3.5. MODAL RECONSTRUCTION OF INTENSITY PROFILES

---

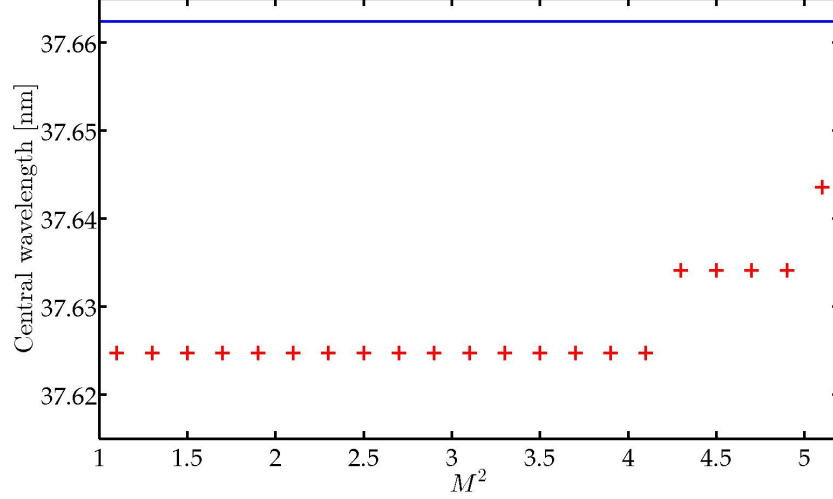


Figure 3.9: Central wavelength in the spectra after three undulators for different  $M^2$  (red crosses). The blue line indicates the central wavelength of the SASE case. The clustering at three different wavelength is an artefact of the limited spectral resolution of the used simulation code.

averaged intensity distribution in the waist is then given by

$$I(x, y) = \sum_{n, n', m, m'=0}^{\infty} [A_{nm} G_n(x) G_m(y) \times A_{n'm'}^* G_{n'}(x) G_{m'}(y)] \quad (3.14)$$

Here one makes use of the fact that the Guoy phase in Eq. (5c) in Ref. [96] can be generalized as:

$$\theta_{m,n} = (m + n + 1) \arctan \left( \frac{z}{z_R} \right) \stackrel{z=0}{=} 0 \quad (3.15)$$

and is zero at the waist. Assuming that the modes are independent of each other, the time-averaged intensities can be added. That means that the elements  $A_{nm} A_{n'm'} = c_{nm} \delta_{nn'} \delta_{mm'}$ , where  $\delta_{mn}$  stands for the Kronecker symbol. For the time-averaged intensity Eq. (3.14) reduces to

$$\bar{I}(x, y) = \sum_{n,m=0}^{\infty} (c_{nm} G_n^2(x) G_m^2(y)) \quad (3.16)$$

where  $c_{nm}$  are the weights representing the intensity content of the individual modes. These coefficients can be calculated as shown in [95] using the Fourier

transform  $\tilde{I}(p_x, p_y)$  of the intensity distribution where  $p_x, p_y$  are the space-frequency variables.

$$c_{nm} = C_0 \int_0^\infty \int_0^\infty \left[ \tilde{I}(p_x, p_y) \Psi_m(\pi^2 w_0^2 p_x^2) \times \Psi_n(\pi^2 w_0^2 p_y^2) p_x p_y dp_x dp_y \right] \quad (3.17)$$

where  $\Psi_n(t) = L_n(t) \exp(-t/2)$  with  $L_n$  the  $n$ -th order Laguerre polynomial. The constant  $C_0$  is a normalization factor which is used to adjust the total power of the reconstructed field to the measured one. Although the method provides unique solutions for the power content coefficients, in practice one has to set an upper limit for the expected highest mode number. This means that the summation in Eq. (3.16) does not go to infinity but is limited to upper summation bounds  $n_{\max}, m_{\max}$ . In the following analysis of experimental data,  $n_{\max} = 8$  was set since the reconstructed intensity profiles yield more than 95% of the original intensity contained within a  $2\sigma$  boundary. The upper bounds depend on the considered profile and have to be adjusted for each particular case. It is worth noting that the precise calculation of  $M^2$  requires high number of modes as noted in [96]. However, the higher order modes tend to have very small intensities, close to the noise level of the detector, and therefore it is difficult to obtain a precise estimate for their power intensity coefficients from experimental data. From this point of view the choice of  $n_{\max}, m_{\max}$  is a compromise between the need to correctly measure  $M^2$  and the desire to keep the measurement error small. These issues have been covered in the discussion on the measurement errors in the section below. In our analysis the waist size  $w_0$  of the fundamental mode ( $w_{00}$ ) is a free parameter which can be fitted with the maximum likelihood approach using the following numerical algorithm: One starts with some initial guess for  $w_0$  and computes the mode content coefficients  $c_{nm}$  where  $n, m = 0 \dots n_{\max}$ . Based on these coefficients, the intensity distribution  $\hat{I}$  using Eq. (3.16) is evaluated. The algorithm then adjusts  $w_{00}$  until the difference  $(\bar{I} - \hat{I})^2$  reaches a minimum.

### 3.6 Comparison to experimental results

The procedure described above has been used to analyze the 38 nm HHG seed pulse at the sFLASH direct seeding experiment [77, 94]. The transverse intensity distribution at the waist is shown in Figure 3.10. Apparently the measured intensity distribution is tilted and asymmetric. There are three sources for this [101].

### 3.6. COMPARISON TO EXPERIMENTAL RESULTS

---

1. The injection beam line which transports the seed pulse from the harmonics source to the undulators rotates the beam by about  $11^\circ$ , thus introducing coupling between x and y.
2. Astigmatism which comes directly from the source leads to asymmetry and has been experimentally studied in [94].
3. The NIR laser beam used for the production of the harmonics is also already astigmatic.

This asymmetry leads to odd modes contributing to the intensity distribution. Since in our analysis two-dimensional Fourier transform of the intensity distribution has been done, the decomposition algorithm is not restricted to even modes, to which the algorithm was limited before in the simulations, and to determine the modal content of this intensity profile the odd modes have been included.

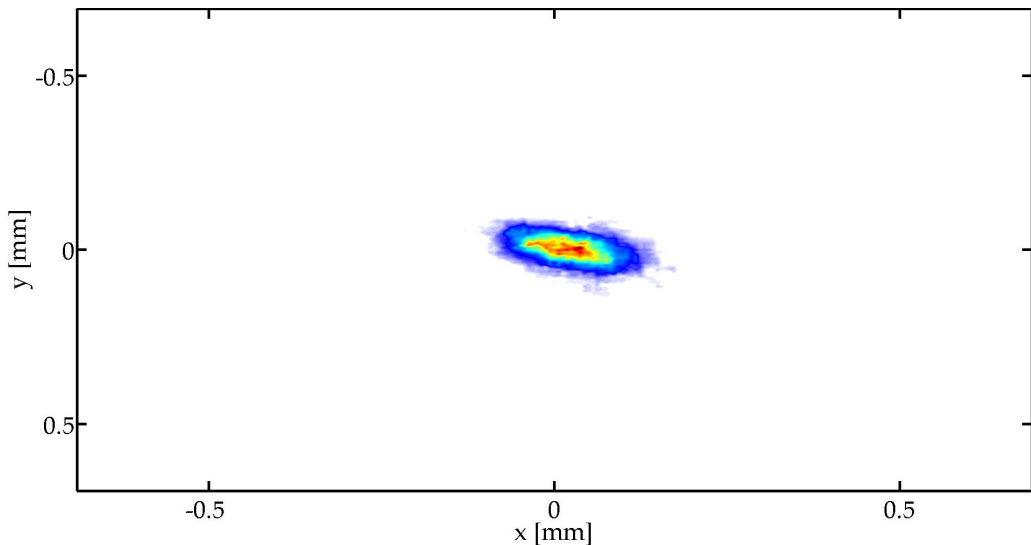


*Figure 3.10: Transverse intensity distribution of the 38 nm HHG seed beam used at the direct seeding experiment sFLASH. It was measured waist, color coded is the intensity measured by the camera.*

The modes decomposition yields the power content coefficients as shown in Figure 3.11. With these power coefficients one can calculate  $M^2$  of the field. There are at least two possibilities to do this. The first option is to use the formula derived in Ref. [96] which directly relates the beam quality

### 3.6. COMPARISON TO EXPERIMENTAL RESULTS

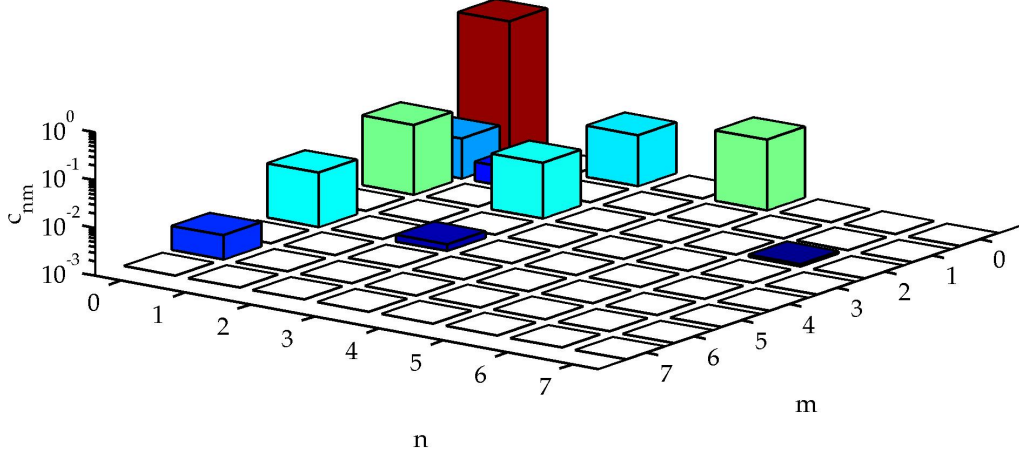


Figure 3.11: Power content coefficients  $c_{nm}$  of the harmonics beam shown in Fig. 3.10. The  $TEM_{00}$  mode is with around 90% of the overall intensity the strongest mode. Power content coefficients smaller than  $10^{-3}$  are colored white. More than 96% of the pixel value intensity is contained in the 64 reconstructed modes.

factor to the power content coefficients:

$$M_x^2 = \frac{\sum_{n,m=0}^{\infty} ((2m+1) c_{nm})}{\sum_{n,m=0}^{\infty} c_{nm}} \quad \text{and} \quad M_y^2 = \frac{\sum_{n,m=0}^{\infty} ((2n+1) c_{nm})}{\sum_{n,m=0}^{\infty} c_{nm}} \quad (3.18)$$

Applying Eq. (3.18) yields  $M_x^2 = 2.45$  and  $M_y^2 = 2.39$ . This result is in a very good agreement with the result obtained with the second method which is to numerically propagate the field over a certain distance and thus obtain the dependence of the beam size versus longitudinal position  $w(z)$  and then analyze this data in the same way as a focus scan technique by exploiting the formula  $M^2 = \frac{\pi w_0}{\lambda z} \sqrt{w^2(z) - w_0^2}$ . One can estimate the  $M^2$  of the HHG seed beam to be  $M_x^2 = 2.2 \pm 0.6$  and  $M_y^2 = 2.0 \pm 0.6$ . The error estimation for the first contribution has been done using a Monte Carlo simulation considering uncertainties in the determination of the wavelength and beam size due to finite camera pixel size, yielding an error of about 20%. This Monte Carlo simulation works as follows: First, a field consisting of a random set of modes is generated and the corresponding intensity profile calculated. This continuous profile is then converted to a grid with a size corresponding to the size of the camera pixel, typically in the order of few  $\mu\text{m}$ . Then noise is added and finally a modal reconstruction takes place. An uncertainty of 10%

### 3.6. COMPARISON TO EXPERIMENTAL RESULTS

---

in the wavelength is the worst estimate. Since in the reconstruction the error on  $w_0$  dominates by a far, the error in wavelength is almost negligible. After the reconstruction, the  $M^2$ -value is calculated. Obviously, due to the introduced noise, finite grid size and wavelength uncertainty the calculated  $M^2$  differs from the true one. The above described procedure has been repeated  $10^5$  times, which is roughly a factor of 100 for noise and grid size, and an additional factor of 10 for the wavelength uncertainty. For different assumed measurement errors, the resulting values are plotted in Fig. 3.12. The graph in this figure shows the probability for a given measurement result to occur. Another error to the measurement is introduced if the measurement has not been done directly at the waist position. This error source has also been studied by scanning the z-position. It turns out that within one Rayleigh length this leads to an error of 20% or less, independent of the actual numerical value. This error adds quadratically to the errors due to noise, finite grid size and wavelength uncertainty which gives a final random error on the  $M^2$  value of approx. 28%. Bunch-to-bunch fluctuations are not an error source as this method can be applied to single intensity images, although they would be interesting to study.

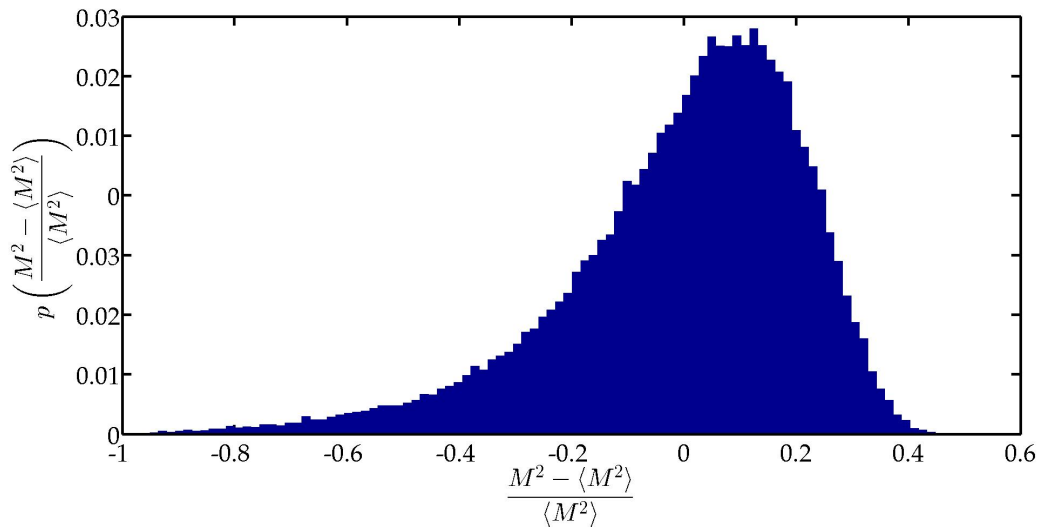


*Figure 3.12: Probability distribution of the  $M^2$  values determined using Monte Carlo simulation. This only covers uncertainties from the measurement, not bunch-to-bunch fluctuations.*

A modal decomposition of the measured seed profile shown in Fig. 3.10 has been performed and an input field distribution for GENESIS containing the power content coefficients from the modal reconstruction has been prepared. It has been assumed that the profile was taken at the waist and the phase

### 3.6. COMPARISON TO EXPERIMENTAL RESULTS

differences between the modes have been assumed to be zero. All modes are generated in roughly the same time in the same, small volume. One can then say they all should have the same phase. During the transport, the shortness of the seed pulse should prevent heating of the mirrors to change photon pulse properties during the irradiation. As all modes have the same wavelength, dispersion is not an issue. At the waist, in the undulator, the Gouy phase is 0. If we assume the wavefront of the seed pulse in the gas cell to be plane, than the phase relation in the focus will be the same as in the source. The FEL output power for the seeded and unseeded case has been calculated for the parameters listed in Table 6.1. The power contrast along the internal bunch coordinate is plotted in Fig. 3.13 behind the last undulator. The simulated contrast for this case is in a good agreement with the expected value for an  $M^2$  of 2.2 in Figure 3.4 and with the experimentally measured energy contrast reported in [77]. It should be stressed that in this reference, an energy contrast is reported with a ratio between the SASE photon pulse length and the seed pulse length of about 4. The seeded FEL pulse energy was  $(1.3 \pm 0.5) \mu\text{J}$  while the unseeded SASE pulse had an energy of about 300 nJ. The duration of the seeded FEL pulse is determined by the duration of the seed pulse of approx. 15 fs rms while about 60 fs rms where estimated to lase at SASE mode.

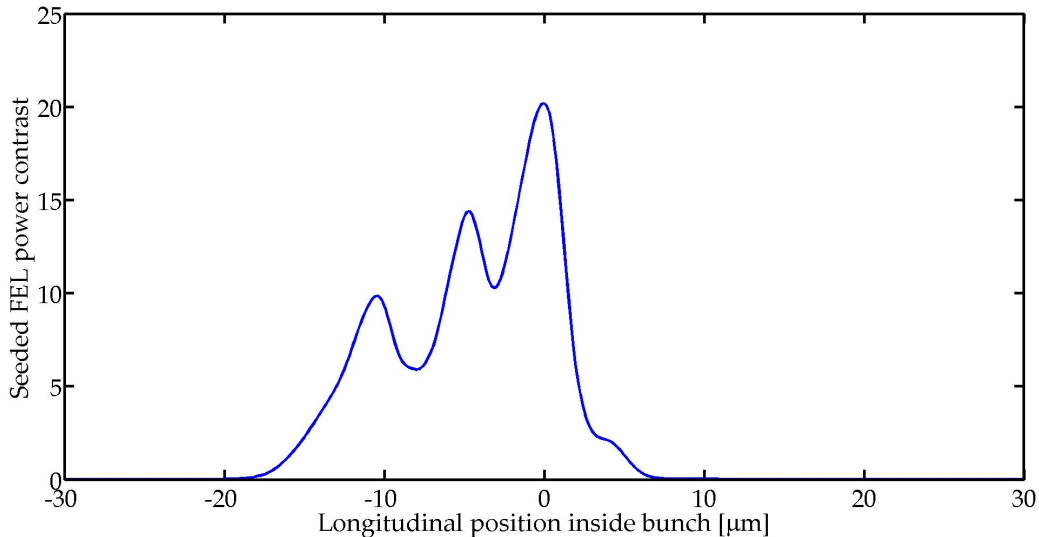


*Figure 3.13: Simulated power contrast along the internal bunch coordinate  $s$ . This is one typical result for one electron bunch.*

## 3.7 Conclusion

The influence of  $M^2$  onto the achievable power contrast between the directly seeded FEL radiation and SASE has been studied considering the hardware setup and the electron beam properties. It has been found that the power contrast decreases rapidly with  $M^2$  reaching 0 at an  $M^2$  of about 5. A modal decomposition using a single transverse intensity profile has been discussed as a method for  $M^2$  measurement. This technique has been applied to the experimental data obtained at the sFLASH experiment and it has been shown that the power contrast from a GENESIS simulation using the reconstructed field is in a good agreement with the experimental observation at sFLASH, taking into account the measured  $M^2$  data and the ratio between seed pulse and bunch duration.

# Chapter 4

## Optimization of the Source Point of a Direct HHG-seeded FEL

In the range from 10 to 40 nm a direct high-harmonic generation (HHG) seeding option was one of the possible seeding schemes foreseen for FLASH2 to improve the FEL radiation quality. For experiments it is important to have the saturation point of the FEL radiation at a constant longitudinal position, close to the end of the undulator. On the other hand, one would like to keep the waist of the HHG seed at a fixed longitudinal position, too, for all wavelengths. In this paper, we present an optimized and adaptable configuration of the undulator positions, assuming fixed positions for both, the HHG seed waist and the FEL radiation saturation point.

### 4.1 Seeding option at FLASH2

For a wavelength range between 10 nm and 40 nm an HHG seeding option was one possible seeding scheme to be realized. A novel gas jet target has been developed for the seed source [102], which is necessary as the needed seed power increases with decreasing wavelength, while the conversion efficiency goes down with the harmonic number [103]. Alternatively, for the longer wavelengths, a target similar to the one of the sFLASH experiment (where seeding at 38.1 nm has already been demonstrated [77, 104]) can be used. In order to reduce the overall number of mirrors and therefore the technical complexity of the HHG seed injection beam line, it is desirable to keep the seed waist position fixed. According to **zemax** calculations for the HHG setup at FLASH2, this point is inside the third undulator. Seeding with HHG is

## 4.2. NUMERICAL SIMULATIONS

---

done with a gas target. For longer wavelengths, a single gas-cell setup can be used, similar to the one used at sFLASH. It has been demonstrated to work at a wavelength below 40 nm, although only at 10 Hz [77]. In order to exploit the advantage of superconducting accelerators, namely the high bunch-to-bunch repetition rate, a laser system at DESY has been developed that has the required stability and power needed to drive an HHG source [105, 106]. This source fulfilled specifications, however it has not been tested at FLASH2.

The photon users have to image the saturation point of the radiation to the respective sample. This requires high-precision adjustment of XUV optical elements. In general, for each wavelength in the undulator the longitudinal position where the FEL goes into saturation (the so-called source point) is different. Since the users may want to have different wavelengths in the experiment, they have to re-align the setup after every wavelength change. The position of the saturation point depends among others on the FEL gain length and wavelength. The required effective undulator length increases with decreasing wavelength. For SASE one can move the saturation point by opening (or closing) undulators upstream such that the required saturation length is achieved inside the last undulator. If the position of the source point (the onset of FEL saturation) is kept at a fixed position, then from the users point of view, a focus adjustments will not be needed.

## 4.2 Numerical Simulations

The goal of the numerical studies is to determine the optimal undulator configuration (gaps closed or opened), while keeping the HHG seed waist and FEL saturation point position fixed.

The individual simulations were performed using the full 3D FEL simulation code GENESIS 1.3 [107]. The FLASH2 undulator system consists of 12 variable gap undulators. The undulator parameters are given in Table 4.1. For seeding, only the undulators #3 through #12 are used, as for the shortest possible wavelength of 4 nm ten undulators are sufficient to reach saturation with seeding. For SASE, however, all twelve would be used. The position of the waist of the HHG beam is located in undulator module #3. It is assumed that the gap of this undulator is always closed as the interaction of the seed and the electron beam takes place here. It has been also assumed that undulator gap #12 is always closed since the saturation point should be located here. The gaps of the remaining eight undulators #4 through #11 can be opened or closed independently. Undulators with gaps opened are treated as drift spaces. All consecutive drift spaces are simulated as one long drift space. The gap of undulators #4 through #11 is assumed to be either

### 4.3. OPTIMIZATION OF UNDULATOR GAPS CONFIGURATION

Table 4.1: Typical FLASH2 parameter set used in the numerical simulations. For seeding only 10 undulators are considered. These parameters are design parameters for the operation of FLASH 2

<b>Undulators</b>		
Number of undulators		10 (out of 12)
Undulator period	$\lambda_u$	31.4 mm
Undulator length	$L_u$	2.3864 m
Periods per undulator	$N_{\text{periods}}$	76
Undulator intersection	$L_{\text{drift}}$	87.92 cm
Max. K parameter (rms)	$K_{\text{rms}}$	2.0
<b>HHG pulse</b>		
Temporal shape		Gaussian
Wavelength	$\lambda_{\text{HHG}}$	37.6 nm
Pulse energy	$E_{\text{HHG}}$	70 pJ
Peak power	$P_{\text{max,HHG}}$	2.5 kW
Duration (rms)	$\tau_{\text{HHG}}$	12 fs
Rayleigh length	$z_{\text{ray}}$	2 m
$M^2$	$M^2$	1
<b>Electron beam</b>		
Peak current	$I_{\text{max}}$	2.5 kA
Bunch Length (rms)	$\sigma_{e^-}$	30 $\mu\text{m}$
Energy	$E$	700 MeV
Energy spread	$\sigma_E$	500 keV
Normalized emittance	$\epsilon_{x,n}$	1.4 mm · mrad
	$\epsilon_{y,n}$	1.4 mm · mrad

opened or closed. Additional 2.5 m of virtual undulator length are simulated downstream of undulator #12 to check for FEL saturation.

### 4.3 Optimization of undulator gaps configuration

For many wavelengths the total available undulator length at FLASH2 ( $\approx 30$  m) will be considerably longer than the saturation length. In such cases some of the undulator gaps have to be opened in order to reach saturation in the last undulator (i.e. to keep the saturation point fixed). Obviously, more than one possible undulator gap configurations are possible. In this section the

### 4.3. OPTIMIZATION OF UNDULATOR GAPS CONFIGURATION

optimization process for the undulator configuration will be shown using the initial conditions listed in table 4.1. With these initial conditions a number of steady-state simulations has been performed in order to find a starting point for further optimization. The used figure of merit has been the peak power of the FEL radiation in the last undulator. The undulator configuration with the highest output power has been used in the next iteration of the optimization. After this time-independent run, a time-dependent simulation has been performed in order to check spectral properties of this undulator setting.

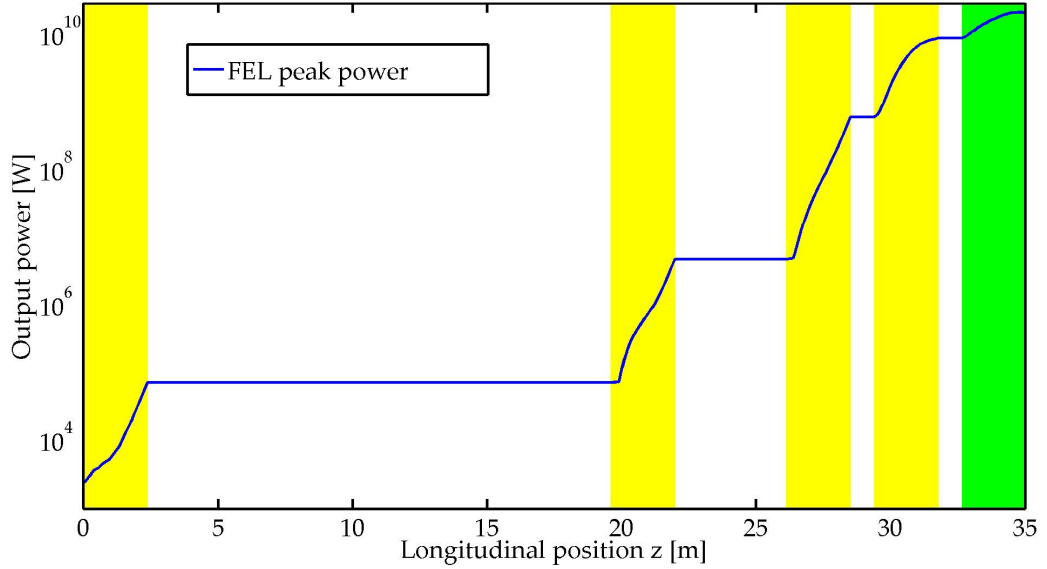


Figure 4.1: Best undulator gap configuration for a time-dependent simulation of HHG seeding at 38 nm at FLASH 2. Yellow bars mark closed undulators. The green bar is an additional undulator added for the simulation to check whether the FEL is in saturation or not. The blue line is the FEL peak power.

For the optimal setting, one can simulate the difference of SASE and seeding performance of the FEL. This is shown in Fig. 4.2. At the longitudinal position with the highest energy contrast, the power spectra are shown in Fig. 4.3(a) and the longitudinal power distributions are shown in Fig. 4.3(b) the radiation pulse yields around  $1.2 \mu\text{J}$  SASE pulse energy (about 12 MW of power) and about  $21 \mu\text{J}$  (roughly 1 GW) in seeded operation. This is inside an undulator, which means that in the experiment one might change beam parameters slightly to increase the saturation length a little, so that the point of the maximum contrast would move towards the end of the undulator.

As shown in Fig. 4.1 for the optimal setting, five consecutive undulator gaps have to be opened. This large drift space of about 17 m is introducing

### 4.3. OPTIMIZATION OF UNDULATOR GAPS CONFIGURATION

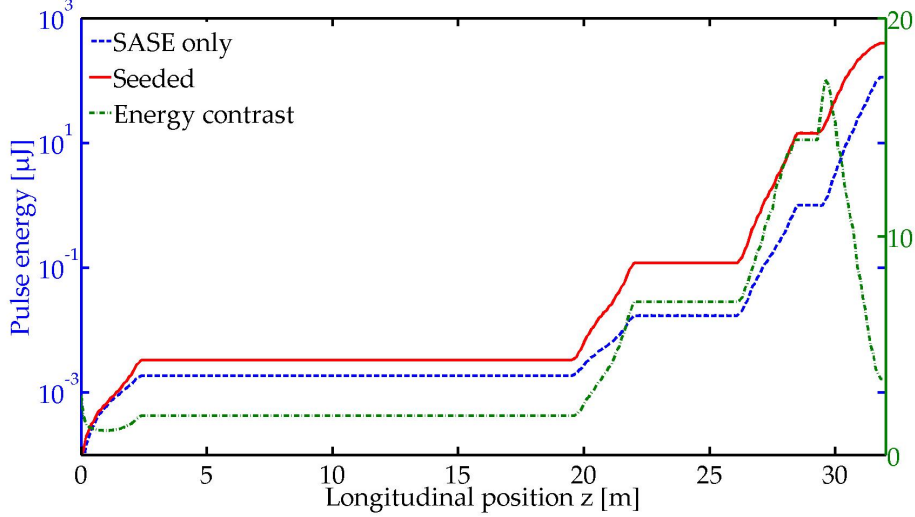
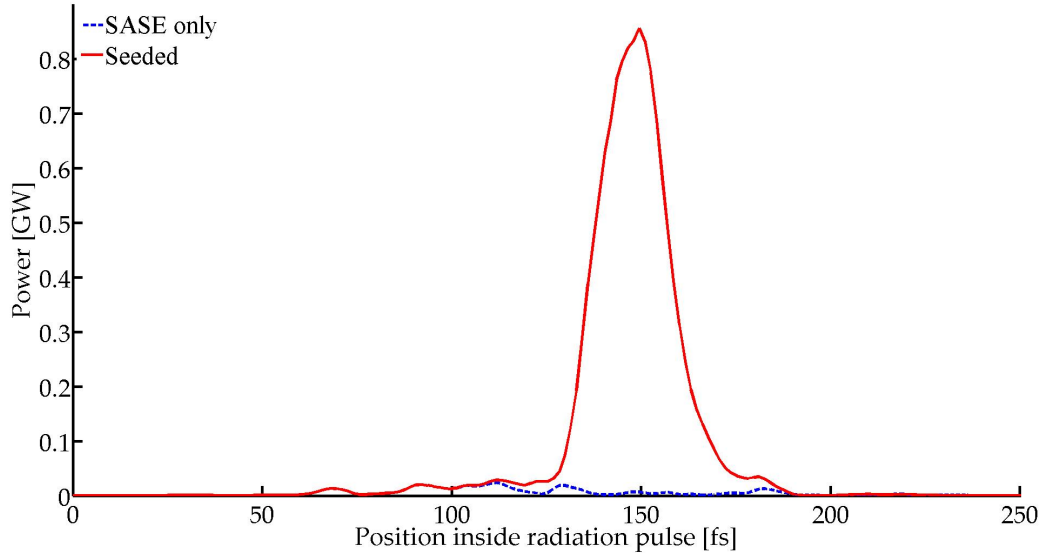


Figure 4.2: FEL pulse energies and energy contrast. Since the seeded FEL has a shorter saturation length, the energy contrast increases with the active undulator length. At around 30 m, the seeded FEL runs into saturation, while the SASE FEL pulse energy still increases, therefore the contrast decreases.

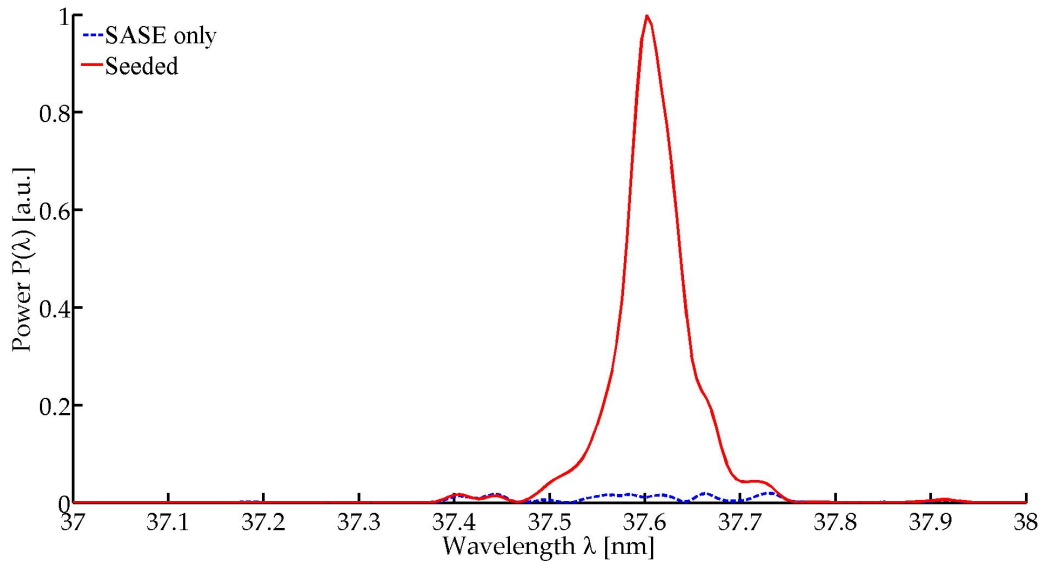
a slippage between electron bunch and FEL radiation. Due to the irregular arrangement of active undulators the slippage between radiation and electron motion introduces a complicated temporal profile of electron bunching and FEL radiation the effect of which is illustrated in Fig. 4.4(a). Inside undulator #9 the bunching introduced in undulator #3 will cause radiation while the radiation pulse from undulator #3, carrying a peak power of about 75 kW, will "seed" the bunch at a different longitudinal position. In undulator #11, after another drift space, the first (left) and second (right) bunched regions inside the bunch start radiating. Due to the slippage inside the undulator, the first bunched region becomes wider. In undulator #12, both bunched regions radiate FEL pulses with a temporal difference. The undulator configuration is imprinted to the electron bunch in terms of bunching.

Since the pre-pulse seen in Fig. 4.4(a) carries a significant amount of power, it could decrease the contrast and/or the temporal resolution of the user experiment. In order to study how to reduce the negative effect of this pre-pulse, several simulations were performed using different temporal delays within in a range of  $\pm 6\tau_{\text{HHG}}$  between the HHG seed and electron bunch. As shown in Fig. 4.5(a) the second pulse almost vanishes when the power peak of the seed pulse passes the first undulator entrance 7 fs prior to the maximum of the current of the electron bunch. The profiles for the optimal contrast

### 4.3. OPTIMIZATION OF UNDULATOR GAPS CONFIGURATION



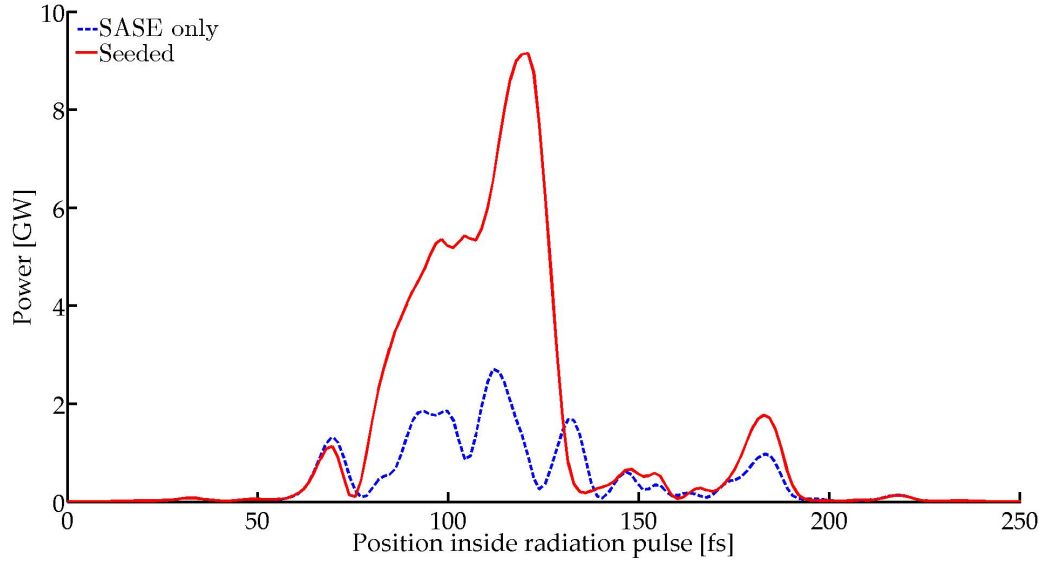
(a) Longitudinal power distribution



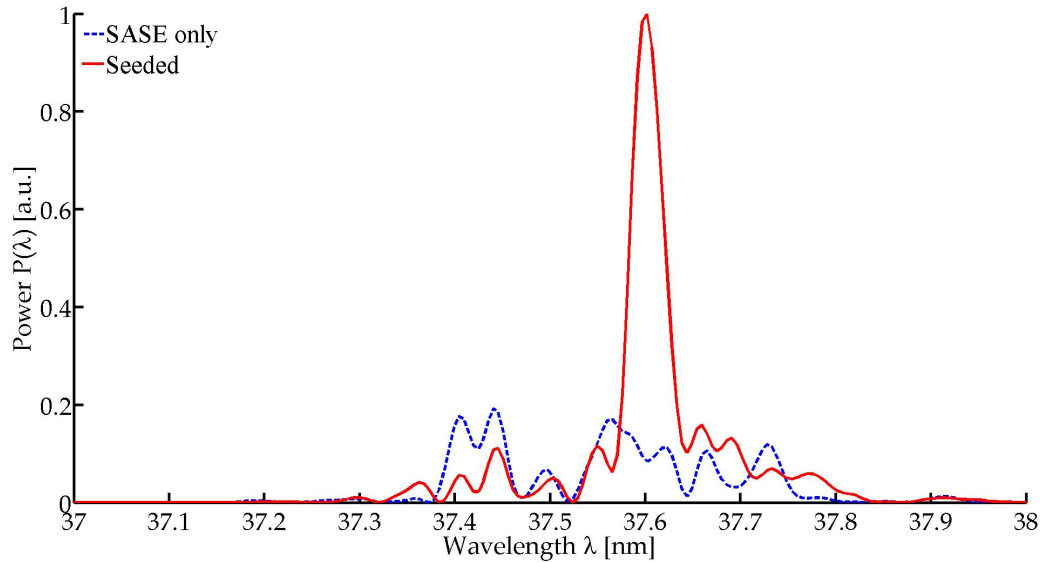
(b) Spectra

Figure 4.3: Longitudinal power distribution (a) and spectra (b) at the position of the highest energy contrast (instead of the end of the last undulator as in Fig. 4.5 and Fig 4.4)) for the optimized temporal offset of 7 fs, optimized in terms of pre-pulse reduction. The head of the pulse is to the right. The radiation pulse yields an energy of 21  $\mu$ J.

### 4.3. OPTIMIZATION OF UNDULATOR GAPS CONFIGURATION



(a) Longitudinal power distribution



(b) Spectra

Figure 4.4: Longitudinal power distribution (a) and spectra (b) for a temporal offset of 54 fs, i.e. the electron bunch peak current arrives at the entrance of the first undulator 54 fs earlier than the HHG seed pulse. The head of the pulse is to the right. The radiation pulse yields an energy of 328  $\mu$ J.

#### 4.4. SUMMARY AND OUTLOOK

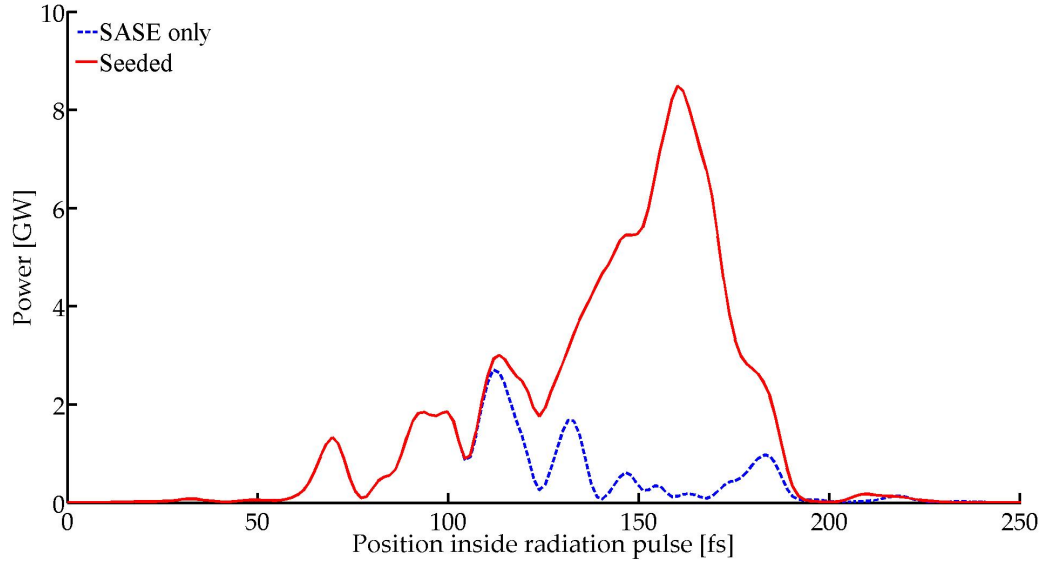
---

don't have this feature and show a nice, almost perfect Gaussian shape. One has to point out that the spectra and power distributions in Fig. 4.4, 4.5, 4.3(b) are typical results of the **GENESIS** simulations for a variety of random number seeds. In this case the seeded FEL pulse has an energy of about  $395 \mu\text{J}$ , while SASE contributes  $114 \mu\text{J}$  (see Fig. 4.2). However, one has to note that in the studies presented above a optimistic estimation of the HHG seed pulse parameters has been considered, e.g. the  $M^2$  of 1. As listed in Table 4.1 the assumed HHG pulse energy is about  $70 \text{ pJ}$  at the undulator entrance. Since  $70 \text{ pJ}$  is a optimistic estimation, a number of simulations has been performed for HHG seed pulse energies in the range from  $50 \text{ pJ}$  to  $10 \text{ nJ}$ . The maximum energy contrast which can be expected from simulation can be seen in Fig. 4.6. The pulse length for the seeded FEL pulse is about  $15 \text{ fs}$  compared to  $40 \text{ fs}$  for the SASE case.

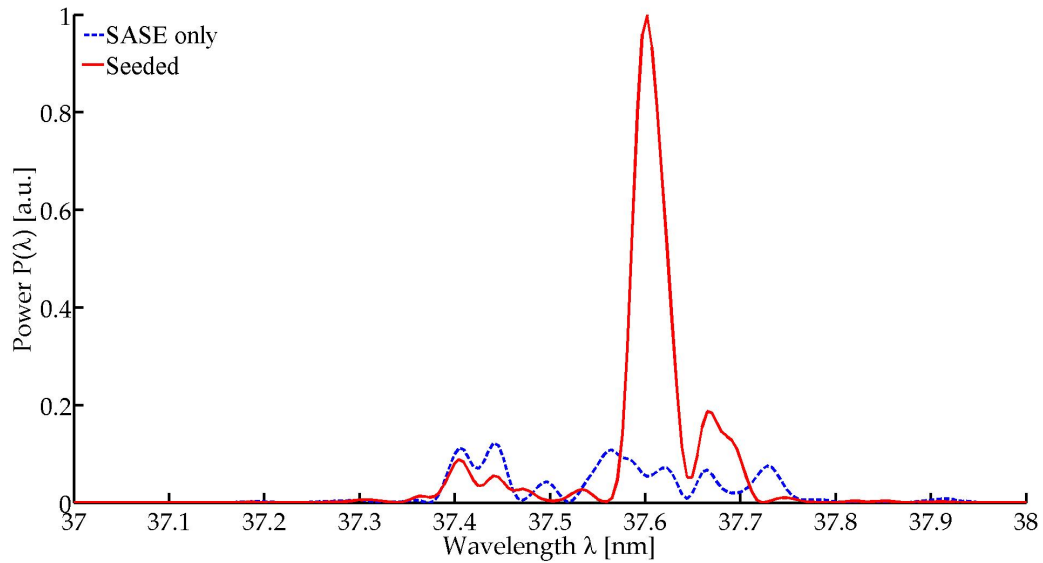
## 4.4 Summary and outlook

The direct HHG seeding option for FLASH II has been studied by the means of numerical simulations, assuming fixed positions for the HHG seed waist and the FEL saturation point. For a set of design FLASH2 and HHG parameters an optimized undulator gap configuration has been found and investigated. The effect of the temporal offset between HHG seed and electron bunch on the longitudinal power distribution has been examined. However, optimization of this parameters leads to a longer FEL radiation pulse. It has been shown that at the position of the maximum energy contrast the radiation pulse is shorter but also less powerful and carrying less energy.

For shorter wavelength, the saturation length becomes longer, thus more undulators need to be used. This means the number of possible undulator setting changes until at the shortest wavelength only one possible setting, all undulators closed, exists. The investigations presented in this chapter should be repeated for a set of representative, shorter wavelength.



(a) Longitudinal power distribution



(b) Spectra

Figure 4.5: Longitudinal power distribution (a) and spectra (b) for a different timing offset. The peak power of the HHG seed radiation pulse arrives 7 fs earlier than the peak current of the electron beam (i.e. the seed pulse has been shifted by +61 fs with respect to Fig. 4.4). The head of the pulse is to the right. The radiation pulse yields an energy of 395  $\mu\text{J}$ .

#### 4.4. SUMMARY AND OUTLOOK

---

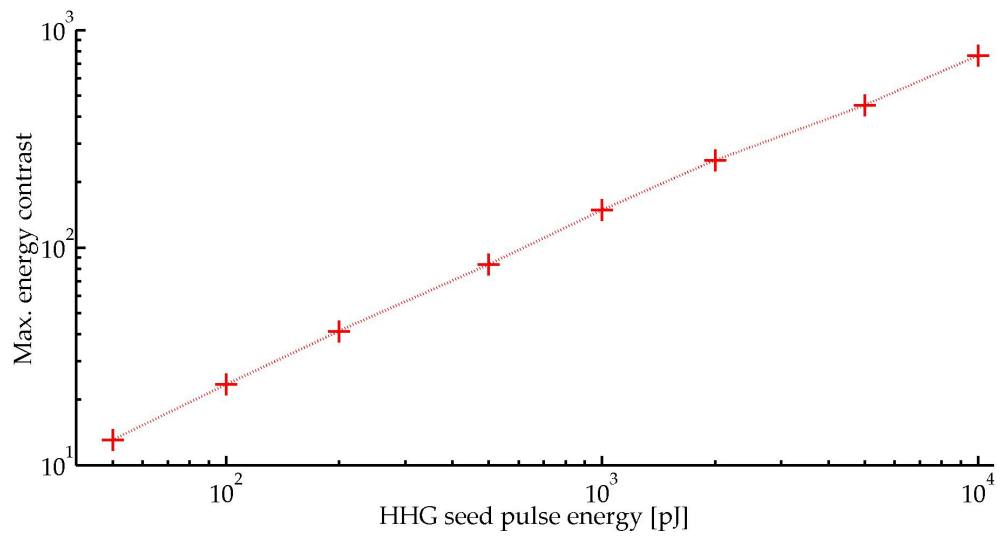


*Figure 4.6: Maximum pulse energy contrast in dependence of the HHG seed pulse energy. The simulation assumed the optimum timing offset and undulator configuration and shows values for the position of best contrast along the undulator beam line.*

# Chapter 5

## High-gain harmonic generation

### 5.1 Data handling between different simulation codes

In order to simulate the process of high-gain harmonic generation (HG HG) one usually splits up the simulation into three parts (compare Fig. 5.1).

- Modulator simulation: Simulate energy modulation due to electron-laser overlap (FEL-Simulation)
- Dispersive section simulation: Electron tracking through a dispersive section, e.g. dipole chicane (beam tracking)
- Radiator simulation: Simulate FEL radiation process due to the induced bunching (FEL-Simulation)

`GENESIS1.3` is capable of loading not only average sliced radiation and beamlet files (called "radiation files" and "beam files") where the radiation and electron beam properties are averaged over a longitudinal distance but also particle distribution files and radiation field files which contain properties of the individual particles and volumes. In addition it is capable to track the input particle distribution through a symmetric D-shape chicane consisting of 5 drift spaces and 4 dipole magnets. However, all drift spaces and dipoles respectively have equal lengths. In addition, collective effects as space charge, coherent synchrotron radiation and so on, are not covered within the simulation of a chicane. However, `GENESIS1.3` offers the possibility to apply 6D transfer matrices to any imported particle distribution. Those matrices describing the second order particle behaviour - but no collective effects - can be obtained using `elegant`.

## 5.1. DATA HANDLING BETWEEN DIFFERENT SIMULATION CODES

---

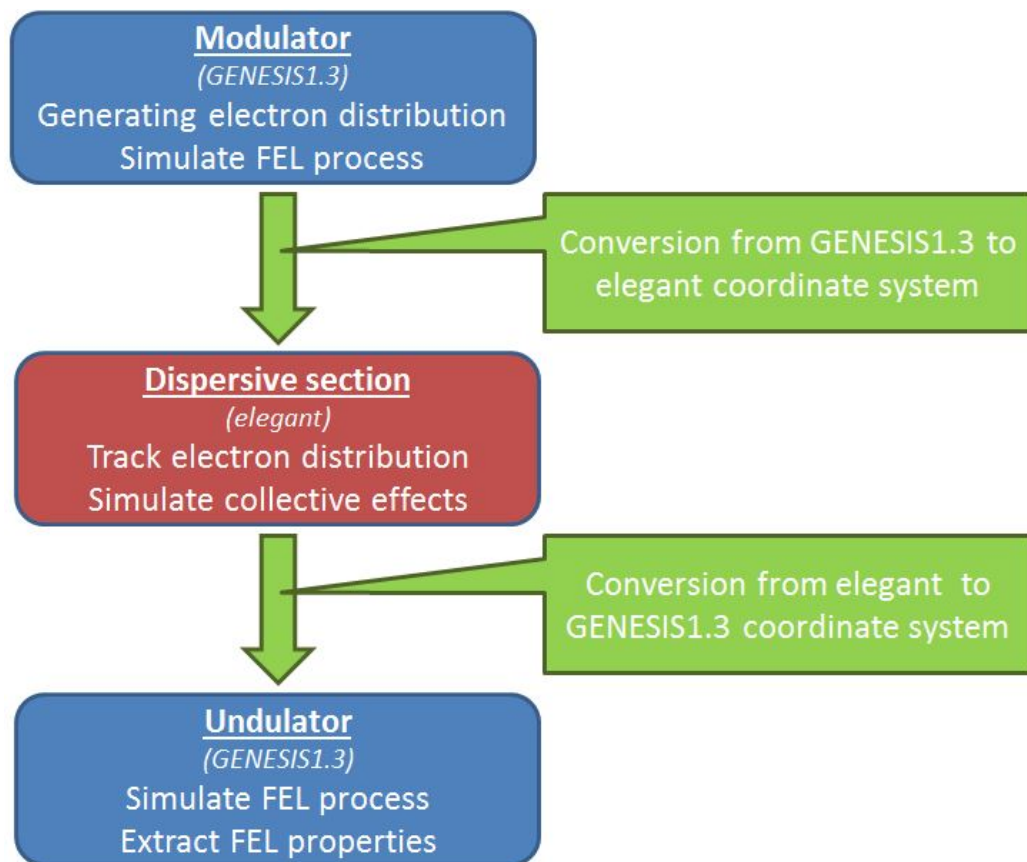


Figure 5.1: Usual HGHG simulation using three individual simulations (Modulator, dispersive section, and radiator)

Several codes have been developed in order to deal with such collective effects and more. While importing electron beam tracking results to FEL simulations is widely used, one usually does not import particle distributions out of FEL simulations to electron tracking codes. In the rare examples found averaged beam properties are used, not the particle distributions. Since `GENESIS` and `elegant` have different coordinate systems, a conversion is needed.

### 5.1.1 Data exchange from `GENESIS1.3` to `elegant`

One of the frequently used 6D particle tracking codes is `elegant` [108] developed at APS-ANL. `elegant` uses the self-describing data sets format ("SDDS") to save data, which is convenient as many codes such as `ASTRA` and `CSRwake` are also capable of importing SDDS particle distributions. The code `GENESIS1.3` uses the hierarchical data format ("HDF") which is freely available and supported by for example `MatLab`, `Java`, `Mathematica`, and `Python`. Both data types are convertible to each other. But `GENESIS1.3` and `elegant` not only differ in the file format, but in the data that is saved:

`GENESIS1.3` has the same number of particles for each longitudinal simulation slice. In order to model a current distribution along the longitudinal axis for each of the slices a beamlet current is assigned - this means that not all simulation particles have the same charge! For each particle within a slice 6 coordinates are saved. The transverse position  $x$  and  $y$  in meter, the transverse particle momentum  $p_x$  resp.  $p_y$ , the energy in terms of the relativistic Lorentz factor  $\gamma_r$  and the longitudinal position inside the slice in terms of the ponderomotive phase  $\Theta \in [-\pi : \pi]$ .

`elegant` has a beam current assigned to each particle distribution file, while each individual particle has the same charge. The 6 phase-space coordinates are the transverse positions  $x$  and  $y$ , the angle between the beams tangential and the particles trajectory  $x'$  and  $y'$ , the particles relativistic Lorentz factor  $\gamma_r$  and the longitudinal position inside the bunch in meter  $z$ . See Table 5.1 for more details.

In order to model the correct current distribution in `elegant` one needs to know the current distribution. For the modeling of the current distribution, not all particles out of a `GENESIS1.3` distribution will be taken, but a number  $N_{\text{selected}}$  scaling with the current will be randomly chosen from the available particles.

$$N_{\text{selected}} = N_{\text{slice}} \frac{I_{\text{slice}}}{I_{\text{max}}} \quad (5.1)$$

with  $N_{\text{selected}}$  the number of particles to be written to the elegant particle

## 5.1. DATA HANDLING BETWEEN DIFFERENT SIMULATION CODES

---

distribution,  $N_{\text{slice}}$  the number of particles per slice in GENESIS,  $I_{\text{slice}}$  the current of the slice and  $I_{\text{max}}$  the current of the slice with the maximum current.

*Table 5.1: Coordinate systems and conversion between GENESIS1.3 and elegant*

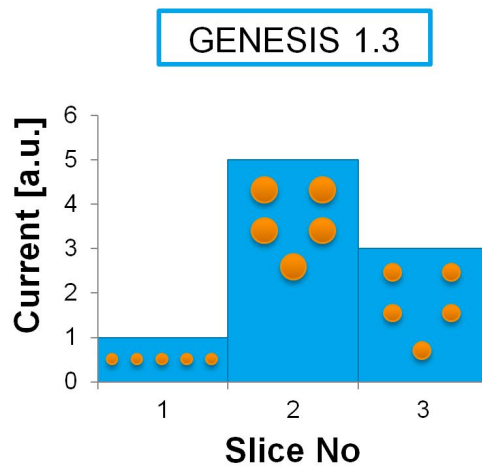
Property	GENESIS1.3	elegant	conversion
Transverse position	$x$	$x$	$x = x$
	$y$	$y$	$y = y$
Transverse angle	$x_p$	$x'$	$\frac{x_p}{\beta_z \gamma_r} = x'$
	$y_p$	$y'$	$\frac{y_p}{\beta_z \gamma_r} = y'$
Longitudinal position	$N_{\text{slice}}, \Theta$	$z$	$\left(\frac{\Theta}{2\pi} - \frac{1}{2} + N_{\text{slice}}\right) \cdot \lambda_{\text{rad}} = z$
Energy	$\gamma_r$	$\gamma_r$	$\gamma_r = \gamma_r$
Charge/Current	$I_{\text{slice}}(n)$	$Q_{\text{bunch}}$	$\sum (I_{\text{slice}}(n)) \frac{\lambda_{\text{rad}}}{c} = Q_{\text{bunch}}$

### 5.1.2 Data exchange from elegant to GENESIS1.3

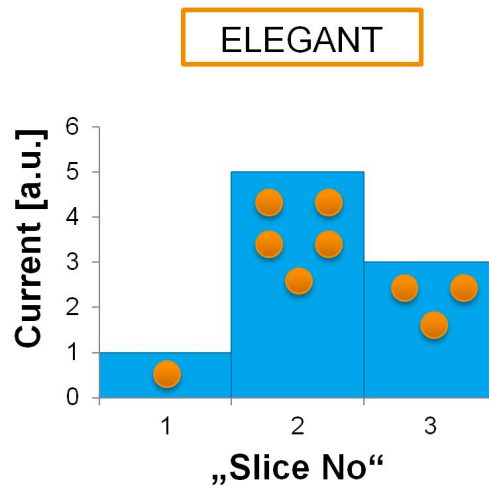
After `elegant` has tracked the particle distribution through whatever beam line, the conversion of the resulting data has to take place. This is needed as `GENESIS1.3` assigns the current a property that is constant over the length of one slice while `elegant` calculates the current from the number of particles per length (See Fig. 5.2). There are several conditions that must be fulfilled:

All particles have to be sorted by their longitudinal position in the bunch. Then the bunch is cut into  $N_{\text{total}}$  slices, which - depending on their motion in the simulated longitudinal phase-space can lead to a bunch with a different number of slices than the imported particle distribution. The number of particles per slice is then used to assign a current  $I_{\text{slice}}$  to each of the slices.

In the next step, one needs to fulfill the conditions required for `GENESIS1.3` particle distribution files: First, all slices have to have the same number of particles per slice, which then has to be an integer multiple of the number of simulation bins (`NBINS`), which by itself needs to be a multiple of 4. For most simulations, `NBINS` is 32. According to the `GENESIS1.3` manual, it has to be at least two times the number of the highest harmonic in the FEL spectra to be calculated plus 2. The information of the number of slices and the length of the individual slices as well as their distance has to be saved to the parameter area of the `GENESIS1.3` particle distribution file. The length of all slices is the same and corresponds to one radiation wavelength.



(a) GENESIS particle distribution. Each slice has the same number of particles while current is treated as an external slice property..



(b) ELEGANT particle distribution. Current is handled as particles per volume.

Figure 5.2: Comparison of a GENESIS1.3 and ELEGANT particle distribution.

### 5.1.3 Challenging particle distributions

Since the number of particles per slice needs to be the same for **GENESIS1.3** particle distributions where the current varies strongly are difficult to handle and many particles are thrown away in the remodeling process. This means that full gaussian particle distributions wider than  $6\sigma$  cannot be used together with this method effectively due to large noise. For the simulation of SASE or the seeding process with the complete electron beam, this method should not be used. For direct seeding and HGHG seeding, one of the beneficial effects is the short pulse duration imprinted to the electron distribution by the means of a short pulse high power laser. This means that in general - unless one deals with ultrashort electron pulses, one can on purpose study only a short section of the electron bunch, and simulate the effect of seeding for the section of the bunch that is overlapped with the laser alone. This means that the application of this method requires the seed pulse to be much shorter as the electron beam. One should, however, take care to include any slipping between electrons and radiation field. For the optimization of seeding, this means one has to do many simulations to find the optimal position inside of the bunch to be overlapped with the seed.

## 5.2 Energy spread measurements

As discussed in the theory section the energy spread is an important figure of merit for the simulation of HGHG, so a realistic number for this is needed. Therefore, measurements on the initial, uncorrelated energy spread at FLASH have been performed using the main dipole of FLASH that is usually used to separate the electron beam and the FEL photons.

First, a calibration constant was found for the screen in the dispersive section. At an energy of 685 MeV, the final two superconducting accelerating modules are switched off and do not contribute to the energy gain of the electrons. Those modules were used to change the energy to  $\pm 1\%$ . The position of the beam on the screen in the dispersive section is then depending on the energy of the electrons. Beam position monitors were used to ensure that the incoming orbit won't change with the energy. The energy resolution of the dump dipole screen was determined to be  $106.48 \pm 0.33$  px/MeV which is  $9.39 \pm 0.03$  keV/px.

After determining the energy resolution ACC67 was put at zero crossing, introducing an energy chirp onto the beam which will enlarge the beam size in the dump like an additional, uncorrelated energy spread. Since the beam size behaves like  $\sigma = \sqrt{\beta\epsilon + \delta^2 D^2}$ , we reduced the  $\beta$ -function by means of a

## 5.2. ENERGY SPREAD MEASUREMENTS

quadrupole to have better resolution.

We then increased the gradient of ACC67 to increase the added energy chirp onto the bunch. The amount of additional energy spread can be calculated if the bunch length is known. This was measured using a transverse deflecting cavity to be 7.2 ps which is in good agreement with the maximum possible bunch length from the photo cathode injector laser.

Then, the beam size was fitted against the additional energy spread (see Fig. 5.3)

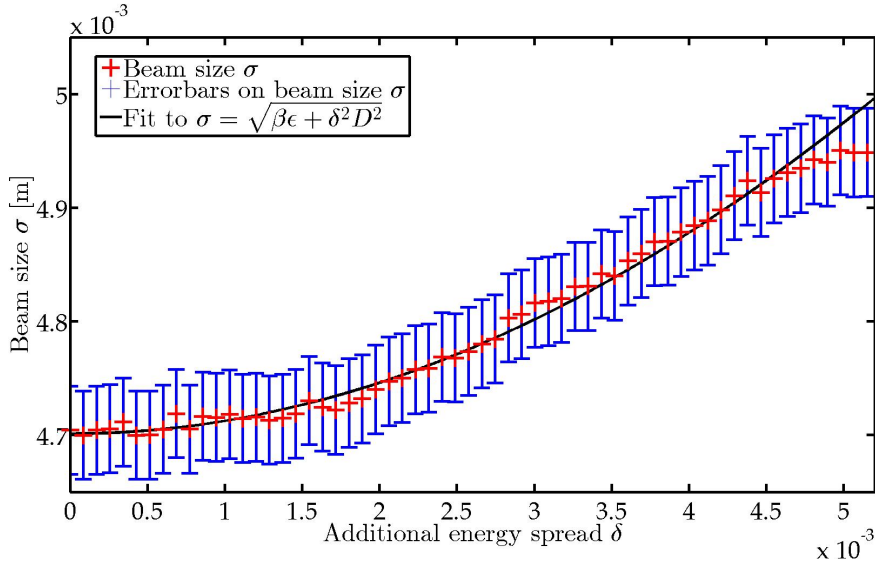


*Figure 5.3: Fit of the energy spread against the beam size. The flattening at an additional energy spread of about  $5 \cdot 10^{-3}$  is a consequence of the limited energy spread that can be transported without losses.*

The result of this fit is that  $\beta\epsilon = (22.10 \pm 0.01)$  m mm mrad which for an assumed emittance of 1.7 mm mrad means  $\beta = (13.000 \pm 0.006)$  m. This means for no additional energy spread the beam size should be  $(4.7011 \pm 0.0011)$  mm, and was measured at  $(4.7043 \pm 0.039)$  mm. Any difference in beam size is an effect of the uncorrelated energy spread for the uncompressed FLASH electron bunch. From this agreement, we can conclude that the contribution of any uncorrelated energy spread to the beam size result from an energy spread smaller than 44 keV.

### 5.3 Modulation depth vs. seed pulse beam quality

In section 3.3 it has been shown how to generate field distribution files that can be used as input radiation for GENESIS simulations. These input files can be generated at an arbitrary wavelength, thus they can be used in long-wavelength HGHG seeding simulations as well. For this simulation, input radiation files at 266 nm, were produced. A simulation based on the foreseen HGHG hardware setup at FLASH was performed using the HGHG simulation framework of T. Plath for different  $M^2$  values.

As seen in the previous chapter, an increasing  $M^2$  leads to a lower peak power contrast with respect to SASE. In the case of HHG the amplification process starts from the externally generated seed which needs to overcome the shotnoise to initiate the seeding process at the desired wavelength.

For HGHG, the topic of this chapters, one needs to imprint an energy modulation onto the electron bunch. This process is the same that takes place at the beginning of an HHG seeded FEL. Since the important feature is the coupling of energy of the seed field to the electrons, smaller  $M^2$  should imprint higher energy modulations in the modulator.

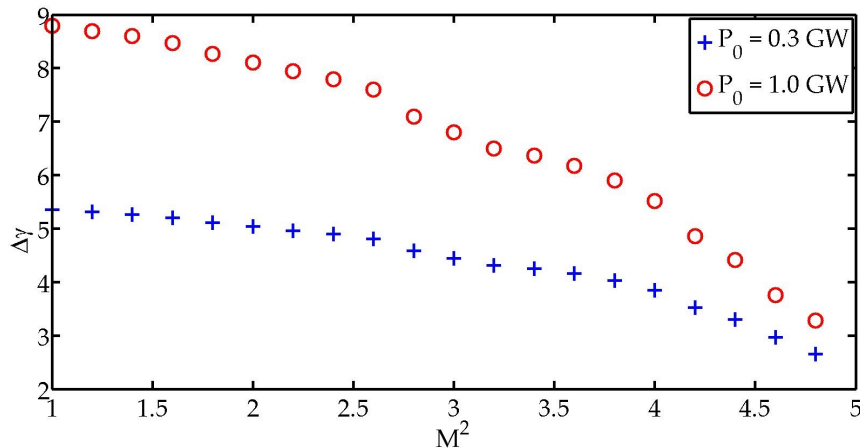


Figure 5.4: Energy modulation at the entrance of the first undulator module for an initial laser seed of 300 MW (blue) and 1 GW (red).

One short modulator has been simulated. In Fig. 5.4 one can see the peak-to-peak modulation amplitude vs the  $M^2$  value of the seed pulse which proves the assumption above: For a seed beam with 1GW peak power containing only the fundamental mode, the modulation amplitude has its maximum at

### 5.3. MODULATION DEPTH VS. SEED PULSE BEAM QUALITY

---

about 8.9 in terms of  $\gamma$  which means roughly 5 MeV and drops to about 4 (2 MeV) at an  $M^2$  of 5.

The simulated particle distributions have then been tracked through a magnetic chicane which converted the energy modulation into a density modulation. The electron bunch was then used for a **GENESIS** simulation in order to predict FEL properties for the different  $M^2$  values.

# Chapter 6

## Achievements in seeding at FLASH

### 6.1 High-harmonic generation

The seeding project at FLASH was the first experiment to show direct HHG seeding in the wavelength range below 40 nm [55]. An external, highly coherent source of radiation, the so-called high-harmonic generation source, provides a radiation field that is used to seed the sFLASH FEL amplifier [94]. The numbers and figures presented in this section are taken from the publication [55].

The setup used for the successful demonstration of HHG seeding below 40 nm is the sFLASH beam line that has been described in Chapter 1. FLASH was operated at a repetition rate of 10 Hz and an energy of 700 MeV. The four-dimensional, spatial overlap is achieved by the means of screens: The electron beam is imaged by an OTR screen, and the XUV beam by the fluorescence on an YAG-screen. The overlap in the wavelength regime is set by matching the gap of the undulator for the wavelength at the given electron energy. The correct radiation wavelength could be checked by the means of a spectrometer. In order to achieve the temporal overlap, three steps are needed:

- (1) For the coarse overlap, a photomultiplier is used. The measured signal is the NIR beam used to generate the XUV beam, and the synchrotron radiation emitted from a five-period electromagnetic wiggler.

- (2) If the coarse overlap is set, the radiation can be sent to a streak camera instead of the photomultiplier which can be used to set the relative timing of the two beams within down to  $\pm 2$  ps.

- (3) In order to get sub-ps precision, which is needed due to the only

## 6.1. HIGH-HARMONIC GENERATION

---

*Table 6.1: Parameters during the first demonstration of HHG seeding at FLASH.*

<b>Electron beam</b>	
Energy	700 MeV
Energy spread rms	$2 \cdot 10^{-4}$
Emittance	1.7 mm · mrad
Bunch charge	0.5 nC
Peak current	1 kA
FEL power gain length	0.70 m
Average beam size	170 $\mu$ m
<b>Seed laser beam</b>	
Pulse energy at source	9 nJ
Pulse energy stability rms	10%
Central wavelength	38.2 nm
Spectral bandwidth rms	0.09 nm
Pulse duration	$< 15$ , fs
Average beam size rms	280 $\mu$ m

tens to hundreds of  $fs$  long electron bunches, the coherent enhancement of optical undulator radiation is used. Therefore, a second electromagnetic wiggler, tuned to 400 nm, the second harmonic of the 800 nm NIR drive laser, will produce a coherent enhancement of undulator radiation initiated by the energy modulation imprinted to the electron beam by its interaction with the NIR laser in the first undulator and the subsequent chicane translating the energy modulation into a density modulation.

Since the relative timing between the seed laser and electron beam fluctuates one needs to scan the relative timing. This is done by changing the timing delay of the laser using a device called “vector modulator” that changes the phase of an externally distributed 1.3 GHz signal that is used for the synchronization of the laser oscillator, working as an electronic delay stage.

At each measurement point of the time scan the NIR laser, and thus the XUV pulse, was toggled so that one can be sure that the observed effect of seeding is not related to the timing alone. In fig. 6.1 one can see the combined results of this timing scan. When the HHG source is active, one can see a temporal region where the FEL maximum pulse energy exceeds the average FEL pulse energy by a factor of up to 5. The same scan without XUV seed pulses shows no such region. From that one can be sure that the

## 6.1. HIGH-HARMONIC GENERATION

enhancement in FEL pulse energy comes from the overlapped XUV pulse. In addition the spatial overlap was changed and the enhancement was also dependent on this parameter.

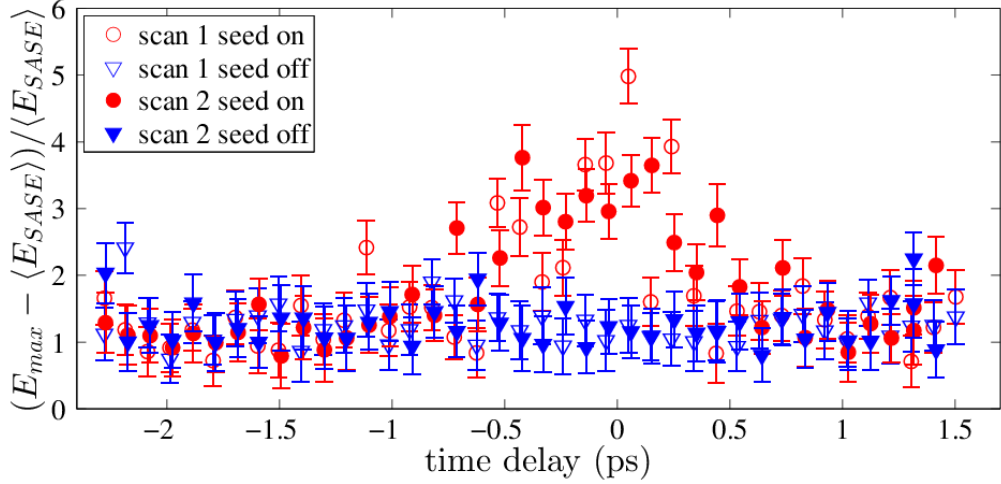
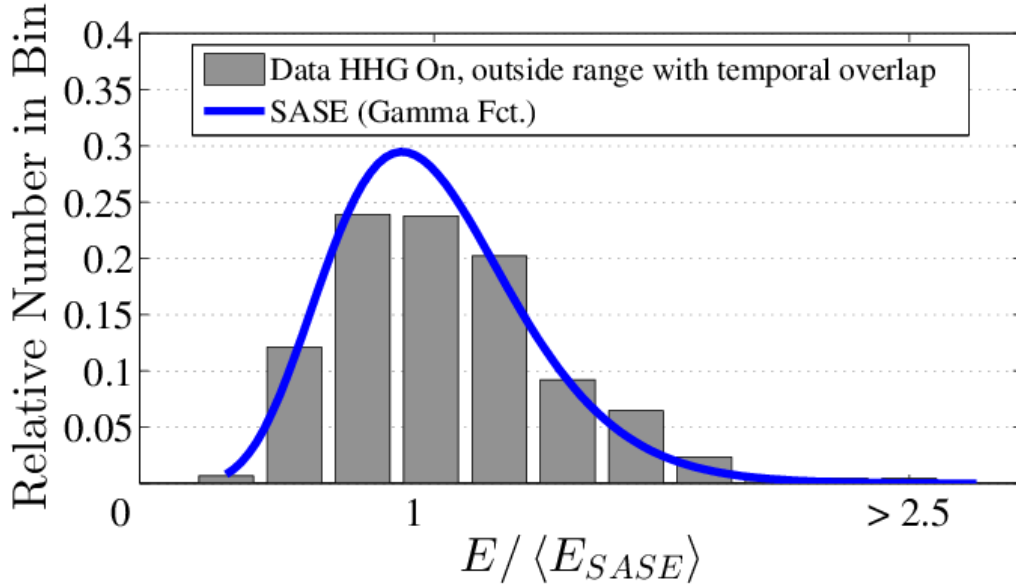


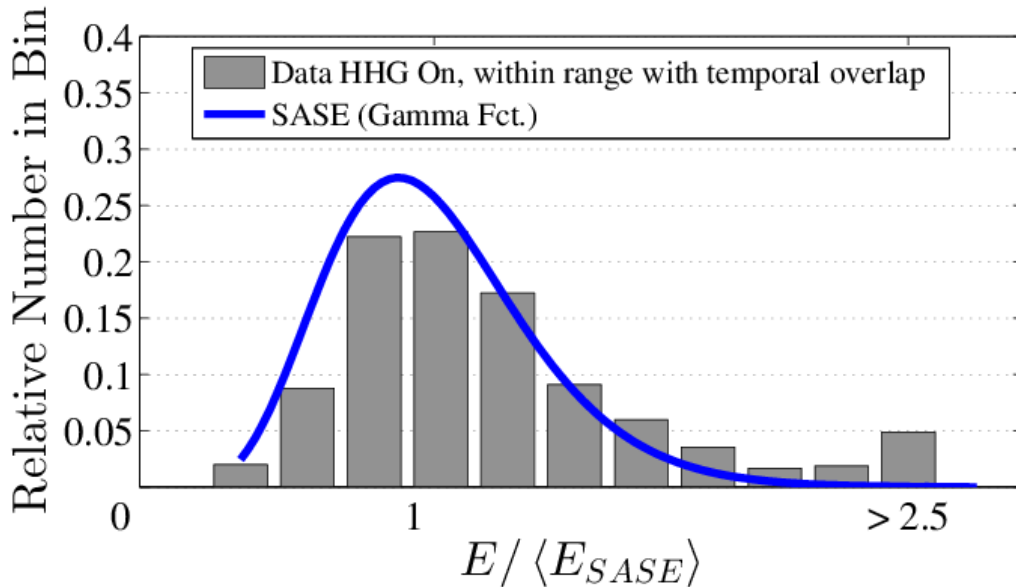
Figure 6.1: Result of the seed scan. One can see that for the laser off (blue) cases there is no change of the FEL energy while for the laser on (red) case a significant enhancement of the FEL energy is present within a certain time delay range. The 0 ps is set arbitrarily to the maximum energy contrast.

Another visualization of the observed seeding effect can be seen in Fig. 6.2. In Fig. 6.2(a) one can see the FEL photon pulse energy distribution without the seed pulse. The distribution of FEL puls energies is a gamma distribution. In Fig. 6.2(b) the seed pulse is overlapped with the electron beam. The same gamma function as in (a) is visible. The histogram shows an excess in photon pulse energies above 2.5 fold the average SASE pulse energy.

In addition to energy enhancement measurement spectra of the FEL radiation at the fundamental and second harmonic of the XUV radiation have been measured. The spectrum of the first harmonic is shown in Fig. 6.3, while consecutive one-shot spectra of the second harmonic are shown in Fig. 6.4



(a) Histogram of FEL energy with the laser timing moved off of the electron bunches. One can see that the FEL photon energy distribution can be described using the gamma distribution characteristic for SASE mode. There are only few shots exceeding the mean SASE FEL pulse energy by more than a factor of 2.5



(b) Histogram of FEL energy with the laser timing on the electron bunches. One can see that the FEL photon energy distribution can be described using the gamma distribution plus an additional gaussian distribution. There are many shots exceeding the mean SASE energy by a factor of more than 2.5. This can clearly be assigned to successful seeding.

*Figure 6.2: Histograms of FEL pulse energies for seeded and unseeded cases. The pulse energy was measured using a multi-channel plate detector.*

## 6.1. HIGH-HARMONIC GENERATION

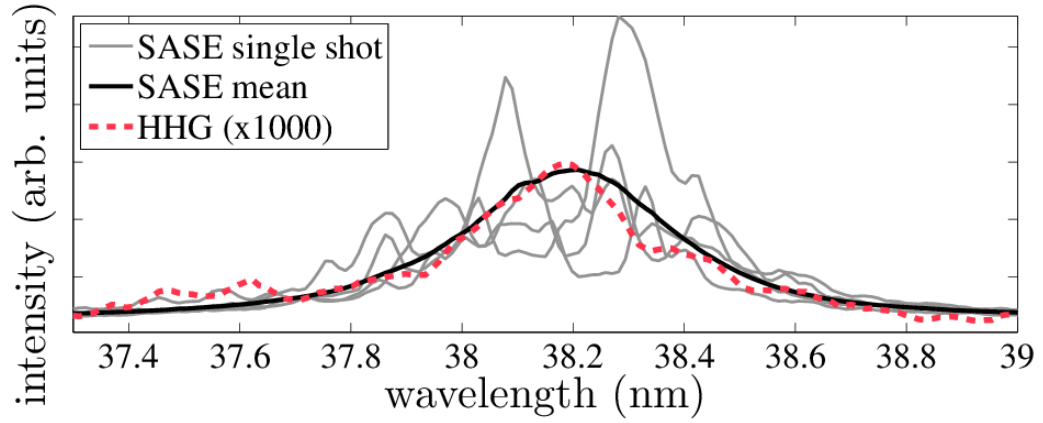


Figure 6.3: Spectrum of the XUV radiation of the sFLASH undulators for SASE at the fundamental undulator wavelength and the HHG seed pulse

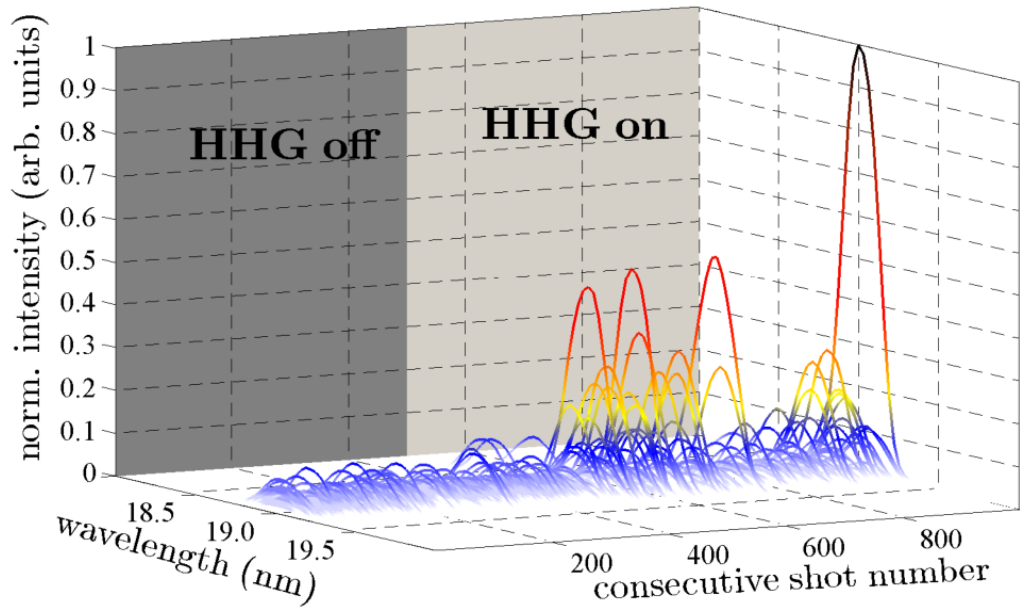
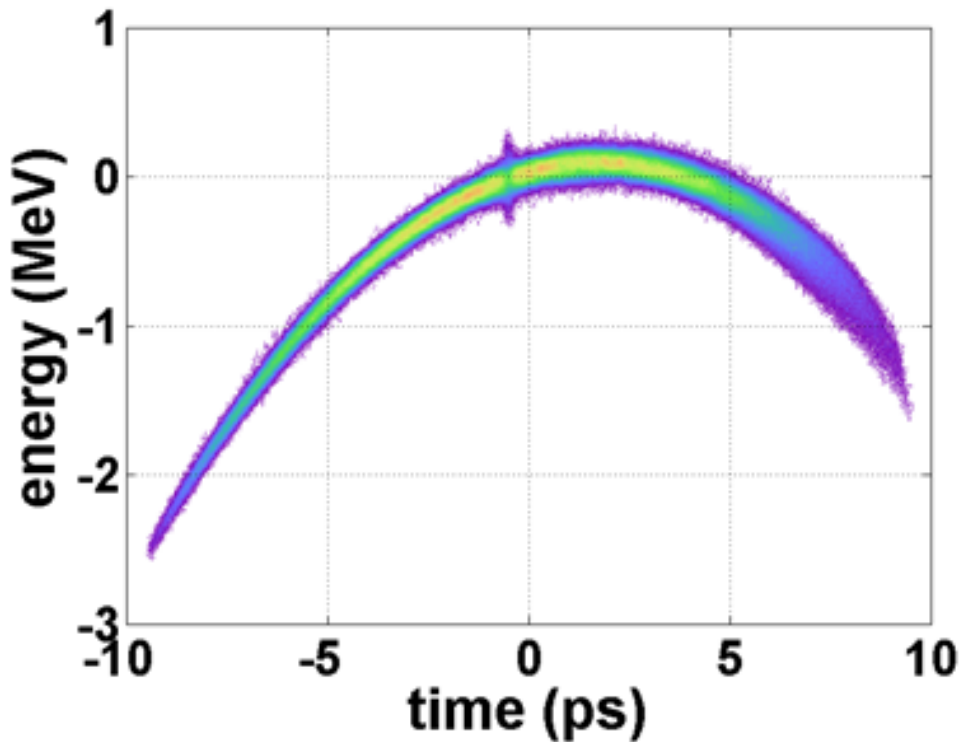


Figure 6.4: Individual single-shot spectra of the second harmonic of the FEL radiation for seed laser off (left) and seed laser on (right). One can see that high energy shots on the second harmonic only occur if the seed laser has been switched on.

## 6.2 HGHG

Recently (April 2015) the first evidence for HGHG seeding at 38 nm was found in the seeding experiment at FLASH. Publications on this success are in preparation. The following numbers and figures are taken from the electronic logbook. As the pulse energy of the 266 nm laser is much higher compared to the XUV beam used for HHG, the energy modulation can be observed using a transverse deflecting structure. This is also a direct measurement of the relative timing between UV pulse and electron bunch. This can be seen in Fig. 6.5.



*Figure 6.5: Longitudinal phase-space distribution of the electron bunch measured using the transverse deflecting cavity. The energy modulation in the electron bunch induced by the UV seed can be seen as a hole in the curved bunch profile*

Comparison to simulation work performed by Ch. Behrens can be used to obtain the modulation amplitude of about 350 keV. (see Fig. 6.6)

After the optimization of the undulator gaps and phase shifter settings, the UV beam timing was synchronized to the electron beam. The FEL

## 6.2. HGHG

Table 6.2: Parameters during the first demonstration of HGHG seeding at FLASH.

<b>Electron beam</b>	
Energy	700 MeV
Bunch charge	0.3 nC
Bunch duration	500 fs
Peak current	0.6 kA
Typ. beam size in radiator	100...200 $\mu\text{m}$
<b>Seed laser beam</b>	
Pulse energy at source	250 $\mu\text{J}$
Rayleigh length	1.4 m
Central wavelength	266 nm
Pulse duration	120..150, fs
Typ. beam size in modulator FWHM	1 mm

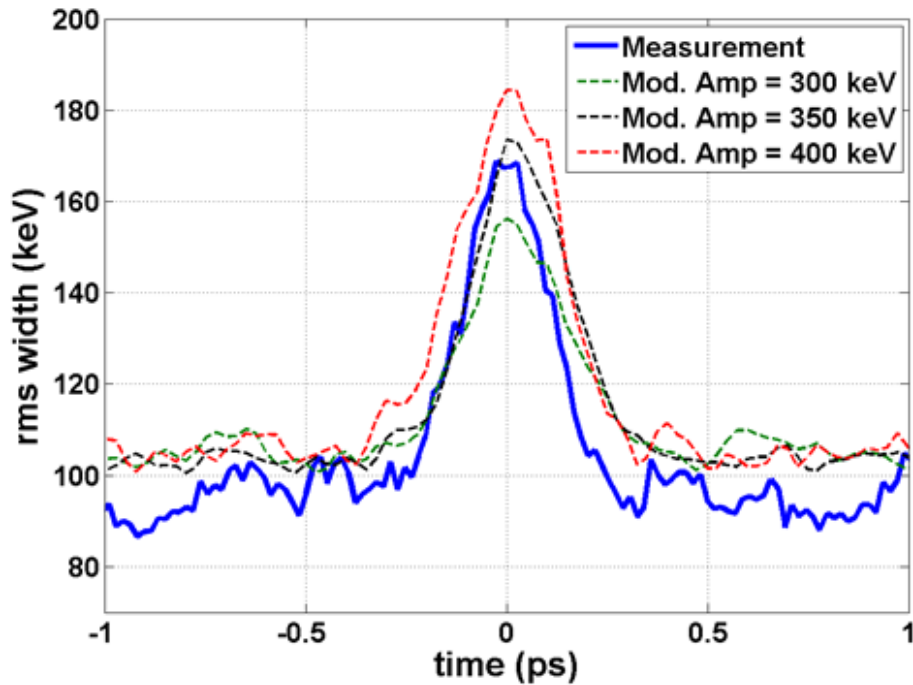


Figure 6.6: Measured rms width of the electron beam in a given time interval compared to several simulated energy modulation amplitudes.

output energy was measured while the seed laser was toggled. There was a clear correlation between seed laser status and FEL energy. The energy contrast was a factor of about 100. (See Fig. 6.7)

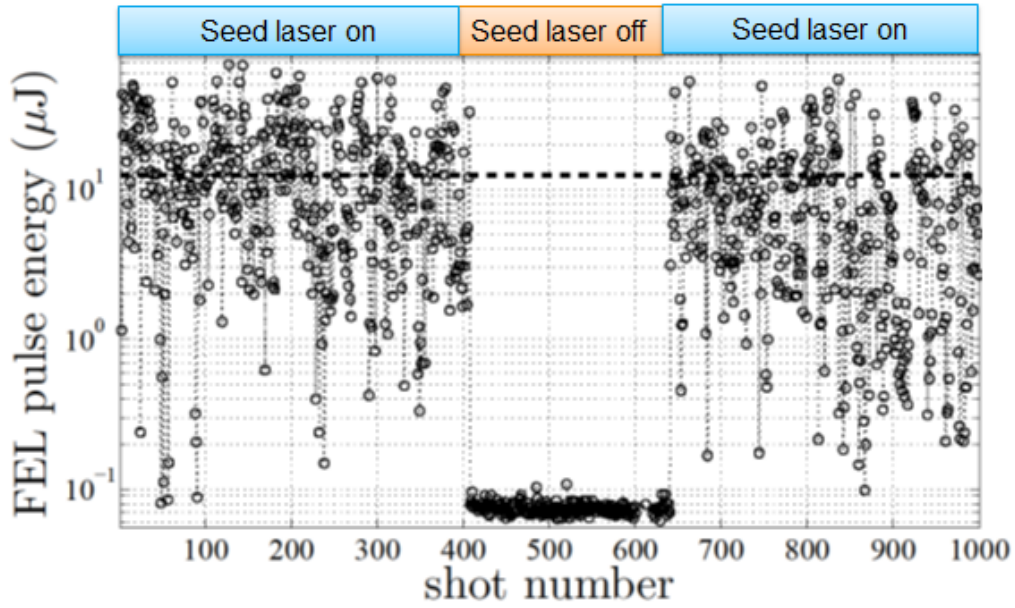


Figure 6.7: FEL pulse energy vs. shot number. The mean FEL energy with the seed laser on is about a factor of 100 higher than for those cases when the laser was switched off.

The spectra shown in Fig. 6.8 shows the HGHG radiation spectra compared to SASE spectra, while the latter has been multiplied by a factor of 1000 to improve the visibility. Finally, an image of the HGHG FEL radiation on a screen is shown in Fig. 6.9

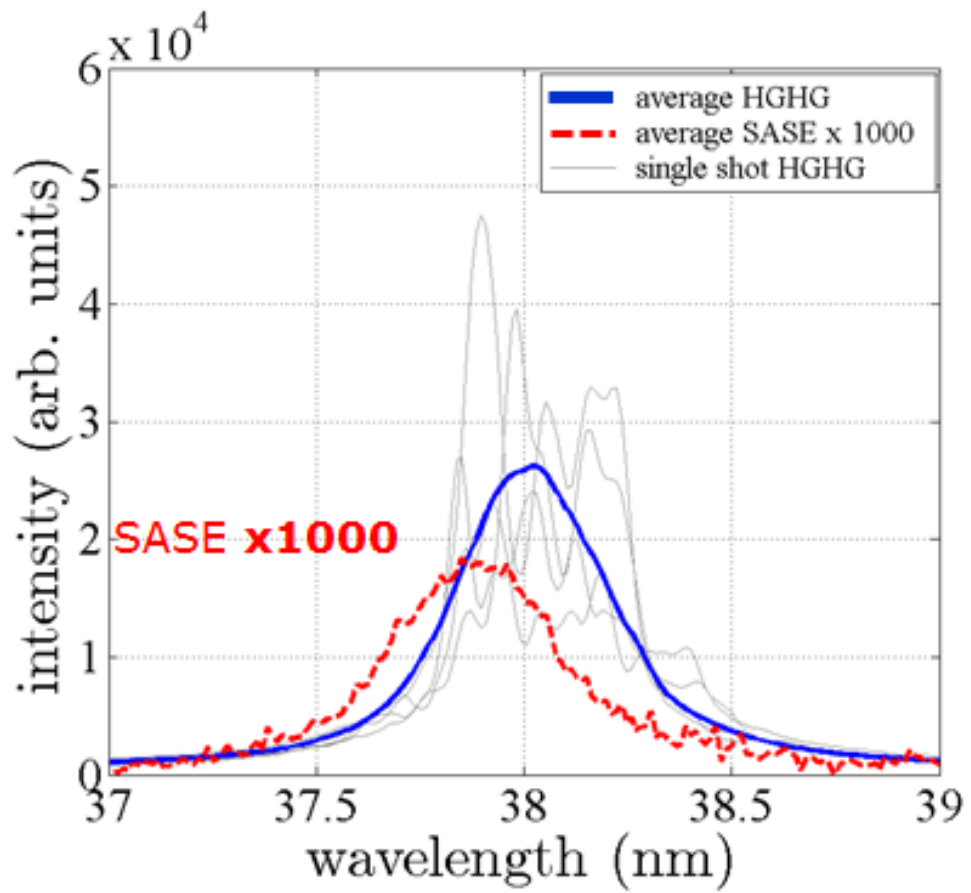
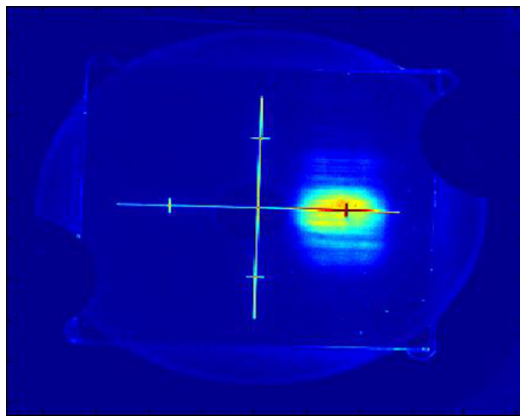


Figure 6.8: Spectra of average HGHG radiation, single-shot HGHG spectra and average SASE radiation. The SASE spectrum has beam multiplied by 1000 in order to enhance visibility, thus having a contrast of about 1000 for the averaged spectra.



*Figure 6.9: Profile of the seeded FEL radiation using a screen.*

# Chapter 7

## Parallel operation of two FEL beam lines

### 7.1 Introduction

The increased number of scientific photon users at the FLASH facility made an extension of the existing photon science facilities at DESY necessary. Additionally, the new undulator beam line is planned to deliver seeded FEL radiation to the users. In this chapter the FLASH extension will be introduced, several different methods of FEL-multiplexing are discussed, the injector laser tests are presented, and finally the first results of parallel operation are shown [109].

While the first undulator beam line, FLASH1 has been described earlier, FLASH2 consists of the following components. In order to generate FEL radiation, twelve planar hybrid permanent-magnet, variable gap undulators with a total magnetic length of 30 m are installed in the new tunnel. This length is sufficient to saturate the FEL at a wavelength of 4 nm in SASE mode. The undulators are, apart from minor modifications, the same U32 undulators that are also used in the sFLASH experiment (see chapter 1). The foreseen optics is a FODO lattice. The general layout of the FLASH-facility after completing the installation of FLASH2 can be seen in Fig. 7.1. The design parameters for the two beam lines at FLASH are summarized in Table 7.1.

The extension is mainly designed to increase the amount of available beam time by providing photon pulses to two users simultaneously.

The most important demands from the user's side are:

- Ensure maximum flexibility in several parameters such as photon pulse length and wavelength.

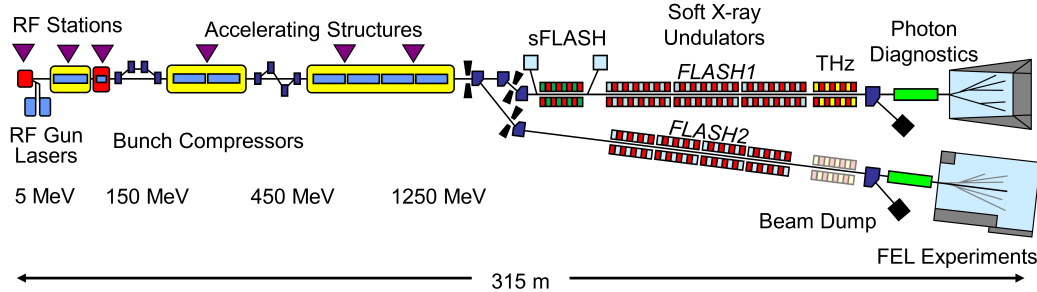


Figure 7.1: Layout of the FLASH facility after the installation of FLASH2. The total length is about 315 m. This sketch is not to scale.

- Deliver bunch trains to both users at a repetition rate of 10 Hz.
- Provide each beam line with bunch trains of different duration and spacing

### 7.1.1 The timing system

Offering the maximum possible flexibility for two FEL beam lines has huge implications on the complete accelerator. Each component like beam loss monitor, beam position monitor, toroids etc. needs to know which bunch train belongs to which FEL beam line, which parameter each bunch train needs, when the bunch train starts, how long it is, when it ends, and in which order the FLASH1 and FLASH2 bunch trains are produced within the 10 Hz macro pulse cycle. The timing system has to deliver this information to the individual accelerator components and data acquisition in order to correctly assign the measured information to the two bunch trains. Basically, the timing system contains and distributes the information what kind of bunch pattern can be expected for each part of the machine. A few important hardware components relying on this information are the kicker, the RF acceleration and compression system and lasers.

Also machine protection for the two FEL beam lines should, whenever possible, only affect the corresponding beam line. In addition, any feedback applied should only change parameters for the bunch train it is working on, which would in most cases be safest to be achieved by blocking the corresponding laser. The development and deployment of such an advanced timing system is also one important step for the European XFEL. The components used to run two FEL beam lines are controlled by the timing system and introduced in the next subsections.

## 7.1. INTRODUCTION

---

Table 7.1: Expected parameters for FLASH2.

	FLASH1	FLASH2
<b>Electron Beam</b>	<b>Value</b>	<b>Value</b>
Energy Range	0.5 – 1.25 GeV	0.5 – 1.25 GeV
Peak Current	2.5 kA	2.5 kA
Bunch Charge	0.06 - 1 nC	0.02 - 1 nC
Normalized Emittance	1.4 mm mrad	1.4 mm mrad
Energy Spread	0.2 MeV	0.5 MeV
Average $\beta$ -function	10 m	6 m
Rep. rate	10 Hz	10 Hz
Number of Bunches per second*	7500	7500
Bunch separation	1-25 $\mu$ s	1-25 $\mu$ s
<b>Undulator</b>	<b>Value</b>	<b>Value</b>
Type	Planar, fixed gap	Planar, variable gap
Period	27.3 mm	31.4 mm
K	0.9	0.5 - 2
Segment length	4.5 m	2.5 m
Minimum gap height	9 mm	9 mm
Number of segments	6	12
<b>Photon Beam SASE</b>	<b>Value</b>	<b>Value</b>
Wavelength range (fundamental)	4.2 - 52 nm	4 - 90 nm
Average single pulse energy	1 - 500 $\mu$ J	1 - 500 $\mu$ J
Pulse duration (FWHM)	10 - 200 fs	10 - 200 fs
Peak power (from av.)	1 - 5 GW	1 - 5 GW
Spectral width (FWHM)	$\approx$ 0.5 - 2 %	$\approx$ 0.5 - 2 %
Peak Brilliance	$10^{28}$ - $10^{31}$	$10^{28}$ - $10^{31}$

\*Shared between FLASH1 and FLASH2, assuming the highest possible repetition rate of 1 MHz.

### 7.1.2 Intra-bunch train switching

The superconducting linac driving the FLASH FEL provides bunch trains with a repetition rate of 10 Hz. Each of these bunch trains consists of up to 800 bunches at a bunch repetition rate of 1 MHz, or less for lower repetition rates. Since not all users need the complete 800  $\mu$ s of the RF pulse, but want to keep the 10 Hz macro pulse repetition rate, one needs a kicker with switching times much shorter than the RF pulse duration. To maintain the flexibility in bunch-to-bunch repetition rate at FLASH a flat-top kicker is used to separate the two bunch trains produced in the linac by a 1 mrad angle. Downstream a DC septum deflects the beam by 6.5 degrees horizontally. Since FLASH delivers long bunch trains, the kicker amplitude, causing the electron beam deflecting angle, needs to have a flat-top of the duration of the deflected bunch train. The flat top of the kicker makes then changes in the repetition rate independent from kicker settings. More information can be found in [110].

### 7.1.3 Dual injector laser setup

Before FLASH2, at FLASH one could switch between two photo cathode injector laser systems. One was the laser system used for operation, while the second one was installed as a backup solution. For FLASH2, both laser systems are used simultaneously and can be set to any of the available repetition rates between 40 kHz and 1 MHz, completely independent from each other. Using two lasers systems offers the possibility to choose pulse properties like bunch-to-bunch repetition rate and bunch charge completely independently from each other. For the optimum performance one has to be sure that both injector lasers hit the cathode under the same angle and at the same position. For FLASH, both laser systems have different pulse durations. This means the electron bunches generated will differ in their temporal shape which needs to be compensated for by means of RF compression. The start time of both lasers can be set independently based on the user demands. If the FLASH1 user needs 200 bunches per macropulse, then there are up to 550 bunches per macropulse left for the user at FLASH2.

### 7.1.4 Changes in the RF system

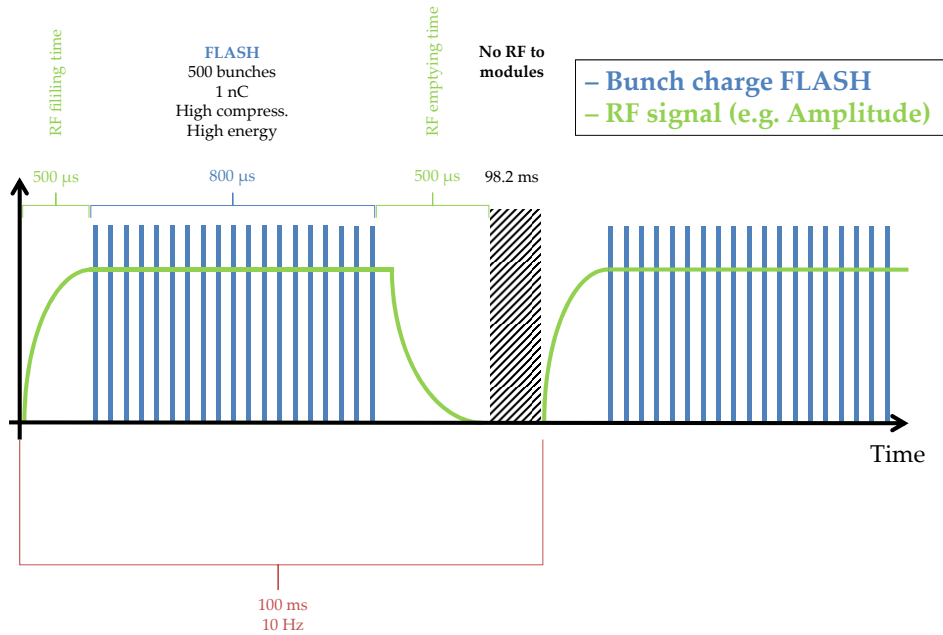


Figure 7.2: Timing pattern for FLASH before the extension. The superconducting cavities are filled. Electron bunches are then injected and accelerated during the up to  $800 \mu\text{s}$  long flat top, in this example only 500 bunches are present. The remaining flat-top is unused.

In order to adjust the photon pulse duration one needs to adjust the electron bunch length. This is mainly done by changing the pulse energy of the injector laser, thus changing the charge which in first place does not change the bunch length. The compression needs to be adjusted as a certain peak current is needed for the operation of the FEL. For FLASH this is done using different RF acceleration gradients and phases and fixed magnetic chicanes, called bunch compressors. Since the bunch compressors consist of dipole magnets, they cannot be used to change the compression of the electron bunches within the needed timescale that lies in the order of the rise time or fall time of the extraction kicker of tens of  $\mu\text{s}$ . This argument is also valid for any other magnet both bunch trains share. One has to adjust

## 7.1. INTRODUCTION

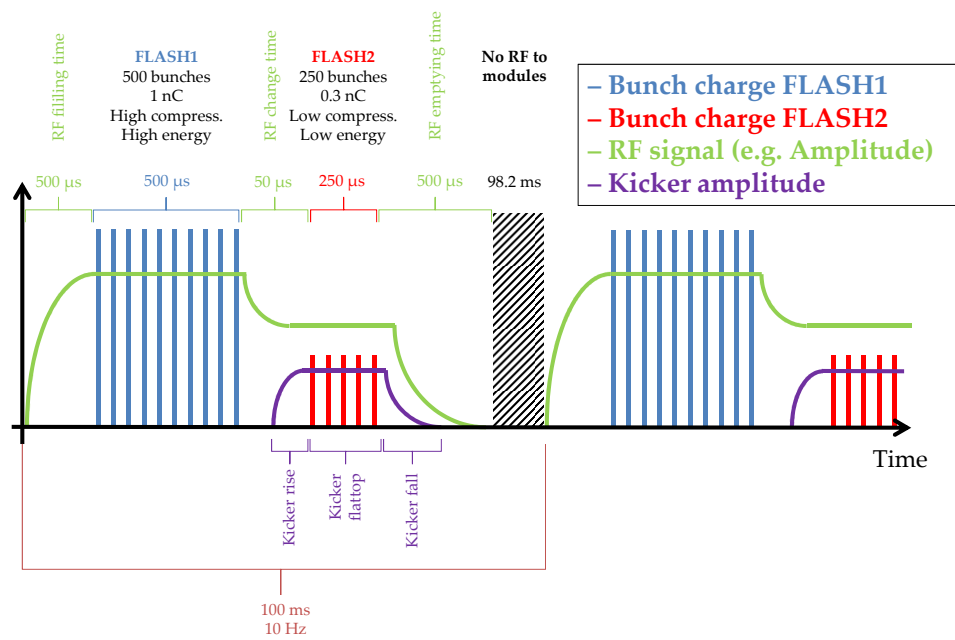


Figure 7.3: Timing pattern for FLASH after the extension. The superconducting cavities are filled. Electron bunches generated by means of the first injector laser are then injected and accelerated during the first flat top. After the first bunch train ends, the flat top of the RF is changed. At the same time, the kicker voltage is rising to its flat top value. When the RF and the kicker reached the flat top, the second injector laser generates electron bunches which will be kicked to FLASH2.

RF parameters to change the bunch length. Therefore the modules need to deliver two flat-tops in the RF pulse separated by a transition time that is shorter than the kicker rise time (see Fig.??). One has to note that changing RF parameters in superconducting cavities takes much longer than in normal conducting modules due to the high Q factor. Since the FLASH1 beam line features fixed-gap undulators, the central energy of the emitted FEL photons can only be adjusted by changing the electron energy. Especially user experiments studying resonances need the exact FEL radiation wavelength within a margin of only tens of picometers. For FLASH1 at 700 MeV, an adjustment of 50 pm means a change of about 1 MeV. Such changes also need to be covered by the RF system and transported to the undulator. In the commonly shared part of the accelerator, the optics will be mismatched for one of the beams if the energy is changed. This mismatch can be corrected by means of quadrupoles in the FLASH1 and FLASH2 beam line. However, the electron beam energy still needs to be in the energy acceptance of the energy collimators, which is about  $\pm 3\%$  at FLASH1. Experimental tests have been performed that show some evidence that in deed that  $\pm 3\%$  could possibly be transported. In Fig. 7.2 the old timing is visualized with one RF flat top, one bunch train and one injector laser. In comparison, Fig. ?? shows the new timing, with the kicker and a second RF flat top, bunch train and injector laser.

## 7.2 FLASH2 hardware commissioning results

Although it was clear from the start that the flexibility of FLASH1 and FLASH2 operation is in principle possible, a large number of proof-of-principle tests have been performed even before FLASH2 was built. For this, the components mentioned in Sec. 7.1 earlier have been tested. The results are presented in this section. The kicker used to extract the second bunch train must rise as fast as possible and provide a stable and constant electromagnetic field over the complete duration of the FLASH2 bunch train as the kicker is the only time-dependent component for the extraction; the septum is DC-powered. The kicker system has been installed in the FLASH1 tunnel and tested with beam: A current of 100 A was applied. The resulting orbit deviation was corrected by DC corrector magnets and the SASE level compared to the original orbit without kicker and orbit correction. The fluctuations on SASE intensity introduced by the kicker did not exceed the instabilities one would expect from the natural SASE fluctuations. The kicker is usually housed in a metal cage. In a first test, this led to a slope on the area where the kicker should deliver a flat top, as shown by the yellow line in Fig. 7.4. This had of course a massive impact on the SASE performance. The same test was repeated with a different cage. The flat top was as flat as needed, as can be seen by the other line in Fig. 7.4. Only moving the timing of the beam near the edges of the flat top within 10  $\mu$ s resulted in a decrease of the SASE intensity.

## 7.2. FLASH2 HARDWARE COMMISSIONING RESULTS

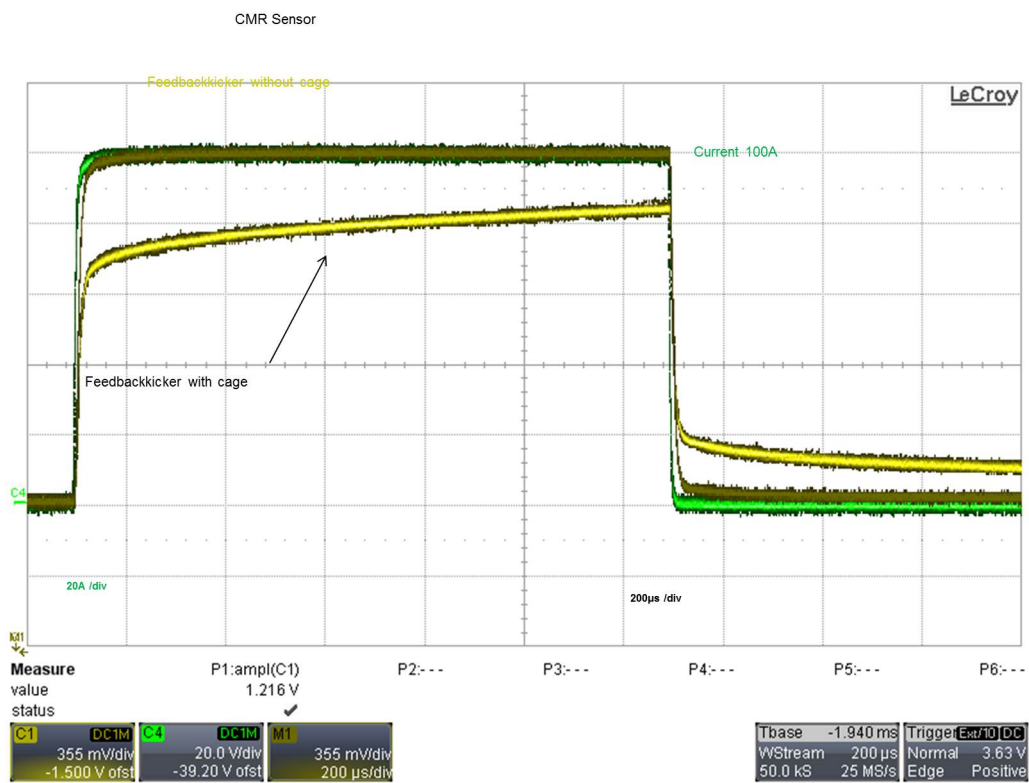


Figure 7.4: Flatness of the long-pulse flat top extraction kicker with (yellow) and without (ocher) casing. One can see that with the casing, the kicker flatness is stable but not constant.

## 7.2. FLASH2 HARDWARE COMMISSIONING RESULTS

Changing the electron bunch length requires the change of the bunch charge and RF parameters. The range of RF parameters that can be reached using the double flat top was tested. One example for three flat tops within one pulse can be seen in Fig. 7.5. The results for the RF parameter range are shown in Table 7.2. The RF is sufficiently flexible to allow for the optimum compression for oth bunch trains. In another experiment, the charge of the electron bunches was changed for one RF flat-top and the SASE performance optimized, while the second bunch train maintained its charge and RF setting. The goal of this experiment is to demonstrate that a high and a low charge beam can be transported and produced optimized FEL radiation at the same time while only touching fast switching RF parameters. Two typical operating points of FLASH, 0.7 GeV and 1.1 GeV have been used for this measurement. The results can be seen in Table 7.3.

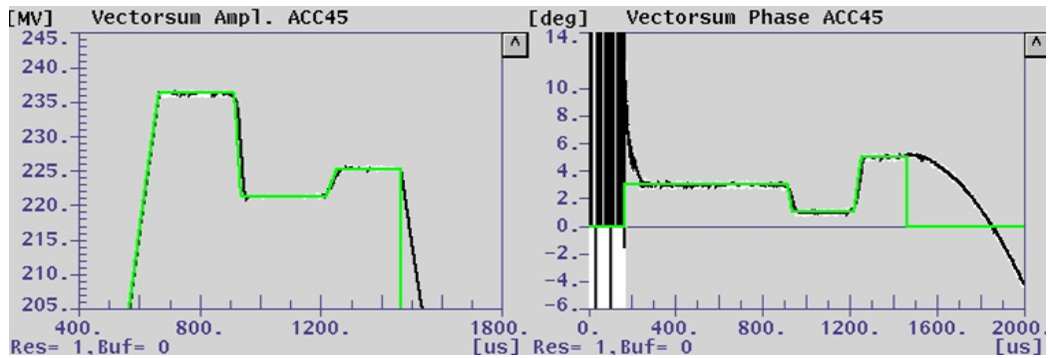


Figure 7.5: Envelope of the RF pulse measured at the accelerating module ACC45, gradient (left) and phase (right). There are three flat tops visible where the third flat top is already foreseen for FLASH3.

## 7.2. FLASH2 HARDWARE COMMISSIONING RESULTS

---

*Table 7.2: RF changes within an RF pulse checked for various RF stations. These values were the differences between the first and second flat top for optimum performance of both FEL beam lines individually under SASE conditions.*

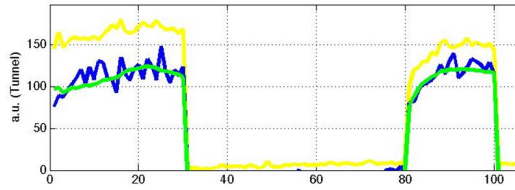
RF Station	Phase (Deg.)	Ampl. (MV)	Transition time ( $\mu$ s)
Gun	+5	-0.1	50
ACC1	+/-2	+/-3.0	30
ACC39	+/-9	-3.0	60
ACC23	+/-3	-15.0	100
ACC45	+/-5	+/-15.0	100
ACC67	-	-	-

*Table 7.3: This table shows the SASE dependence on the electron bunch charge for two different electron energies. The scans were performed by decreasing the charge, and afterward only touching RF parameters which can be changed within the split RF pulse, and the pointing of the electron beam into the undulator. At the lowest charge, the machine was optimized again for 700 MeV, increasing SASE from 30 to 55 and the scan has been repeated increasing the charge.*

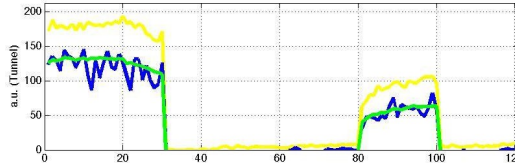
Charge (nC)	SASE ( $\mu$ J)	SASE ( $\mu$ J)
	at 0.7 GeV	at 1.1 GeV
0.60	210	165/110
0.30	170	80/100
0.15	110	75
0.07	30/55	35

## 7.2. FLASH2 HARDWARE COMMISSIONING RESULTS

For the same bunch charge and compression in each bunch train the lasing is the same. One can change the SASE energy by reducing the bunch charge in one train without touching the other. The measurement were performed using the FLASH1 beam line. Usually, half the bunch charge does not result in the half FEL pulse energy, because the gain length gets shorter. Changing the RF parameters leads to the same peak curent and then the FEL energy scales with the bunch length. This can be seen in Fig. 7.6.



(a) Both bunch trains have the same charge per bunch.



(b) The second bunch train has about 50% of the charge per bunch than the first one.

*Figure 7.6: Measured photon pulse energy on a Gas Monitor Detector for two bunch trains seperated by  $50 \mu\text{s}$ . The first train has 30 pulses while the second one has 20 pulses. The vertical axis shows the photon pulse energy in arbitrary units, the horizontal scale is the time (roughly in microseconds). The yellow line is the maximum value, the green line the exponentially filtered average and blue line the instantaneous value. The gap of about  $50 \mu\text{s}$  is foreseen for the kicker to rise and to adjust the RF parameters. For the top figure, the cathode lasers were setup to deliver he same charge, for the bottom figure, for the 2nd pulse train the charge was reduced to half. RF parameters were adjusted to optimize lasing for each bunch train individually.*

In addition to test the dependency on the photon pulse energy of the different lasers, test were performed on the bunch length as a function of the bunch charges. The results of this measurement is displayed in Fig. 7.7.

## 7.2. FLASH2 HARDWARE COMMISSIONING RESULTS

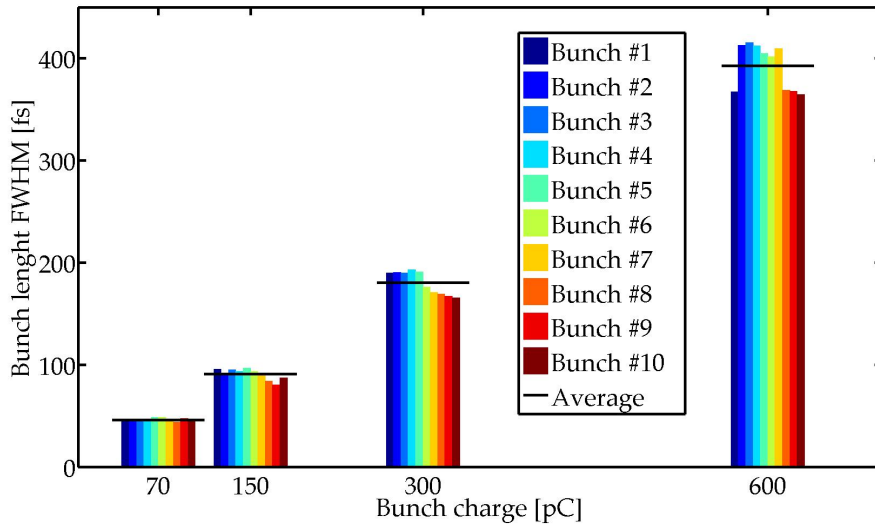


*Figure 7.7: Charge dependence of the electron bunch length after the optimum compression. Color coded is the bunch number in the train. The black line is the average.*

## 7.2. FLASH2 HARDWARE COMMISSIONING RESULTS

---

An additional test was to demonstrate that small deviations in electron beam energy can be transported through FLASH1 while maintaining lasing. To this end, the gradient of the second RF flat top was changed. The difference in total energy was 3 MeV, as shown in Fig. 7.8. This resulted in different radiation wavelength as can be seen on the spectrometer camera in Fig. 7.9

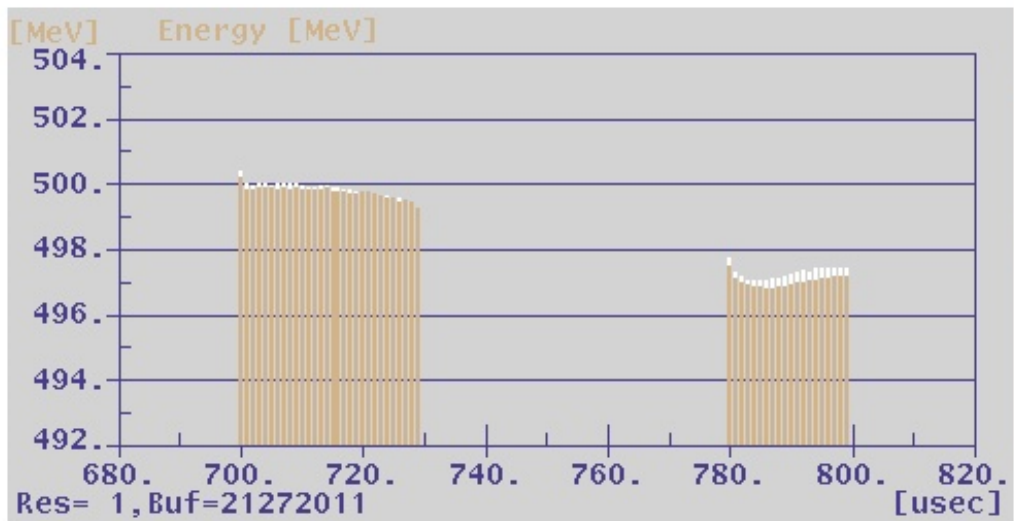
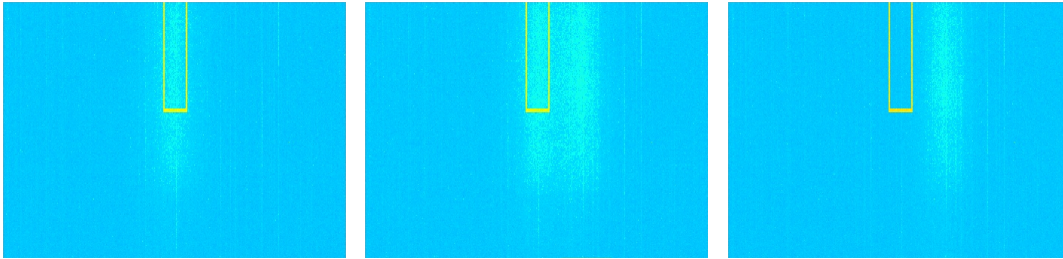


*Figure 7.8: Energy of the individual bunches. Bunch train 1 consisting of 30 bunches has about 500 MeV total energy, bunch train 2 consisting of 20 bunches about 497 MeV.*

## 7.2. FLASH2 HARDWARE COMMISSIONING RESULTS

---



(a) Bunch train 1 with an energy of 500 MeV only. (b) Both bunch trains on spectrometer. (c) Bunch train 2 with an energy of 497 MeV only.

*Figure 7.9: XUV-Spectrometer camera image of the FEL radiation driven by two bunch trains of different energies. Smaller wavelengths are to the left. The yellow box has a width of about 0.1 nm. One can estimate that the two bunch trains are separated by about 3 times the box' width. This would mean a difference of 0.3 nm. This corresponds to an energy deviation of  $\frac{\Delta E}{E} = 0.6\%$  which is in a good agreement to the measured energy deviation of  $\frac{3\text{MeV}}{500\text{MeV}} = 0.6\%$ .*

### 7.3 FLASH2 beam line commissioning

Since the official beam permission, many tests have been performed to show that FLASH2 can fulfill the demands of the photon users and to show the flexibility offered by the FLASH2 setup. In Fig. 7.10 one can see the expected spectral range and its dependence on the gap as well as the wavelength that were already demonstrated. In Fig. 7.11 one can see the FEL radiation profiles taken on a YAG screen inside the photon beam line at different beam times sorted by wavelengths for different electron beam energies, while in Fig. 7.12 four images of the FEL radiation on a YAG screen are shown that were taken during a wavelength scan within about 30 minutes at a fixed electron beam energy. The wavelength was changed by varying the gap of the undulators.

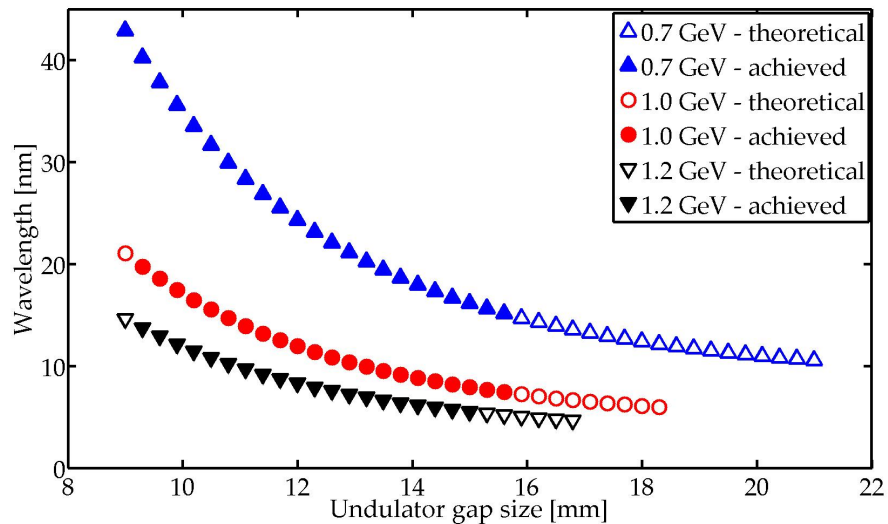


Figure 7.10: Theoretical and achieved wavelength of the FLASH2 undulator system for three different electron beam energies. A filled marker indicates that this wavelength has been demonstrated experimentally.

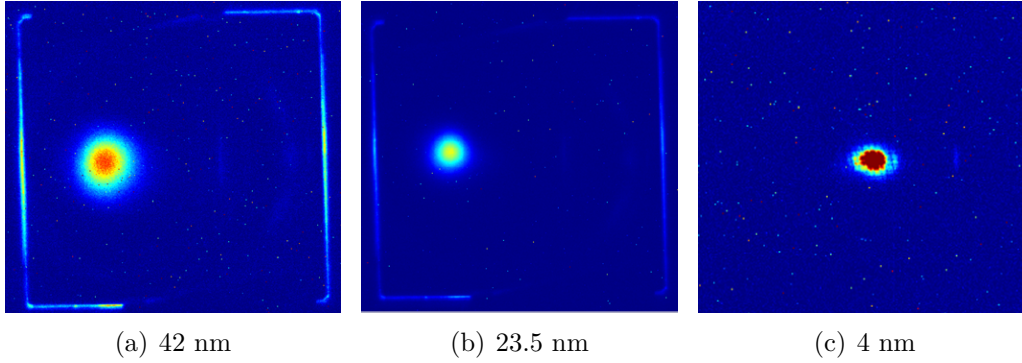


Figure 7.11: Profiles of the FEL radiation on a YAG screen in the photon beam line for different wavelengths between 4 nm and 42 nm.

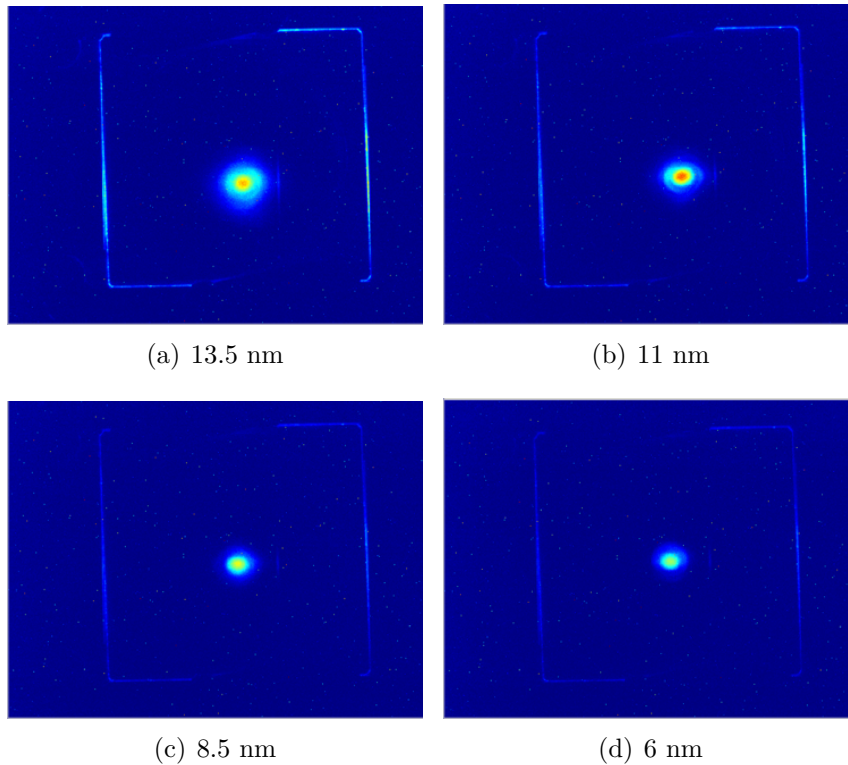


Figure 7.12: Some profiles of the FEL radiation on a YAG screen for a wavelength scan from 13.5 nm to 6 nm that was performed in 0.5 nm steps. FLASH1 was running at 5 nm during the complete scan, which took about 30 min.

## 7.4 Examples for other FEL multiplexing facilities

As shown before, FLASH1 and FLASH2 give the maximum flexibility possible for simultaneous delivery of two pulse trains for users. There are however other methods, though not as flexible, still used to increase beam time for users. FLASH features an electromagnetic undulator downstream the main XUV undulator beam line used for the generation of coherent radiation in the terahertz-regime used for two-wavelength experiments. As the wavelengths differ by a large amount, the micro bunching and energy spread introduced in the XUV wavelength range will not be harmful to the THz radiation production. It might, on the opposite, even be helpful as it contains noise on longer wavelengths.

Another example is the beam line SASE3 at the European X-Ray Free-Electron Laser. Here one uses the spent beam of the first undulator beam line and transports it through a dipole magnet. This magnet separates the electrons from the photon beam and thus it introduces an angle between the photon beams of SASE1 and SASE3. The following undulator beam line produces then FEL radiation for the second user. (See Fig. 7.13) The disadvantages here are that the exact same beam drives two undulator systems, which means they cannot vary in terms of pulse duration, electron energy or pulse pattern. In addition, using a spent beam one always has to consider the degraded electron beam quality due to the lasing process in the first undulator. Any changes in the electron orbit or optics for the first undulators will make corrections for the second undulator inevitable. For the electron orbit, which can be measured without degrading the electron beam, the correction can be handed over to an orbit feedback system. The electron beam optics however can only be determined by the beam size, which is a destructive measurement. Thus, it can only be corrected if the users abdicate a fraction of their beam time.

For normal conducting accelerators with repetition rates of around 100 Hz, one can also use fast kickers to apply an orbit kick to the electron beam on a bunch-to-bunch time scale. For SACLA, the Japanese XFEL facility, the following scheme, applicable for normal conducting FELs, has been proposed [112]: The charging of the high voltage power supplies starts with a trigger signal generated based on the power line frequency (which, for the case of the prefecture of Hyogo where RIKEN is situated, is 60 Hz). A reference RF clock and counter unit is used to deal with timing jitter and provides adjustable timing delays. The main linac produces bunch trains at 60 Hz with a kinetic energy of 6.8 GeV. The last RF modules are operated

#### 7.4. EXAMPLES FOR OTHER FEL MULTIPLEXING FACILITIES

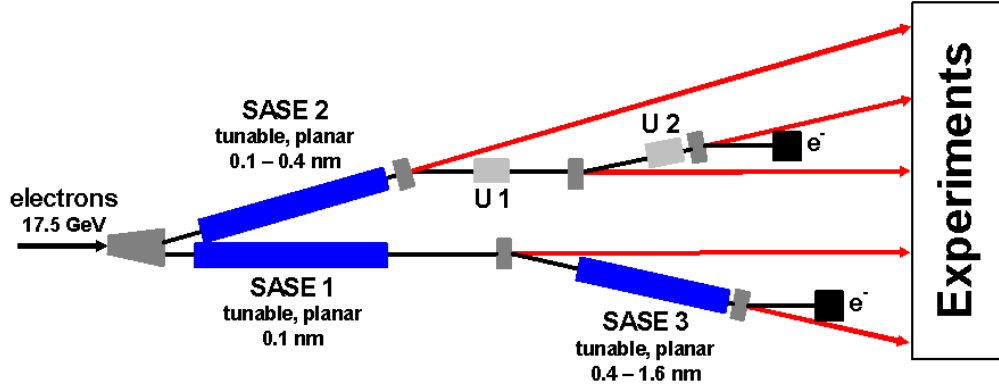


Figure 7.13: Undulator section of the XFEL. One can see that SASE3 uses the spent beam of SASE1. The grey block between both undulators is the dipole magnet. Image taken from [111].

at gradients of 200 MeV per module at lower frequencies, four modules at 30 Hz and two at 15 Hz. That means that the FEL can operate at three different wavelengths, but the total rate of pulses is decreased for each energy. Although three different electron energies are produced, the flexibility is limited in terms of electron charge, compression, bunch pattern and repetition rate.

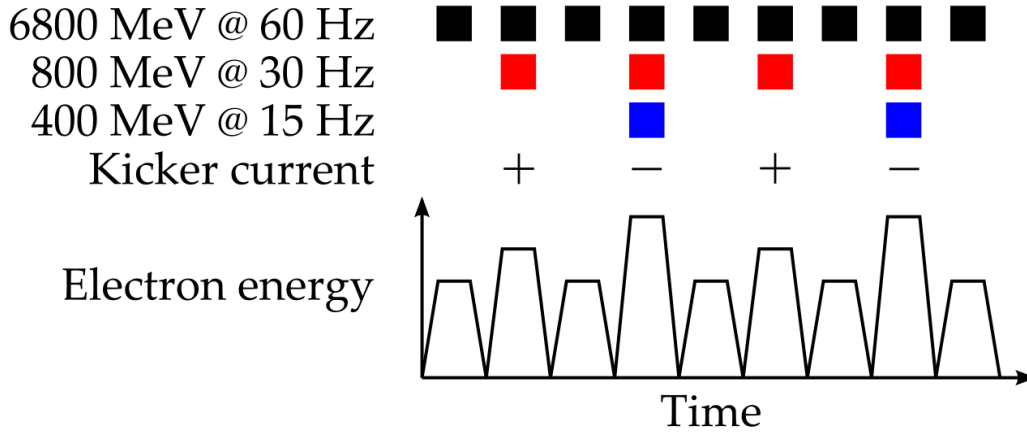


Figure 7.14: SACLA Timing pattern

# Chapter 8

## Summary and Outlook

The FEL output power in dependence of the  $M^2$  of the incoming XUV beam has been studied in simulation. The results lead to the conclusion that the power contrast comes almost completely from the embedded fundamental TEM<sub>00</sub> mode, while higher order modes contribute only little to the power contrast. In addition, there is no evidence that the presence of higher order modes has a negative effect on the contrast. The behaviour of the gain curves has been studied. For an  $M^2$  up to 4 the gain curves show the same behaviour as for the  $M^2 = 1$  case. The  $M^2$  of the FEL radiation has been shown to be independent of the incoming XUV seed beam and a fixed number, which is in agreement with the theoretical description in [85]. For the reliable operation of a seeded FEL one would however like to have a more dedicated device for the measurement of  $M^2$  that would be installed in the vicinity of the undulator and deliver measurement results with lower measurement errors.

It has been shown that a modal reconstruction using Hermite-Gaussian modes is possible. The obtained  $M^2$  has a large error in the order of 28%. However, the  $M^2$  obtained by this method can be used to characterize the FEL seed beam in the vicinity of the undulator, where only single screens are present. An XUV transverse profile obtained during a measurement shift at FLASH has been used to generate a seed beam for the simulation out of the deconstructed modes. It led to the same power contrast, and, with the assumptions on the FEL pulse lengths, to the same energy contrast that has been observed.  $M^2$  measurements of an THG tripler have been performed and are also in agreement with the ISO measurement method. In the future one would like to repeat the measurements on successful seeding shifts in order to show the effect of  $M^2$  in the experiment.

A direct HHG seeding option for FLASH2 has been studied under the conditions that the focus of the XUV beam should be situated in the first undulator and the source point for the users of the FEL radiation should

---

be in the last one. All possible combinations of the independently operating variable gap undulators have been studied in order to obtain the best FEL performance in terms of power contrast in the SASE case. The simulation shows that for the optimal performance it will be necessary to change electron beam parameters to move the point of the best contrast towards the end of the last undulator. Simulation will be needed to find this optimum electron beam settings. Furthermore, these calculations have to be repeated for some shorter, representative wavelengths (e.g. 30, 20, 10, 5 nm) and different  $M^2$  values.

For HGHG, the energy spread is an important figure. Therefore the dispersion has been measured at the end of the undulator, using the dump dipole as an electron spectrometer. The upper limit of the energy spread through the complete FEL can be estimated to be 40 keV. A new method for tracking particle distributions through a magnetic chicane (or other magnetic lattices) has been developed and used to optimize the energy modulation amplitude for two different laser seed beam powers and different  $M^2$ . Furthermore, during the time of this thesis, HHG and HGHG seeding has been demonstrated successfully at sFLASH. This is an important step for the future seeded operation of FLASH2. One would like to use the dump dipole as an electron energy spectrometer in a way such that one could directly observe the energy spread introduced by the seeding process as it is done in FERMI@ELETTRA.

Before FLASH2 was ready to be operated, important pre-tests were performed. One of those is the study on the influence of the extraction kicker that separates the bunches between the FLASH1 and FLASH2 electron beam line on the SASE performance. Those intensity fluctuations did not exceed the fluctuations one expects in SASE operation. The needed flexibility in the RF system has been tested. The flexibility in the RF system to drive two FEL beam lines is achieved by providing two flat-tops in the temporal RF power distribution, although in the pre-test three flat-tops were successfully tested, as it is foreseen to extend the FLASH2 beam line by a third beam line - FLASH3. As soon as the second injector laser was installed tests were performed using two flat tops. One could show that for equal bunch charges on both flat-tops the SASE performance was the same, and that for smaller bunch charges with optimized compression using RF parameters of the second flat top the FEL performance followed the expected behaviour. The charge dependence of the electron bunch length under optimum compression was studied and it was shown that the RF is capable of offering enough flexibility to cope with the needed compression changes. Finally, two electron bunches with different kinetic energies were used to produce FEL radiation. This was successfully done, with a clear spectrogram of two SASE

---

wavelength of the two electron beams. Switching the energy of either beam was possible without any changes of the electron optics.

Whithin several months the commissioning of the hardware was done. The beam extraction was successful, and transmission to the dump was achieved soon. All of the wavelengths that were planned for FLASH2 could be shown to lase. An electron energy scan, corresponding to a wavelength change from 13.5 nm down to 6 nm, was performed in less than 30 minutes. Right now, first user beam is delivered at FLASH2.

Most tests at FLASH2 were performed during user operation at FLASH1. FLASH1 and FLASH2 were already operated simultaneously, both with long bunch trains.

# Bibliography

- [1] Elder, F.R., Gurewitsch, A.M., Langmuir, R.V., et al. “Radiation from Electrons in a Synchrotron”. In: *Physical Review*, vol. 71: pp. 829–830 (Jun. 1947). doi: 10.1103/PhysRev.71.829.5
- [2] Altarelli, M. and Salam, Abdus. “The quest for brilliance: light sources from the third to the fourth generation”. In: *Europhysics News*, vol. 35 (2): pp. 47–50 (2004). doi: 10.1051/epn:2004204
- [3] Berkelman, K. “A Personal History of CESR and CLEO: Updated October 2001”. Tech. rep. (2002)
- [4] Balewski, K., Brefeld, W., Decking, W., et al. “PETRA III: A low emittance synchrotron radiation source. Technical design report”. Tech. rep. (2004)
- [5] Ginzburg, V.L. In: *Izvestiya Akademii Nauk Armyanskoi SSR, Seriya Fiziko*, vol. 11 (2): p. 165 (1947)
- [6] Motz, H., Thon, W., and Whitehurst, R.N. “Experiments on Radiation by Fast Electron Beams”. In: *Journal of Applied Physics*, vol. 24 (7): pp. 826–833 (1953). doi: 10.1063/1.1721389
- [7] Madey, J.M. “Stimulated Emission of Bremsstrahlung in a Periodic Magnetic Field”. In: *Journal of Applied Physics*, vol. 42 (5): pp. 1906–1913 (Apr 1971). doi: 10.1063/1.1660466
- [8] Elias, L.R. “Free-electron laser research at the University of California, Santa Barbara”. In: *Quantum Electronics, IEEE Journal of*, vol. 23 (9): pp. 1470–1475 (Sep 1987). doi: 10.1109/JQE.1987.1073554
- [9] Amersfoort, P.V., Best, R., Faatz, B., et al. “Status of the dutch free electron laser for infrared experiments”. In: *Nuclear Instruments and Methods in Physics Research Section A: Accelerators, Spectrometers, Detectors and Associated Equipment*, vol. 285 (1–2): pp. 67 – 70 (1989). doi: 10.1016/0168-9002(89)90427-0

## BIBLIOGRAPHY

---

- [10] Ortega, J., Bergher, M., Chaput, R., et al. “CLIO: Collaboration for an infrared laser at Orsay”. In: *Nuclear Instruments and Methods in Physics Research Section A: Accelerators, Spectrometers, Detectors and Associated Equipment*, vol. 285 (1–2): pp. 97 – 103 (1989). doi: 10.1016/0168-9002(89)90432-4
- [11] Brunken, M., Döbert, S., Eichhorn, R., et al. “First lasing of the Darmstadt cw free electron laser”. In: *Nuclear Instruments and Methods in Physics Research Section A: Accelerators, Spectrometers, Detectors and Associated Equipment*, vol. 429 (1–3): pp. 21 – 26 (1999). doi: 10.1016/S0168-9002(99)00060-1
- [12] Kulipanov, G., Litvinenko, V., Pinaev, I., et al. “The VEPP-3 storage-ring optical klystron: Lasing in the visible and ultraviolet regions”. In: *Nuclear Instruments and Methods in Physics Research Section A: Accelerators, Spectrometers, Detectors and Associated Equipment*, vol. 296 (1–3): pp. 1 – 3 (1990). doi: 10.1016/0168-9002(90)91179-F
- [13] Couprie, M.E., Billardon, M., Velghe, M., et al. “Free-electron-laser oscillation on the Super-ACO storage ring at Orsay”. In: *Nuclear Instruments and Methods in Physics Research A*, vol. 296: pp. 13–19 (Oct. 1990). doi: 10.1016/0168-9002(90)91182-B
- [14] Litvinenko, V., Burnham, B., Park, S., et al. “First UV/visible lasing with the OK-4/Duke storage ring FEL”. In: *Nuclear Instruments and Methods in Physics Research Section A: Accelerators, Spectrometers, Detectors and Associated Equipment*, vol. 407 (1–3): pp. 8 – 15 (1998). doi: 10.1016/S0168-9002(97)01357-0
- [15] Nölle, D., Garzella, D., Geisler, A., et al. “First lasing of the FELICITA I FEL at DELTA”. In: *Nuclear Instruments and Methods in Physics Research Section A: Accelerators, Spectrometers, Detectors and Associated Equipment*, vol. 445 (1–3): pp. 128 – 133 (2000). doi: 10.1016/S0168-9002(00)00044-9
- [16] Walker, R., Clarke, J., Couprie, M., et al. “First lasing and initial performance of the European UV/VUV storage ring FEL at ELETTRA”. In: *Nuclear Instruments and Methods in Physics Research Section A: Accelerators, Spectrometers, Detectors and Associated Equipment*, vol. 475 (1–3): pp. 20 – 27 (2001). doi: 10.1016/S0168-9002(01)01529-7

- 
- [17] Kondratenko, A. and Saldin, E. “Generating of coherent radiation by a relativistic electron beam in an undulator”. In: *Part.Accel.*, vol. 10: pp. 207–216 (1980)
- [18] Bonifacio, R., Pellegrini, C., and Narducci, L. “Collective Instabilities and High Gain Regime in a Free Electron Laser”. In: *Opt.Commun.*, vol. 50: pp. 373–378 (1985). doi: 10.1016/0030-4018(84)90105-6
- [19] Sheffield, R.L. “Progress in Photoinjectors for LINACs”. In: “Linear Accelerator Conference, 1990, Albuquerque, NM, September 10-14, 1990”, (1990)
- [20] Travier, C. “Rf guns: bright injectors for FEL”. In: *Nuclear Instruments and Methods in Physics Research Section A: Accelerators, Spectrometers, Detectors and Associated Equipment*, vol. 304 (1–3): pp. 285 – 296 (1991). doi: [http://dx.doi.org/10.1016/0168-9002\(91\)90870-V](http://dx.doi.org/10.1016/0168-9002(91)90870-V)
- [21] Murokh, A., Agustsson, R., Babzien, M., et al. “Properties of the ultrashort gain length, self-amplified spontaneous emission free-electron laser in the linear regime and saturation”. In: *Phys. Rev. E*, vol. 67: p. 066501 (Jun 2003). doi: 10.1103/PhysRevE.67.066501
- [22] Milton, S.V., Gluskin, E., Arnold, N.D., et al. “Exponential Gain and Saturation of a Self-Amplified Spontaneous Emission Free-Electron Laser”. In: *Science*, vol. 292 (5524): pp. 2037–2041 (2001). doi: 10.1126/science.1059955
- [23] Andruszkow, J. et al. “First observation of selfamplified spontaneous emission in a free electron laser at 109-nm wavelength”. In: *Phys.Rev.Lett.*, vol. 85: pp. 3825–3829 (2000). doi: 10.1103/PhysRevLett.85.3825
- [24] Ackermann, W. et al. “Operation of a free-electron laser from the extreme ultraviolet to the water window”. In: *Nat Photon*, vol. 1 (6): pp. 336–342 (Jun. 2007). doi: 10.1038/nphoton.2007.76
- [25] Schreiber, S. “First Lasing in the Water Window with 4.1 nm at FLASH.” (p. 2). 33rd International Free Electron Laser Conference, Shanghai(China), 2011-08-22 - 2011-08-26, JACoW, Geneva (2011-08-22 - 2011-08-26 2011)
- [26] Faatz, B. et al. “Flash II: Perspectives and challenges”. In: *Nuclear Instruments and Methods in Physics Research Section A: Accelerators,*

## BIBLIOGRAPHY

---

- Spectrometers, Detectors and Associated Equipment*, vol. 635 (1, Supplement): pp. S2 – S5 (2011). doi: 10.1016/j.nima.2010.10.065
- [27] Shintake, T. “First lasing at SCSS”. In: “Free electron laser. Proceedings, 28th International Conference, FEL 2006, Berlin, Germany, August 27-September 1, 2006”, (pp. 16–17) (2006)
- [28] Allaria, E., Appio, R., Badano, L., et al. “Highly coherent and stable pulses from the FERMI seeded free-electron laser in the extreme ultraviolet”. In: *Nat Photon*, vol. 6 (6): pp. 633–704 (Sep. 2012). doi: 10.1038/nphoton.2012.233
- [29] Emma, P., Akre, R., Arthur, J., et al. “First lasing and operation of an ångstrom-wavelength free-electron laser”. In: *Nat Photon*, vol. 4 (4): pp. 641–647 (Aug. 2010). doi: 10.1038/nphoton.2010.176
- [30] Pile, D. “X-rays: First light from SACLA”. In: *Nat Photon*, vol. 5 (5): pp. 456–457 (Nov. 2011). doi: 10.1038/nphoton.2011.178
- [31] Abela, R., Aghababayan, A., Altarelli, M., et al. *XFEL: The European X-Ray Free-Electron Laser - Technical Design Report*. DESY, Hamburg (2006). doi: 10.3204/DESY06 – 097
- [32] Oh, J., Ko, I., Namkung, W., et al. “Design study on 0.3-nm PAL-XFEL”. Tech. rep. (2004)
- [33] “SwissFEL Conceptual Design Report”. Tech. rep.
- [34] Blau, J. “Free Electron Lasers in 2013”. (p. 486). 35th International Free Electron Laser Conference, Manhattan(USA), 2011-08-26 - 2011-08-30, JACoW (2013-08-26 - 2013-08-30 2013)
- [35] Michel, P., Gabriel, F., Grosse, E., et al. “First lasing of the ELBE MID-IR FEL”. In: “Free electron laser. Proceedings, 26th International Conference, FEL 2004, Trieste, Italy, August 29-September 3, 2004”, (2004)
- [36] Patel, C.K.N., Faust, W.L., McFarlane, R.A., et al. “Laser action up to 57.355 nm in gaseous discharges (Ne, He-Ne)”. In: *Applied Physics Letters*, vol. 4 (1): pp. 18–19 (1964). doi: 10.1063/1.1723574
- [37] Tavella, F., Willner, A., Rothhardt, J., et al. “Fiber-amplifier pumped high average power few-cycle pulse non-collinear OPCPA”. In: *Optics express*, vol. 18: pp. 4689–4694 (2010). doi: 10.1364/OE.18.004689

- 
- [38] Akasaki, I., Sota, S., Sakai, H., et al. “Shortest wavelength semiconductor laser diode”. In: *Electronics Letters*, vol. 32 (12): pp. 1105–1106 (Jun 1996). doi: 10.1049/e1:19960743
- [39] Ewing, J. “Excimer laser technology development”. In: *Selected Topics in Quantum Electronics, IEEE Journal of*, vol. 6 (6): pp. 1061–1071 (Nov 2000). doi: 10.1109/2944.902155
- [40] Schmäser, P., Dohlus, M., Rossbach, J., et al. *Free-Electron Lasers in the Ultraviolet and X-Ray Regime : Physical Principles, Experimental Results, Technical Realization; 2nd ed. 2014, Springer Tracts in Modern Physics*, vol. 258. Springer International Publishing, Cham (2014). doi: 10.1007/978-3-540-79572-8
- [41] Ackermann, W., Asova, G., Ayvazyan, V., et al. “Operation of a Free-electron Laser from the Extreme Ultraviolet to the Water Window.” In: *Nature photonics*, vol. 1: p. 336 (2007). doi: 10.1038/nphoton.2007.76
- [42] Bödewadt, J. “private communication”
- [43] Schlarb, H. “Normal conducting cavity for arrival time stabilization”. In: “FEL Beam dynamics group meeting talk”, (2011)
- [44] Feldhaus, J., Saldin, E., Schneider, J., et al. “Possible application of X-ray optical elements for reducing the spectral bandwidth of an X-ray SASE FEL”. In: *Optics Communications*, vol. 140 (4–6): pp. 341 – 352 (1997). doi: 10.1016/S0030-4018(97)00163-6
- [45] Treusch, R., Brefeld, W., Feldhaus, J., et al. “The seeding project for the FEL in TTF phase II”. In: “Ann. report 2001”, (2001)
- [46] Miltchev, V., Rossbach, J., Faatz, B., et al. “Simulation studies on the self-seeding option at FLASH”. In: , (pp. 162–165) (2006)
- [47] Saldin, E., Schneidmiller, E., Shvyd’ko, Y., et al. “X-ray FEL with a meV bandwidth”. In: *Nuclear Instruments and Methods in Physics Research Section A: Accelerators, Spectrometers, Detectors and Associated Equipment*, vol. 475 (1–3): pp. 357 – 362 (2001). doi: 10.1016/S0168-9002(01)01539-X
- [48] Amann, J., Berg, W., Blank, V., et al. “Demonstration of self-seeding in a hard-X-ray free-electron laser”. In: *Nat Photon*, vol. 6 (6): pp. 693–698 (Aug. 2012). doi: 10.1038/nphoton.2012.180

## BIBLIOGRAPHY

---

- [49] Seres, J., Seres, E., Verhoef, A.J., et al. “Demonstration of self-seeding in a hard-X-ray free-electron laser”. In: *Nature*, vol. 433 (433): p. 596 (Feb. 2005). doi: 10.1038/433596a
- [50] Maltezopoulos, T., Mittenzwey, M., Azima, A., et al. “A high-harmonic generation source for seeding a free-electron laser at 38 nm”. In: *Applied physics / B*, vol. 115 (1): pp. 45–54 (2014). doi: 10.1007/s00340-013-5571-6
- [51] SeresV, J., Yakovlev, S., Seres, E., et al. “Coherent superposition of laser-driven soft-X-ray harmonics from successive sources”. In: *Nature*, vol. 775 (3): pp. 878–883 (Nov. 2007). doi: 10.1038/nphys775
- [52] Pullen, M.G., Gaffney, N.S., Hall, C.R., et al. “High-order harmonic generation from a dual-gas, multi-jet array with individual gas jet control”. In: *Opt. Lett.*, vol. 38 (20): pp. 4204–4207 (Oct 2013). doi: 10.1364/OL.38.004204
- [53] Hage, A., Landgraf, B., Taylor, M., et al. “New design of a multi-jet target for quasi phase matching”. In: *Review of Scientific Instruments*, vol. 85 (10): 103105 (2014). doi: 10.1063/1.4897269
- [54] Togashi, T., Takahashi, E.J., Midorikawa, K., et al. “Extreme ultraviolet free electron laser seeded with high-order harmonic of Ti:sapphire laser”. In: *Opt. Express*, vol. 19 (1): pp. 317–324 (Jan 2011). doi: 10.1364/OE.19.000317
- [55] Ackermann, S., Azima, A., Bajt, S., et al. “Generation of Coherent 19- and 38-nm Radiation at a Free-Electron Laser Directly Seeded at 38 nm”. In: *Physical review letters*, vol. 111 (11): p. 114801 (2013). doi: 10.1103/PhysRevLett.111.114801
- [56] Yu, L. “Generation of intense uv radiation by subharmonically seeded single-pass free-electron lasers”. In: *Phys.Rev.*, vol. A44: pp. 5178–5193 (1991). doi: 10.1103/PhysRevA.44.5178
- [57] Yu, L. and Wu, J. “Theory of High Gain Harmonic Generation: an Analytical Estimate”. In: *Nucl.Instrum.Meth.*, vol. A483: pp. 493–498 (2002). doi: 10.1016/S0168-9002(02)00368-6
- [58] Doyuran, A., Babzien, M., Shaftan, T., et al. “Characterization of a High-Gain Harmonic-Generation Free-Electron Laser at Saturation”. In: *Phys. Rev. Lett.*, vol. 86: pp. 5902–5905 (Jun 2001). doi: 10.1103/PhysRevLett.86.5902

- 
- [59] Allaria, E., Castronovo, D., Cinquegrana, P., et al. “Two-stage seeded soft-X-ray free-electron laser”. In: *Nature photonics*, vol. 7: pp. 913–918 (2013). doi: 10.1038/nphoton.2013.277
- [60] Xiang, D. and Stupakov, G. “Echo-enabled harmonic generation free electron laser”. In: *Phys. Rev. ST Accel. Beams*, vol. 12: p. 030702 (Mar 2009). doi: 10.1103/PhysRevSTAB.12.030702
- [61] Schreiber, S. “RF Guns at FLASH” (2014). OA
- [62] Aune, B. “TESLA Test Facility: Status and Results”. Tech. Rep. DESY M 96-20 (1996)
- [63] Brinkmann, R. “The TESLA Superconducting Linear Collider”. Tech. Rep. DESY M 97-04 (1997). OA
- [64] Vogel, E., Albrecht, C., Baboi, N., et al. “Test and Commissioning of the Third Harmonic RF System for FLASH.” (pp. 4281–4283). 1st International Particle Accelerator Conference, Kyoto(Japan), 2010-05-23 - 2010-05-28, JACoW, Geneva (2010-05-23 - 2010-05-28 2010)
- [65] Pfluger, J. and Nikitina, Y. “Planar undulator schemes with strong focusing properties for the VUV-FEL at the TESLA test facility”. In: *Nucl.Instrum.Meth.*, vol. A381: pp. 554–559 (1996). doi: 10.1016/S0168-9002(96)00720-6
- [66] Tiedtke, K., Feldhaus, J., Hahn, U., et al. “Gas detectors for x-ray lasers”. In: *Journal of Applied Physics*, vol. 103 (9): 094511 (2008). doi: 10.1063/1.2913328
- [67] Richter, M., Gottwald, A., Kroth, U., et al. “Measurement of gigawatt radiation pulses from a vacuum and extreme ultraviolet free-electron laser”. In: *Applied Physics Letters*, vol. 83 (14): pp. 2970–2972 (2003). doi: 10.1063/1.1614417
- [68] Tiedtke, K., Azima, A., Bargon, N.v., et al. “The soft x-ray free-electron laser FLASH at DESY: beamlines, diagnostics and end-stations”. In: *New journal of physics*, vol. 11: p. 023029 (2009). doi: 10.1088/1367-2630/11/2/023029
- [69] Wellhöfer, M., Hoeft, J.T., Martins, M., et al. “Photoelectron spectroscopy as a non-invasive method to monitor SASE-FEL spectra”. In: *Journal of Instrumentation*, vol. 3 (02): p. P02003 (2008)

## BIBLIOGRAPHY

---

- [70] Brenner, G., Kapitzki, S., Kuhlmann, M., et al. “First results from the online variable line spacing grating spectrometer at {FLASH}”. In: *Nuclear Instruments and Methods in Physics Research Section A: Accelerators, Spectrometers, Detectors and Associated Equipment*, vol. 635 (1, Supplement): pp. S99 – S103 (2011). doi: 10.1016/j.nima.2010.09.134. PhotonDiag 2010
- [71] Frassetto, F., Coraggia, S., Gerasimova, N., et al. “Compact spectrometer for photon diagnostics of the extreme-ultraviolet free-electron-laser radiation”. In: *Nuclear Instruments and Methods in Physics Research Section A: Accelerators, Spectrometers, Detectors and Associated Equipment*, vol. 635 (1, Supplement): pp. S94 – S98 (2011). doi: 10.1016/j.nima.2010.11.004. PhotonDiag 2010
- [72] Juranic, P., Bonfigt, S., Ilchen, M., et al. “The new online Photoionization Spectrometer at FLASH”. 1st International Particle Accelerator Conference, Kyoto(Japan), 2010-05-23 - 2010-05-28, JACoW, Geneva (2010-05-23 - 2010-05-28 2010)
- [73] Saldin, E., Schlarb, H., Schmidt, B., et al. “Status of the Optical Replica Synthesizer at FLASH”. In: *Conf.Proc.*, vol. C070625: p. 965 (2007)
- [74] Saldin, E., Schneidmiller, E., and Yurkov, M. “A Simple method for the determination of the structure of ultrashort relativistic electron bunches”. In: *Nucl.Instrum.Meth.*, vol. A539: pp. 499–526 (2005). doi: 10.1016/j.nima.2004.11.002
- [75] *Undulator system for a seeded FEL experiment at FLASH (WE5RFP070)*, Proceedings of the Particle Accelerator Conference 2009 (2009)
- [76] Behrens, C. “Measurement and Control of the Longitudinal Phase Space at High-Gain Free-Electron Lasers.” (p. 97). 33rd International Free Electron Laser Conference, Shanghai(China), 2011-08-22 - 2011-08-26, JACoW, Geneva (2011-08-22 - 2011-08-26 2012)
- [77] Ackermann, S. et al. “Generation of coherent 19 nm and 38 nm radiation at a free-electron laser directly seeded at 38 nm.” In: *Physical Review Letters*, vol. 111 (11): p. 114801 (2013)
- [78] Schoeps, A., Bilani, O., Ramm, T., et al. “Design and commissioning of the FLASH2 undulators”. (pp. 2007–2009). International Par-

---

ticle Accelerator Conference IPAC, Dresden(Germany), 06/15/2014 - 06/20/2014 (06/15/2014 - 06/20/2014 2014)

- [79] Faatz, B., Pfluger, J., and Nikitina, Y. “Study of the undulator specification of the VUV-FEL at the TESLA Test Facility”. In: *Nucl.Instrum.Meth.*, vol. A393: pp. 380–384 (1997). doi: 10.1016/S0168-9002(97)00517-2
- [80] Murphy, J.B., Pellegrini, C., and Bonifacio, R. “Collective instability of a free electron laser including space charge and harmonics”. In: *Optics Communications*, vol. 53: pp. 197–202 (Mar. 1985). doi: 10.1016/0030-4018(85)90331-1
- [81] Singer, A. and Vartaniants, I. “Coherence properties of focused X-ray beams at high-brilliance synchrotron sources”. In: *Journal of synchrotron radiation*, vol. 21 (1): pp. 5 – 15 (2014). doi: 10.1107/S1600577513023850
- [82] Singer, A., Vartanyants, I.A., Kuhlmann, M., et al. “Transverse-Coherence Properties of the Free-Electron-Laser FLASH at DESY”. In: *Phys. Rev. Lett.*, vol. 101: p. 254801 (Dec 2008). doi: 10.1103/PhysRevLett.101.254801
- [83] Schäfer, B., Flöter, B., Mey, T., et al. “{FEL} beam characterization from measurements of the Wigner distribution function”. In: *Nuclear Instruments and Methods in Physics Research Section A: Accelerators, Spectrometers, Detectors and Associated Equipment*, vol. 654 (1): pp. 502 – 507 (2011). doi: 10.1016/j.nima.2011.07.031
- [84] Singer, A., Sorgenfrei, F., Mancuso, A.P., et al. “Spatial and temporal coherence properties of single free-electron laser pulses”. In: *Opt. Express*, vol. 20 (16): pp. 17480–17495 (Jul 2012). doi: 10.1364/OE.20.017480
- [85] Saldin, E., Schneidmiller, E., and Yurkov, M. “Coherence properties of the radiation from X-ray free electron laser”. In: *Optics Communications*, vol. 281 (5): pp. 1179 – 1188 (2008). doi: <http://dx.doi.org/10.1016/j.optcom.2007.10.044>
- [86] Winterfeldt, C., Spielmann, C., and Gerber, G. “ *Colloquium* : Optimal control of high-harmonic generation”. In: *Rev. Mod. Phys.*, vol. 80: pp. 117–140 (Jan 2008). doi: 10.1103/RevModPhys.80.117

## BIBLIOGRAPHY

---

- [87] Lewenstein, M., Balcou, P., Ivanov, M.Y., et al. “Theory of high-harmonic generation by low-frequency laser fields”. In: *Phys. Rev. A*, vol. 49: pp. 2117–2132 (Mar 1994). doi: 10.1103/PhysRevA.49.2117
- [88] Corkum, P.B. “Plasma perspective on strong field multiphoton ionization”. In: *Phys. Rev. Lett.*, vol. 71: pp. 1994–1997 (Sep 1993). doi: 10.1103/PhysRevLett.71.1994
- [89] Wu, J. and Bolton, P.R. “Coherent X-ray Production by Cascading Stages of High Gain Harmonic Generation Free Electron Lasers Seeded by IR Laser Driven High-Order Harmonic Generation”. In: , (pp. 186–189) (2006)
- [90] Brefeld, W., Faatz, B., Feldhaus, J., et al. “Study of frequency multiplication process in multistage HGHG FEL”. In: *Nucl.Instrum.Meth.*, vol. A483: pp. 80–88 (2002). doi: 10.1016/S0168-9002(02)00290-5
- [91] Bachelard, R. et al. “Wavefront analysis of nonlinear self-amplified spontaneous-emission free-electron laser harmonics in the single-shot regime.” In: *Physical Review Letters*, vol. 106 (23): p. 234801 (2011)
- [92] Gautier, J. et al. “Optimization of the wave front of high order harmonics”. In: *The European Physical Journal D*, vol. 48 (3): pp. 459–463 (2008). doi: 10.1140/epjd/e2008-00123-2
- [93] *How to (Maybe) Measure Laser Beam Quality, OSA Trends in Optics and Photonics*, vol. 17. Optical Society of America (1998)
- [94] Maltezopoulos, T. et al. “A high-harmonic generation source for seeding a free-electron laser at 38 nm”. In: *Applied Physics B*, (pp. 1–10) (2013). doi: 10.1007/s00340-013-5571-6
- [95] Gori, F. et al. “Intensity-based modal analysis of partially coherent beams with Hermite—Gaussian modes”. In: *Opt. Lett.*, vol. 23 (13): pp. 989–991 (Jul 1998). doi: 10.1364/OL.23.000989
- [96] Sprangle, P., Freund, H., Hafizi, B., et al. “Optical Beam Quality in Free-Electron Lasers”. In: *IEEE Journal of Quantum Electronics*, vol. 45: pp. 218–222 (2009). doi: 10.1109/JQE.2009.2012508
- [97] Johnston, T.F. “Beam Propagation (M2) Measurement Made as Easy as It Gets: The Four-Cuts Method”. In: *Appl. Opt.*, vol. 37 (21): pp. 4840–4850 (1998)

- 
- [98] Schmidt, O.A. et al. “Real-time determination of laser beam quality by modal decomposition”. In: *Optics Express*, vol. 19 (7): pp. 6741–6748 (2011). doi: 10.1364/oe.19.006741
- [99] Reiche, S. “GENESIS 1.3: a fully 3D time-dependent FEL simulation code”. In: *Nuclear Instruments and Methods in Physics Research, Section A: Accelerators, Spectrometers, Detectors and Associated Equipment*, vol. 429: pp. 243–248 (1999). doi: 10.1016/S0168-9002(99)00114-X
- [100] Nelder, J.A. and Mead, R. “A Simplex Method for Function Minimization”. In: *The Computer Journal*, vol. 7 (4): pp. 308–313 (1965). doi: 10.1093/comjnl/7.4.308
- [101] *Commissioning results of the photon-electron diagnostics unit at aFLASH (MOPD54)*, Proceedings of the DIPAC2011 (2011)
- [102] Willner, A., Tavella, F., Yeung, M., et al. “Coherent control of high harmonic generation via dual-gas multijet arrays”. In: *Physical review letters*, vol. 107: p. 175002 (2011). doi: 10.1103/PhysRevLett.107.175002
- [103] Willner, A. *A high repetition rate XUV seeding source for FLASH2*. Dr., Universität Hamburg, Hamburg (2012). Diss.
- [104] Lechner, C. “First Direct Seeding at 38 nm”. (p. TUOAI01). 34th International Free-Electron Laser Conference, Nara(Japan), 2012-08-26 - 2012-08-31, JACoW, Geneva (2012-08-26 - 2012-08-31 2012)
- [105] Prandolini, M.J., Riedel, R., Schulz, M., et al. “Design Considerations for a High Power, Ultrabroadband Optical Parametric Chirped-Pulse Amplifier”. In: *Optics express*, vol. 22 (2): p. 1594 (2014). doi: 10.1364/OE.22.001594. OA
- [106] Riedel, R., Rothhardt, J., Beil, K., et al. “Thermal Properties of Borate Crystals for High Power Optical Parametric Chirped-Pulse Amplification”. In: *Optics express*, vol. 22 (15): pp. 17607 – 17619 (2014). doi: 10.1364/OE.22.017607. OA
- [107] Reiche, S. “{GENESIS} 1.3: a fully 3D time-dependent {FEL} simulation code”. In: *Nuclear Instruments and Methods in Physics Research Section A: Accelerators, Spectrometers, Detectors and Associated Equipment*, vol. 429 (1–3): pp. 243 – 248 (1999). doi: 10.1016/S0168-9002(99)00114-X

## BIBLIOGRAPHY

---

- [108] Borland, M. “elegant: A Flexible SDDS-Compliant Code for Accelerator Simulation”
- [109] Tiedtke, K., Azima, A., von Bargen, N., et al. “The soft x-ray free-electron laser FLASH at DESY: beamlines, diagnostics and end-stations”. In: *New Journal of Physics*, vol. 11 (2): p. 023029 (2009)
- [110] Scholz, M., Decking, W., Faatz, B., et al. “Extraction Arc for FLASH II”. (p. TUPD33). 34th International Free-Electron Laser Conference, Nara(Japan), 2012-08-26 - 2012-08-31, JACoW, Geneva (2012-08-26 - 2012-08-31 2012)
- [111] Brinkmann, R., Schneidmiller, E.A., and Yurkov, M.V. “Possible operation of the European XFEL with ultra-low emittance beams”. In: *Nucl. Instrum. Meth.*, vol. A616: pp. 81–87 (2010). doi: 10.1016/j.nima.2010.02.121
- [112] Hara, T., Tamasaku, K., Asaka, T., et al. “Time-interleaved multienergy acceleration for an x-ray free-electron laser facility”. In: *Phys. Rev. ST Accel. Beams*, vol. 16: p. 080701 (Aug 2013). doi: 10.1103/PhysRevSTAB.16.080701

The doi-identifiers were obtained using meta-search engines like the DESY publication database, CiteULike, and INSPIRE.

# Chapter 9

## Acknowledgements

As expected in the field of scientific research at large, complex facilities, also this thesis would not be possible without the support of many people.

I want to express my gratitude towards Prof. Dr. Jörg Roßbach for being my supervisor for my doctoral thesis. His vivid and interesting lectures on accelerator physics at the University of Hamburg consolidated my decision on my scientific specialisation into the field of accelerator physics. He was also a supervisor of my diploma thesis. Even after his retirement, he always had time and listened to all of my problems, not only those regarding science.

I would like to gratefully thank Dr. Bart Faatz for being my second supervisor. Our weekly meetings are one of the reasons for the success of this PhD thesis. His will to systematically approach every problem that occurred during the last years ended in many interesting results. I also want to thank him for supporting me becoming an accelerator operator.

I would like to thank Dr. Velizar Miltchev for assisting Dr. Bart Faatz in my supervision and his contribution to my research and all the fruitful discussions we had during the last years.

I am thankful to Dr. Winfried Decking, Dr. Alexander Gamp, and Dr. Klaus Balewski who realized the position I was able to write my PhD thesis on, as well as Swaantje Mette, Christel Övermann, Fenna Reinholdt, Carsten Kluth and Oliver Koschig, who supported me in terms of office and IT infrastructure.

Grateful thanks to all colleagues from the seeding team. It was a pleasure to work with you and I am thankful for all your help. Even after long shifts after unsuccessful seeding, we could laugh together. Especially thankful I am to my PhD colleagues Christoph Lechner (hopefully by now Dr. Christoph Lechner) and Tim Plath, who both never let me down.

I want to express my gratitude to the FLASH management, Dr. Siegfried Schreiber, Dr. Katja Honkavaara, and Dr. Mathias Vogt for their support

---

for the seeding team and my work.

My thanks also go out to the community of machine operators, shift leaders, technical coordinators, machine coordinators, and photon coordinators and all the other people in the control room contributing to successful machine operation. You accepted me fast as "one of yours". You were there to support me when there was much to do, and our scientific and non-scientific discussion, as well as our feasts, will always stay in good memory.

I am very happy to have good friends like Marc and Steffi, who supported me and spend many relaxing times with me. Of course this is also true for "La Familia" and "OMC-HH".

Finally, I want to thank my family for their unconditional support throughout the years and the familial cohesion which we share. I want to thank my all my grandparents which helped me to become the man I am, and of course my parents. Without the help of you, Regina and Roger, neither achieving a PhD, nor a diploma, would have been possible or even thinkable. I can't express the level of gratefulness I feel towards you.

I am happy to have such friends and family. I am looking forward to the many years we all will share together!

## 고생 끝에 낙이 온다

*Korean Proverb: "At the end of hardship comes happiness."*

# Eidesstattliche Versicherung

Hiermit erkläre ich an Eides statt, dass ich die vorliegende Dissertationschrift selbst verfasst und keine anderen als die angegebenen Quellen und Hilfsmittel benutzt habe.

Hamburg, den 28. Juli 2016

Sven Ackermann